The kinematics of central-southern Turkey and northwest Syria revisited

Ali Seyrek[a], Tuncer Demir[b], Rob Westaway[c,d,*], Hervé Guillou[e], Stéphane Scaillet[e], Tom S. White[f], David R. Bridgland[g]

[a] Department of Soil Science, Harran University, 63300 Şanlıurfa, Turkey
[b] Department of Geography, Harran University, 63300 Şanlıurfa, Turkey
[c] School of Engineering, University of Glasgow, Glasgow G12 8QQ, U.K.
[d] Newcastle Institute for Research on Sustainability, Devonshire Building, Newcastle University, Newcastle upon Tyne NE1 7RU, U.K.
[e] Laboratoire des Sciences du Climat et de l'Environnement, Domaine du CNRS, Bâtiment 12, Avenue de la Terrasse, 91198 Gif-sur-Yvette, France
[f] Department of Zoology, University of Cambridge, Downing Street, Cambridge CB2 3EJ, U.K.
[g] Department of Geography, Durham University, South Road, Durham DH1 3LE, U.K.
[*]**Corresponding author** e-mail: robert.westaway@glasgow.ac.uk

Abstract

Central-southern Turkey, NW Syria, and adjacent offshore areas in the NE Mediterranean region form the boundary zone between the Turkish, African and Arabian plates. A great deal of new information has emerged in recent years regarding senses and rates of active crustal deformation in this region, but this material has not hitherto been well integrated, so the interpretations of key localities by different teams remain contradictory. We have reviewed and synthesized this evidence, combining it with new investigations targeted at key areas of uncertainty. This work has led to the inference of previously unrecognized active faults and has clarified the roles of other structures within the framework of plate motions provided by GPS studies. Roughly one third of the relative motion between the Turkish and Arabian plates is accommodated on the Misis-Kyrenia Fault Zone, which links to the study region from the Kyrenia mountain range of northern Cyprus. Much of this motion passes NNE then eastward around the northern limit of the Amanos Mountains, as previously thought, but some of it splays northeastward to link into newly-recognised normal faulting within the Amanos Mountains. The remaining two thirds of the relative motion is accommodated along the Karasu Valley; some of this component steps leftward across the Amik Basin before passing southward onto the northern Dead Sea Fault Zone (DSFZ) but much of it continues southwestward, past the city of Antakya, then into offshore structures, ultimately linking

to the subduction zone bounding the Turkish and African plates to the southwest of Cyprus. However, some of this offshore motion continues southward, west of the Syrian coast, before linking onshore into the southern DSFZ; this component of the relative motion is indeed the main reason why the slip rate on the northern DSFZ, measured geodetically, is so much lower than that on its southern counterpart. In some parts of this region, notably in the Karasu Valley, it is now clear how the expected relative plate motion has been accommodated on active faults during much of the Quaternary: rather than constant slip rates on individual faults, quite complex changes in the partitioning of this motion on timescales of hundreds of thousands of years are indicated. However, in other parts of the region it remains unclear whether additional major active faults remain unrecognised or whether significant relative motions are accommodated by distributed deformation or on the many smaller-scale structures present.

Highlights

-..The evidence for active faulting in and around central-southern Turkey is synthesized

-..Data for both onshore and offshore active faults is integrated

-..Previously unrecognized active faults are identified from offset sediments and lavas

-..Rates of active faulting are compared and contrasted with geodetic data

Key words:

Turkey, Syria, plate kinematics, Pliocene, Pleistocene, Amanos Mountains, Karasu Valley, Amik Basin

1. Introduction

The northeastern corner of the Mediterranean Sea, including central-southern Turkey and northwest Syria (Fig. 1), forms the boundary zone between the Turkish, African and Arabian plates. In recent years an abundance of new data has been documented, regarding the sense, rate and history of Late Cenozoic crustal deformation in this region. This multi-disciplinary dataset includes measurements of

active crustal deformation from GPS (e.g., McClusky et al., 2000; Reilinger et al., 2006; Alchalbi et al., 2010; ArRajehi et al., 2010; Sadeh et al., 2012; Mahmoud et al., 2013; Palano et al., 2013), palaeoseismic and archaeoseismic studies of slip rates on faults (e.g., Meghraoui et al., 2003; Marco et al., 2005; Akyuz et al., 2006; Altunel et al., 2009), detailed studies of relations between volcanism and tectonics, including geochemical analyses and geochronological studies (e.g., Krienitz et al., 2009; Searle et al., 2010; Ma et al., 2011; Trifonov et al., 2011); measurements of Quaternary slip rates from offset basalt flows or other offset landforms (e.g., Seyrek et al., 2007; Abou Romieh et al., 2009, 2012), documentation of Quaternary rates of vertical crustal motion from studies of fluvial and marine terraces (e.g., Bridgland et al., 2008, 2012; Seyrek et al., 2008), documentation of previously unrecognized active faults (e.g., Boulton and Robertson, 2008; Emre and Duman, 2011; Emre et al., 2011, 2012a, 2012b; Duman and Emre, 2013), and clarification of the configuration of active faults in offshore areas using seismic reflection profiling (e.g., Aksu et al., 2005; Hall et al., 2005; Elias et al., 2007; Bowman, 2011). Nonetheless many inconsistencies remain between these different forms of evidence. For example, one team may dismiss the recognition of active faulting by another (cf. Boulton and Robertson, 2008; Karabacak et al., 2010; Karabacak and Altunel, 2013); or one team may model GPS data subject to the assumption of a geometry of active faulting that has been superseded by field studies in the area (cf. Parlak et al., 1997; Seyrek et al., 2008; Mahmoud et al., 2013; Duman and Emre, 2013). The extant literature indeed includes instances where detailed studies by different teams of the same localities are completely contradictory, a notable example being the Latakia area of NW Syria (Hardenberg and Robertson, 2007, 2013; cf., Al Abdalla, 2010; cf. Bridgland et al., 2008; see also below). Duman and Emre (2013) have synthesized established knowledge along with significant new discoveries regarding the active faulting in central-southern Turkey (although they provide no indication which are which) and make some attempt to relate these observations to the motions of the adjoining plates. However, as is discussed below (sections 4 and 5.1), their compilation lacks detail (no site co-ordinates are provided and much of the evidence is only located in the most general terms), omits key evidence at some sites, and sometimes gives

undue prominence to minor structures or seems to conflate active faulting with older crustal deformation.

Figure 1 : regional map
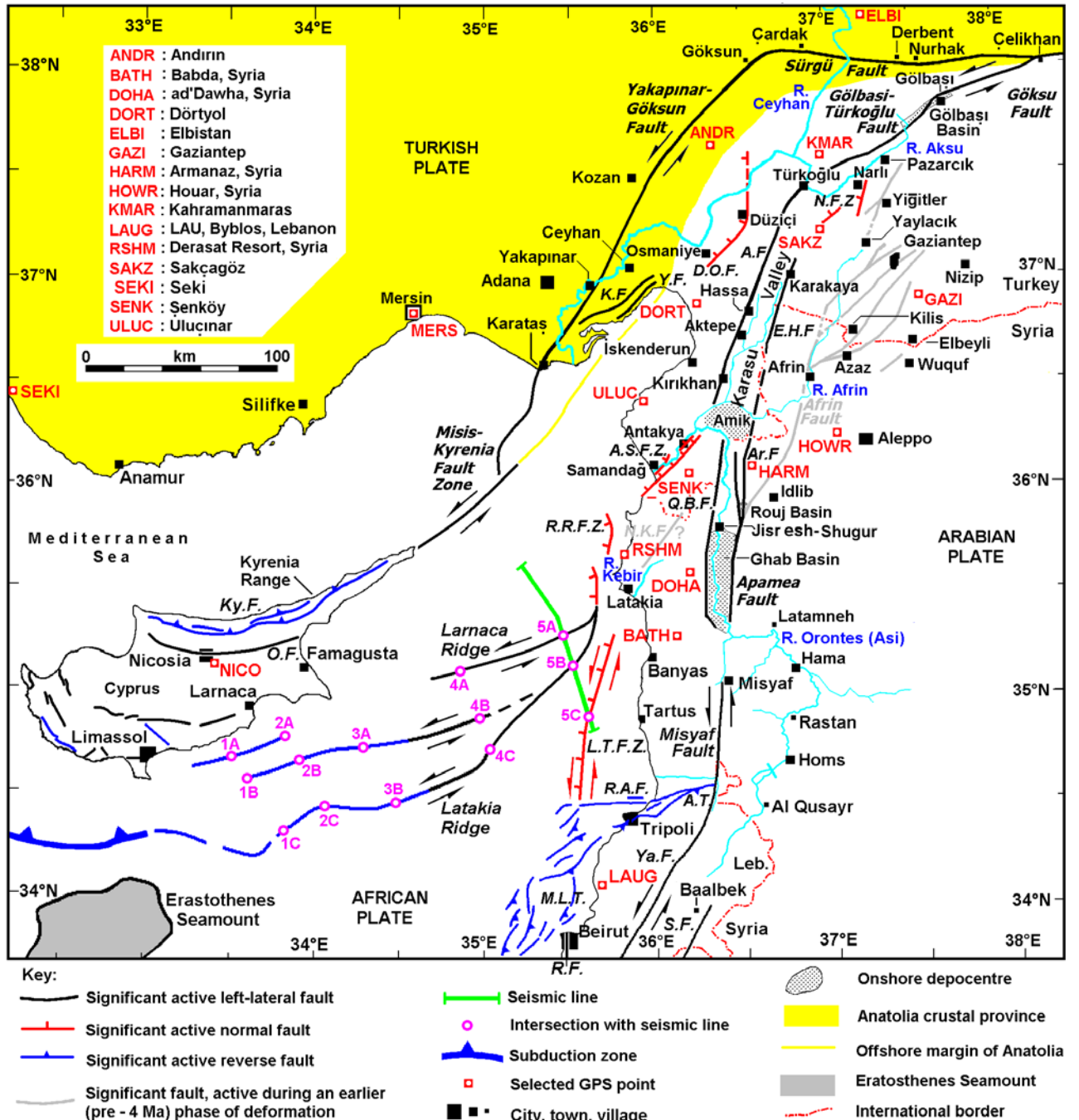
Until about a decade ago the area offshore of Syria was arguably the least well explored part of the Mediterranean Sea (Hall, 2005). Structures showing sea-floor relief had been revealed largely by bathymetric surveys and had been interpreted by some authors as active fault zones, but definitive evidence was lacking. The abundance of new data from offshore seismic surveys (e.g., Hall et al., 2005; Bowman, 2011) demonstrates conclusively that these structures have been active at significant rates during the present (post – Early Pliocene) phase of crustal deformation; however, this evidence has yet to be fully integrated with that from onshore areas. In this paper, we will integrate this evidence to establish the linkage between active faulting offshore of northernmost Syria and onshore in southernmost Turkey. We will then present new field observations and reassessments of existing evidence from key onshore localities on the western flank of the Amanos Mountains, within the Karasu Valley, and in the Amik Basin.

2. Background information

As already noted, the present study region contains the boundary zone between the Turkish, African and Arabian plates. It has experienced many instrumental and historical earthquakes; see, for example, Mahmoud (2012, Figs I.3 to I.5) or Duman and Emre (2013, Fig. 23) for maps, and Ambraseys and Jackson (1998) or Sbeinati et al. (2005) for compilations of historical macroseismic data. These data indicate a broad zone of active deformation but relatively few historical or instrumental events have been associated with any particular active fault. Other sources of information, including field observation and remote sensing imagery, are therefore required to identify important active faults in the region. GPS measurements spanning only a few years can give rates of relative motion that are representative of much longer timescale motions (e.g., ArRajehi et al., 2012), but the interpretation of such data requires knowledge of the locations of major faults in order to relate their slip to the relative motions of the adjoining plates. This section will summarize the background to the present analysis, regarding the geometry and chronology of active faulting in the region.

2.1 Geometry of active faulting

The northern part of the Dead Sea Fault Zone (DSFZ), the boundary between the African and Arabian

Plates, and the East Anatolian Fault Zone (EAFZ), the boundary between the Turkish and Arabian

plates (Fig. 1), were recognized many decades ago as major left-lateral fault zones (e.g., Freund et

al., 1970; McKenzie, 1976). Westaway (1994) subsequently published the first quantitative,

internally consistent kinematic model for this region, which was based on seismic moment

summation for instrumental and historical earthquakes; this estimated left-lateral slip rates of ~7

mm a^{-1} on the DSFZ and ~14 mm a^{-1} on the EAFZ.

When the EAFZ was first identified, primarily from satellite imagery (McKenzie, 1976), it was thought

to continue ENE-WSW in a straight line from the Gölbaşı-Türkoğlu area (Fig. 1) to the vicinity of the

Mediterranean coast (as the Karataş Fault / Yumurtalık Fault in Fig. 1), before running offshore near

Karataş. At that time the DSFZ had been traced northward as far as the Amik Basin in the extreme

south of Turkey (e.g., Freund et al., 1970). The left-lateral faulting in this area is distributed across a

zone some 10-15 km wide, within which Westaway (2003, 2004) recognised two principal active

faults, named the Qanaya-Babatorun Fault and Armanaz Fault (Fig. 1). However, the continuation of

this left-lateral faulting farther north along the Karasu Valley was not recognised by Freund et al.

(1970), and the geometry of any interconnection between it and the EAFZ was for many years

completely unclear. At this early stage the Karasu Valley was indeed thought to be a graben or rift,

unrelated to strike-slip faulting (see Seyrek et al., 2007, for more detailed discussion of historical

research on this topic). Subsequent offshore investigations (e.g., Aksu et al., 1992) revealed a zone of

active faulting linking the Misis mountains in the Karataş area to the Kyrenia mountain range of

northern Cyprus; it was thus realised that the onshore faulting in the Karataş area links ultimately to

the subduction zone between the African and Turkish plates to the SW of Cyprus (Fig. 1) via this

Misis-Kyrenia Fault Zone (MKFZ). However, subsequent work (e.g., Westaway, 2003, 2004; Seyrek et

al., 2008) established that the onshore faulting in the Karataş area does not link in-line to the ENE with the EAFZ; it continues NNE to the Göksun area before turning eastward and merging with the main EAFZ near Çelikhan (Fig. 1). Emre et al. (2012b) and Duman and Emre (2013) have recently documented the active faulting along this zone (which they called the Sürgü-Misis Fault Zone; SMFZ) in considerable detail; it can now be regarded as well established. Many authors (e.g., Karig and Kozlu, 1990; Westaway, 2003, 2004; Seyrek et al., 2007, 2008) have thus regarded the region south and east of this fault zone and west of the Karasu Valley as the northern 'promontory' of the African Plate. Nonetheless, the SMFZ is more complex than is schematically illustrated in Fig. 1; for example, the Sürgü Fault, depicted, has slipped left-laterally by ~4 km, based on structural evidence documented near Derbent by Perinçek and Kozlu (1983), with a time-averaged slip rate of ~1 mm a^{-1} (Westaway, 2004). Duman and Emre (2013) have now proposed that other subparallel fault strands are also active, accounting overall for a higher slip rate and more total slip.

Of particular significance to the regional kinematics is the geometry of active faulting in the Türkoğlu area (Fig. 1), for which a multiplicity of different interpretations have been published in the past. The Gölbaşı-Türkoğlu segment of the EAFZ enters this area from the ENE, locally with S55°W trend (e.g., Westaway et al., 2006). It can be traced along the foot of a bluff flanking the Türkoğlu alluvial plain (Sağlık Ovası) to a point ~6 km ENE of Türkoğlu (circa Universal Transverse Mercator [UTM] co-ordinates CB 15000 43000, near which the fault line is transected by the River Aksu). Along the WNW margin of this plain SW of Türkoğlu (between c. CB 00700 36000 and CB 00350 30000), active faulting is evident, with alluvial fans offset by components of normal slip (Duman and Emre, 2013). The linear bluff along the SSE margin of this plain SE of Türkoğlu (between c. CB 14000 34000 and CB 12000 31500) was also interpreted by Emre et al. (2012b) as marking another active fault. However, the principal active fault in this area is thought (e.g., Westaway, 2004; Emre et al., 2012b; Duman and Emre, 2013) to continue with S35°W trend beneath the alluvial plain, which contained a lake until it was artificially drained for agriculture, rather than along either of its margins. Farther SSW,

near Şekeroba (c. CB 02000 24000; ~18 km SSW of Türkoğlu and ~7 km NNE of Nurdağı) this active fault emerges at the WNW margin of the Karasu Valley and thereafter forms an abrupt escarpment, which continues SSW for ~100 km to the vicinity of Kırıkhan (Fig. 1), that has been mapped by many workers (e.g., Yurtmen et al., 2002; Seyrek et al., 2007; Karabacak et al., 2010; Emre et al., 2012a, 2012b; Duman and Emre, 2013). Active faulting including a component of extension has long been recognised elsewhere in this area, notably on the eastern side of the northern Karasu Valley (e.g., Terlemez et al., 1997), where the land surface steps down to the WNW from the >1000 m a.s.l. Gaziantep Plateau to the ~500 m a.s.l. Narlı plain (Fig. 1). This zone of en echelon oblique normal faults has been named the Narlı Fault Zone by Emre et al. (2012b) and Duman and Emre (2013); part of it slipped in the magnitude ~5 Çöçelli earthquake of 14 November 2012, which involved components of left-lateral and normal slip if the WNW-dipping nodal plane of the focal mechanism was the fault plane (MTA, 2012). However, there is no evidence of any component of active faulting that continues WSW from Türkoğlu, transecting the Amanos Mountains; no major active fault should therefore be assumed in this location, as (for example) features in the recent Mahmoud et al. (2013) analysis.

The first synthesis of GPS results by McClusky et al. (2000) led to a block model for the regional kinematics for which the EAFZ slip rate was deduced to be 9±1 mm a^{-1}, somewhat less than Westaway's (1994) prediction. Reilinger et al. (2006) published a revised bock model based on a longer series of GPS data, in which left-lateral slip at ~10 mm a^{-1} on the EAFZ passed southwestward into left-lateral slip at ~7 mm a^{-1} along the Karasu Valley and ~5 mm a^{-1} on the northern DSFZ, with a component of the relative plate motion that is taken up within the Karasu Valley splaying southwestward from the northern DSFZ in the Antakya area and continuing offshore. Reilinger et al. (2006) also discussed an alternative model for this region, with a different set of plate or block boundaries and relative motions; it thus became evident that GPS data alone cannot resolve the manner in which relative plate motions are accommodated in this region, and that analysis of such

data requires knowledge of the geological evidence, including where significant active faults are located.

The McClusky et al. (2000) GPS synthesis also indicated that the motion of the northern Arabian Plate is oblique to the northern DSFZ, indicating a component of transpression. This led to the idea that the Lebanon / Anti-Lebanon mountains and Jabal Nusayriyah or Syrian Coastal Range have developed synkinematically with the left-lateral slip on the DSFZ (e.g., Westaway, 2003, 2004; Gomez et al., 2006), rather than having developed beforehand as was previously thought (e.g., Brew et al., 2001). At the same time, significant left-lateral faulting has been recognised along the Karasu Valley, from offset Pleistocene basalt flows (Yurtmen et al., 2002; Seyrek et al., 2007) and offset stream channels (Karabacak et al., 2010; Karabacak and Altunel, 2013); we suggest the name Karasu Valley Fault Zone (KVFZ) for this zone of subparallel left-lateral faults. Westaway (2003, 2004) also suggested that the Amanos mountain range to the west of the Karasu Valley might likewise have developed as a result of a northward continuation of this left-lateral transpression, an idea pursued further by Seyrek et al. (2007, 2008). However, it was noted (Westaway, 2003, 2004) that this idea is only tenable if the region west of the Karasu Valley indeed forms a northern 'promontory' of the African Plate; if, instead, it is considered as part of an overall deforming zone between the Turkish and Arabian plates, then no component of transpression would be expected. The summary in Table 1 of the relative motions between key GPS points makes clear that this region should indeed be considered part of a deforming zone between the Turkish and Arabian plates; overall, it accommodates distributed left-lateral simple shear oriented circa NE-SW, across both the SMFZ and KVFZ, together with a subsidiary component of extension (i.e., it is transtensional, not transpressive).

The principal constraints on the present-day regional kinematics are provided by the known rate of left-lateral slip on the EAFZ, estimated geodetically by Reilinger et al. (2006) as 9.9 ± 0.2 mm a^{-1}, and the ~5 mm a^{-1} slip rate on the DSFZ south of Lebanon, which has been determined by several GPS

studies (e.g., 4.4±0.3 mm a[-1], Reilinger et al., 2006; 4.7±0.2 mm a[-1], ArRajehi et al., 2010; 4.9 mm a[-1], Sadeh et al., 2012) and is consistent with geological evidence (e.g., Abou Romieh et al., 2012). On the interseismic timescale, faults can be envisaged as locked to depth D, such that elastic strain accumulates in their surroundings according to

$$b = \frac{V}{\pi}\left(-\tan^{-1}(x/D)\right),$$ (1)

(Savage and Burford, 1973), where V is the rate of transcurrent plate motion and b is the transcurrent velocity at distance x from the fault, relative to zero at x=0. This theoretical treatment predicts that half the relative plate motion (b varying between –V/4 and +V/4) occurs over a distance of ±D on either side of a fault. Reilinger et al. (2006) estimated that D for the EAFZ is ~18 km, but did not consider the full complexity of this zone, the width of which (Fig. 1) will mimic the effect of a high value of D in such calculations. Nonetheless, it is apparent from Table 1 that points close to the active faulting do not record the full left-lateral motion; this is evidently why, for example, the pair ELBI-GAZI indicates less relative motion than does MERS-GAZI (Fig. 1). Table 1 also suggests that maybe half of the relative motion, some 5 mm a[-1], passes onto the SMFZ and MKFZ, the remaining half being accommodated by the KVFZ. However, the geodetic points (ULUC and DORT) used in these calculations are closer to the latter than the former, so the partitioning of elastic deformation will exaggerate the latter somewhat. Duman and Emre (2013) estimated that as a rough 'rule of thumb' the field evidence for Late Pleistocene and Holocene faulting indicates maybe half as much slip on the SMFZ in comparison with the KVFZ, so a reasonable starting point for the present analysis is that left-lateral slip of ~3-4 mm a[-1] passes onto the MKFZ and of ~6-7 mm a[-1] is accommodated by the KVFZ. However, calculations using equation (1) indicate that the DSFZ accommodates left-lateral slip at only ~2-3 mm a[-1] in the Misyaf area and across the Ghab Basin in NW Syria (Alchalbi et al., 2010; Mahmoud et al., 2013), suggesting that a significant component of the relative motion passes southwestward from the KVFZ onto a zone of active faulting along the lower valley of the River

Orontes (Asi), downstream of Antakya in the extreme south of Turkey. Active faulting, combining components of left-lateral slip and extension (i.e., left-lateral transtension) has indeed been recognised onshore along the lower Orontes valley (e.g., Boulton and Robertson, 2008; Boulton and Whittaker, 2009; Tüysüz et al., 2013; Figs 2, 3) although this interpretation has been disputed (Karabacak et al., 2010; Karabacak and Altunel, 2013).

Figure 2 : Antakya field photo

Figure 3 : Antakya field photo

The published GPS data for this region have been depicted as velocity vector maps many times (e.g.,

Reilinger et al., 2006, Fig. 3; Mahmoud et al., 2013, Fig. 2), so such a depiction is not repeated here.

The relative motions between key GPS points depicted in Fig. 1 are instead summarized in Table 1. In

the past few years a multiplicity of interpretations of the regional kinematics on the basis of GPS

data have indeed been published (e.g., Alchalbi et al., 2010; ArRajehi et al., 2010; Sadeh et al., 2012;

Mahmoud et al., 2013; Palano et al., 2013). The differences between these interpretations indicate

the limitations of this technique, especially since it has difficulty resolving relative motions of <~1

mm a^{-1} and many active faults are slipping at rates rather less than this (e.g., Westaway, 2004). As an

illustration of this point, we recall that Mahmoud et al. (2013) have proposed a regional kinematic

model that reinstates the McKenzie (1976) idea of a straight line continuation of the EAFZ from the

Gölbaşı-Türkoğlu area to the Mediterranean coast near Karataş and fits the available GPS data

reasonably well, even though this is at odds with other detailed studies of the same area (e.g.,

Seyrek et al., 2008; Duman and Emre, 2013; see also below, section 4.2) which require a different

geometry of faulting. The evident need for a clear up-to-date synthesis of the geometry of active

faults in the study region to avoid such difficulties in future is one motivating factor behind the

present study.

Table 1 : GPS data

Table 1: Estimated rates of relative motion across fault zones from GPS

Points	Ref.	v_w (mm a^{-1})	v_s (mm a^{-1})	v (mm a^{-1})	α	θ	v_L (mm a^{-1})	v_E (mm a^{-1})	Note	Interpreta
ELBI-GAZI	1,1	6.51±0.87	4.33±0.85	7.82	S56°W	SW	7.67	1.54		Left-latera
ELBI-GAZI	2,3	3.81±0.79	4.45±0.79	5.86	S41°W	SW	5.84	-0.45	1	Left-latera
ELBI-HOWR	2,3	5.24±0.78	5.00±0.79	7.24	S46°W	SW	7.24	0.17		Left-latera
MERS-GAZI	1,1	4.86±0.89	8.76±0.87	10.02	S29°W	SSW	9.95	1.14		Left-latera
MERS-GAZI	4,3	4.02±0.46	6.09±0.44	7.30	S33°W	SSW	7.16	1.38		Left-latera
MERS-HOWR	4,3	5.45±0.43	6.64±0.44	8.59	S39°W	SSW	8.22	2.49		Left-latera
ELBI-KMAR	1,1	3.86±0.74	1.23±0.88	4.05	S72°W	West	3.86	-1.23	1	Left-latera
KMAR-SAKZ	1,1	1.20±0.74	1.03±0.76	1.58	S49°W	SSW	1.41	0.71	2	Left-latera
KMAR-GAZI	1,1	2.65±0.78	3.10±0.78	4.08	S41°W	SSW	3.88	1.26	1,2	Left-latera
ANDR-KMAR	1,1	4.73±1.75	1.69±1.78	5.02	S70°W	West	1.69	4.73		Extension
ANDR-SAKZ	1,1	5.93±1.73	2.72±1.68	6.52	S65°W	SSW	4.78	4.44	2	Left-latera
ANDR-GAZI	1,1	7.38±1.75	4.79±1.69	8.86	S57°W	SSW	7.25	4.99		Left-latera
DORT-SAKZ	1,1	2.93±0.70	2.04±0.71	3.57	S55°W	SSW	3.01	1.93	2	Left-latera

DORT-SAKZ	3,3	2.68±0.44	1.46±0.44	3.05	S61°W	SSW	2.37	1.92	2	Left-latera
DORT-GAZI	1,1	4.38±0.75	4.11±0.73	6.01	S47°W	SSW	5.47	2.47		Left-latera
DORT-GAZI	3,3	3.58±0.54	2.93±0.51	4.63	S51°W	SSW	4.08	2.19		Left-latera
DORT-HOWR	3,3	5.01±0.51	3.48±0.51	6.10	S55°W	SSW	5.13	3.30		Left-latera
SEKI-NICO	1,1	4.89±0.82	3.49±0.79	6.01	S54°W	West	4.89	-3.49		Left-latera
MERS-NICO	1,1	5.35±0.87	-1.83±0.87	5.65	N71°W	West	5.35	1.83	3	Left-latera
MERS-NICO	4,5	4.42±0.21	0.18±0.21	4.42	S88°W	West	4.42	-0.18		Left-latera
MERS-DORT	1,1	0.48±0.85	4.65±0.85	4.67	S6°W	S40°W	3.87	-2.62	1	Left-latera
MERS-DORT	4,3	0.44±0.34	3.16±0.34	3.19	S8°W	S40°W	2.70	-1.69	1	Left-latera
MERS-ULUC	1,1	1.99±1.25	4.77±1.21	5.17	S23°W	S40°W	4.93	-1.54	1	Left-latera
MERS-ULUC	4,3	1.13±0.84	3.35±0.80	3.54	S19°W	S40°W	3.29	-1.29	1	Left-latera
MERS-SENK	1,1	6.47±0.95	5.26±0.93	8.34	S51°W	S40°W	8.19	1.58		Transtensi
MERS-SENK	4,3	5.36±0.53	3.84±0.51	6.59	S54°W	S40°W	6.39	1.64		Transtensi
NICO-SENK	1,1	1.12±0.84	7.09±0.82	7.18	S9°W	S10°W	7.18	-0.13		Left-latera
NICO-SENK	5,3	0.940.53	3.660.51	3.78	S14°W	S10°W	3.77	0.29		Left-latera
NICO-LAUG	1,1	-0.63±1.09	5.28±1.09	5.32	S7°E	S10°W	5.09	-1.54		Mixed; Inc
NICO-LAUG	5,5	-0.87±0.27	3.50±0.27	3.61	S14°E	S10°W	3.30	-1.46		Mixed; Inc
NICO-CSAR	5,4	-0.36±0.24	2.97±0.24	2.99	S7°E	S80°W	0.16	-2.99	2	Shortening
NICO-AREL	5,4	-0.20±0.27	3.50±0.27	3.51	S3°E	S80°W	0.41	-3.48	2	Shortening
DORT-SENK	1,1	5.99±0.82	0.61±0.80	6.02	S84°W	S45°W	4.67	3.80		Left-latera
DORT-SENK	3,3	4.92±0.60	0.68±0.58	4.97	S82°W	S45°W	3.96	3.00		Left-latera
ULUC-SENK	1,1	4.48±1.23	0.49±1.18	4.51	S84°W	S45°W	3.51	2.82		Left-latera
ULUC-SENK	3,3	4.23±0.97	0.49±0.93	4.26	S83°W	S45°W	3.34	2.64		Left-latera
ULUC-HARM	3,3	3.76±0.93	2.38±0.89	4.45	S58°W	S35°W	4.11	1.71	2	Left-latera
ULUC-HOWR	3,3	4.32±0.93	3.29±0.89	5.43	S53°W	S35°W	5.17	1.65		Left-latera
SENK-HARM	3,3	-0.47±0.65	1.89±0.64	1.95	S14°E	South	1.89	-0.47	1,2	Left-latera
SENK-GAZI	1,1	-1.61±0.86	3.50±0.82	3.85	S25°E	South	3.50	-1.61	1	Left-latera
SENK-GAZI	3,3	-1.34±0.67	2.25±0.64	2.62	S31°E	South	2.25	-1.34	1	Left-latera
SENK-HOWR	3,3	0.09±0.65	2.80±0.64	2.80	S2°W	South	2.80	0.09		Left-latera
SENK-DOHA	3,3	-1.02±0.66	1.26±0.65	1.62	S39°E	S10°W	1.06	-1.22	1	Barely res
SENK-BATH	3,3	0.01±0.65	1.44±0.63	1.44	South	S10°W	1.42	-0.26	1	Barely res
RSHM-SENK	3,3	0.76±0.67	1.36±0.65	1.56	S29°E	S10°W	1.21	-0.98	1	Barely res
RSHM-DOHA	3,3	-0.26±0.60	-0.10±0.60	0.28	N69°E	S10°W	-0.04	-0.14	1	No signific
RSHM-BATH	3,3	0.75±0.59	0.08±0.59	0.75	S84°W	S10°W	0.21	0.72		Barely res
BATH-DOHA	3,3	-1.01±0.59	-0.18±0.58	1.03	N80°E	S10°W	-0.35	-0.96	1,4	No signific
LAUG-RSHM	5,3	1.05±0.48	1.52±0.48	1.85	S35°W	S10°W	1.68	0.77		Left-latera
LAUG-BATH	5,3	1.80±0.47	1.60±0.46	2.41	S48°W	S10°W	1.89	1.49		Left-latera
LAUG-DOHA	5,3	0.79±0.47	1.42±0.47	1.62	S29°W	S10°W	1.54	0.53		Left-latera
GLON-RSHM	4,3	-0.27±0.50	1.60±0.49	1.62	S10°E	S10°W	1.53	-0.54	1	Left-latera
GLON-DOHA	4,3	-0.53±0.49	1.50±0.48	1.59	S19°E	S10°W	1.39	-0.78	1	Left-latera
GLON-BATH	4,3	0.48±0.48	1.68±0.47	1.75	S16°W	S10°W	1.74	0.18		Left-latera
GLON-LAUG	4,5	-1.32±0.33	0.08±0.33	1.32	S87°E	S10°E	0.31	-1.29		Left-latera
AZMN-RSHM	4,3	-0.09±0.49	1.40±0.49	1.40	S4°E	S10°W	1.36	-0.33	1	Left-latera
AZMN-DOHA	4,3	-0.35±0.48	1.30±0.48	1.35	S15°E	S10°W	1.22	-0.57	1	Left-latera
AZMN-BATH	4,3	0.66±0.48	1.48±0.47	1.62	S24°W	S10°W	1.57	0.39		Left-latera
AZMN-LAUG	4,5	-1.14±0.33	-0.12±0.33	1.15	N84°E	S10°W	0.08	-1.14		Left-latera
CSAR-GLON	4,4	0.81±0.31	0.45±0.31	0.93	S61°W	N40°W	-0.18	0.91	4	Extension
CSAR-AZMN	4,4	0.63±0.31	0.65±0.31	0.91	S44°W	N40°W	0.09	0.90		Extension
CSAR-RSHM	4,3	0.54±0.47	2.05±0.47	2.12	S15°W	S10°W	2.11	0.18		Left-latera
CSAR-BATH	4,3	1.29±0.45	2.13±0.44	2.49	S31°W	S10°W	2.32	0.90		Left-latera
CSAR-DOHA	4,3	0.28±0.46	1.95±0.46	1.97	S8°W	S10°W	1.97	-0.06	1	Left-latera
AREL-GLON	4,4	0.65±0.33	-0.08±0.33	0.65	N83°W	N40°W	-0.48	0.45	4	Barely res
AREL-AZMN	4,4	0.47±0.33	0.12±0.33	0.49	S76°W	N40°W	-0.21	0.44	4	Barely res
AREL-RSHM	4,3	0.38±0.48	1.52±0.48	1.57	S14°W	S10°W	1.56	0.11		Left-latera
AREL-BATH	4,3	1.13±0.47	1.60±0.46	1.96	S35°W	S10°W	1.77	0.83		Left-latera
AREL-DOHA	4,3	0.12±0.47	1.42±0.47	1.43	S5°W	S10°W	1.42	-0.13	1	Left-latera

Relative velocities are calculated from individual velocities of points, the two velocities used for each pair being listed in the 'Ref.' column. Ref. 1 denotes data from the online supplement of Reilinger et al. (2006) in the reference frame used in that study. Refs. 2-5 denote data from the online supplement of Palano et al. (2013) in the alternative reference frame into which velocity data were transformed for that study, with data sources indicated thus: 2, Reilinger et al. (2006); 3, ArRajehi et al. (2010); 4, Sadeh et al. (2012); and 5, Palano et al. (2013). Point names correspond to the following placenames: ANDR, Andırın, Turkey; AREL, Ariel, Israeli-occupied Palestine; AZMN, Mount Atzmon, Israel; BATH, Babda, Syria; CSAR, Caesaria Beach, Israel; DOHA, ad'Dawha, Syria; DORT, Dörtyol, Turkey; ELBI, Elbistan, Turkey; GAZI, Gaziantep, Turkey; GLON, Gilon, Israel; HARM, Armanaz, Syria; HOWR, Houar, Syria; KMAR, Kahramanmaraş, Turkey; LAUG, Lebanese American University campus, Byblos, Lebanon; MERS, Mersin, Turkey; NICO, Nicosia, Cyprus; RSHM, Derasat seaside resort, Syria; SAKZ, Sakçagöz, Turkey; SENK, Şenköy, Turkey; and ULUC, Uluçınar, Turkey (see Fig. 1 for locations, except for points in Israel – AZMN and GLON, north of the Carmel Fault, and AREL and CSAR, south of this fault - whose locations are illustrated by Sadeh et al., 2012). Like Palano et al. (2013), we have not analysed the Mahmoud et al. (2013) GPS dataset as the short period of observation that it represents has resulted in high uncertainties for the motions of the surveyed points. Values v_w and v_s are the southward and westward components of the velocity of the first point relative to the second, both calculated assuming the uncertainties in the individual velocity measurements are uncorrelated, with v and α denoting the magnitude and azimuth of each overall relative velocity. θ denotes the estimated overall orientation of the deforming zone(s) between each pair of points. Values v_L and v_E denote the calculated components of left-lateral relative motion and extension, parallel and perpendicular to the trends of each of the zones. All calculations assume no rotation of fault-bounded blocks. Notes: 1, A component of extension is expected but the predicted value of v_E is negative indicating an apparent component of shortening, albeit small (within error margins) in most cases; 2, calculations involving points HARM, KMAR and SAKZ seem to underestimate rates of left-lateral slip on the G.T.F., K.V.F.Z. and northern D.S.F.Z. compared with other combinations. This may well be because these points lie so close to the fault zone that some of the transient interseismic accumulation of shear strain is developing farther east (cf. Alchalbi et al., 2010); 3, A component of shortening is expected but the predicted value of v_E is positive indicating an apparent component of extension; 4, The predicted value of v_L is negative indicating an apparent component of right-lateral slip, albeit small (within error margins).

2.2 Chronology of phases of crustal deformation

The chronology of the present phase of deformation in the study region has proved difficult to

establish. However, knowledge of its duration is important, for example to avoid mis-identification

of faults that have been active during different phases of deformation and to facilitate comparison

between measurements of deformation rates (measured, e.g., using GPS) and measurements of

total amounts of deformation, or relative motion, that have occurred during the present phase.

Following the collision between Arabia and Anatolia, which marked the closure of the Southern

Neotethys Ocean and occurred in eastern Turkey during the Eocene (e.g., Aktaş and Robertson,

1984; Allen and Armstrong, 2008), prolonged crustal shortening occurred within Anatolia, lasting

until the Late Miocene when the development of the North Anatolian Fault Zone marked the

formation of the separate Turkish Plate, moving independently of the Eurasian plate. Many reverse faults dating from this NW-SE crustal shortening phase beneath the northeastern Mediterranean Sea are sealed by Messinian evaporates, indicating that the end of this phase of deformation was effectively synchronous with the start of the Messinian Salinity Crisis (MSC) (e.g., Hall et al., 2005). The latter event is now accurately dated to ~6 Ma (e.g., 5.96±0.02 Ma; Krijgsman et al., 1999).

Conversely, Westaway et al. (2008) and others have inferred that the present geometry of faulting onshore in SE Turkey became active circa 3.7 or 3.6 Ma (or, as a first approximation, ~4 Ma). This interpretation is based on comparisons of the total slip to slip rate for the EAFZ and for individual faults within it. The EAFZ is known from the aforementioned geodetic studies (e.g., McClusky et al., 2000; Reilinger et al., 2006) to be accommodating left-lateral relative motion at ~10 mm a^{-1} and is known from geological observations (summarised by Westaway et al., 2008; see also, e.g., Westaway and Arger, 1996) to have slipped a total of ~35 km. As a first approximation, dividing this slip rate into this total slip value gives an age estimate of ~3.5 Ma. More detailed calculations are also possible; for example Westaway et al. (2006) estimated the total slip on the Gölbaşı-Türkoğlu Fault (Fig. 1) as 19 km from a stratigraphic offset and the slip revealed by entrenched river valleys along this fault, since the rate of regional uplift and fluvial downcutting increased around the Mid Pleistocene Revolution (MPR), the change in climatic cyclicity that occurred circa Marine oxygen Isotope Stage (MIS) 22 (~870 ka), as 4.44±0.06 km. A slip rate of 5.10±0.07 mm a^{-1} is thus indicated, which restores the total slip since 3.73±0.05 Ma. The MPR marks the onset of ~100 kyr climate periodicity, associated with increased severity of cold-climate stages (e.g., Mudelsee and Schulz, 1997; Maslin and Ridgwell, 2005), beginning circa MIS 22, that resulted in increased rates of erosion, thus driving more rapid uplift, here and in many other regions worldwide (e.g., Bridgland and Westaway, 2008; Demir et al., 2012). Other calculations of a similar nature are also possible, as detailed by Westaway et al. (2006, 2008).

Elsewhere within the DSFZ, a reorganization in the geometry of faulting is likewise evident during the Pliocene, notably in the Ghab Basin in NW Syria, where a thick Pliocene-Pleistocene lacustrine succession has been emplaced onto much older bedrock (e.g., Domas, 1994; Devyatkin et al., 1997; Brew et al., 2001), indicating that no depocentre existed beforehand. However, it is clear from the disposition of the Homs Basalt (which adjoins the DSFZ south of Misyaf in NW Syria; Fig. 4) that the northern DSFZ in western Syria already existed by this time; this basalt is dated to ~6.0-3.7 Ma (Searle et al., 2010) but some of it cascaded into the linear valley along the DSFZ indicating that the Misyaf Fault (Fig. 1) already existed at the time (Westaway, 2004, 2011). The disposition of this basalt is also influenced by topography that was created by the slip on this fault zone and the associated transpression (Chorowicz et al., 2005). Searle et al. (2010) estimated the upper bound to the left-lateral offset of the Homs Basalt by the Misyaf Fault as 16.8 km; if all this slip occurred since ~3.6 Ma, the subsequent time-averaged slip rate has been ~4.7 mm a^{-1}, this calculated value being likewise an upper bound to the slip rate on this fault (Abou Romieh et al., 2012). Farther south, the initial development of the Hula Basin in the northern Jordan Valley has been assigned a nominal age of ~4 Ma, based on dated volcanism (e.g., Heimann and Steinitz, 1989; Heimann et al., 2009); it marks another leftward step in the DSFZ that did not exist beforehand. It is thus evident that, synchronous with the initiation of the EAFZ, a reorganization in the geometry of the DSFZ occurred during the Early or Mid Pliocene, reflected in the development of the Ghab and Hula pull-apart basins; like Seyrek et al. (2007), we envisage that the Qanaya-Babatorun Fault, the KVFZ, and the active faulting within the Amik Basin (Fig. 1) developed synchronously with this event.

Figure 4 : Syria fault map
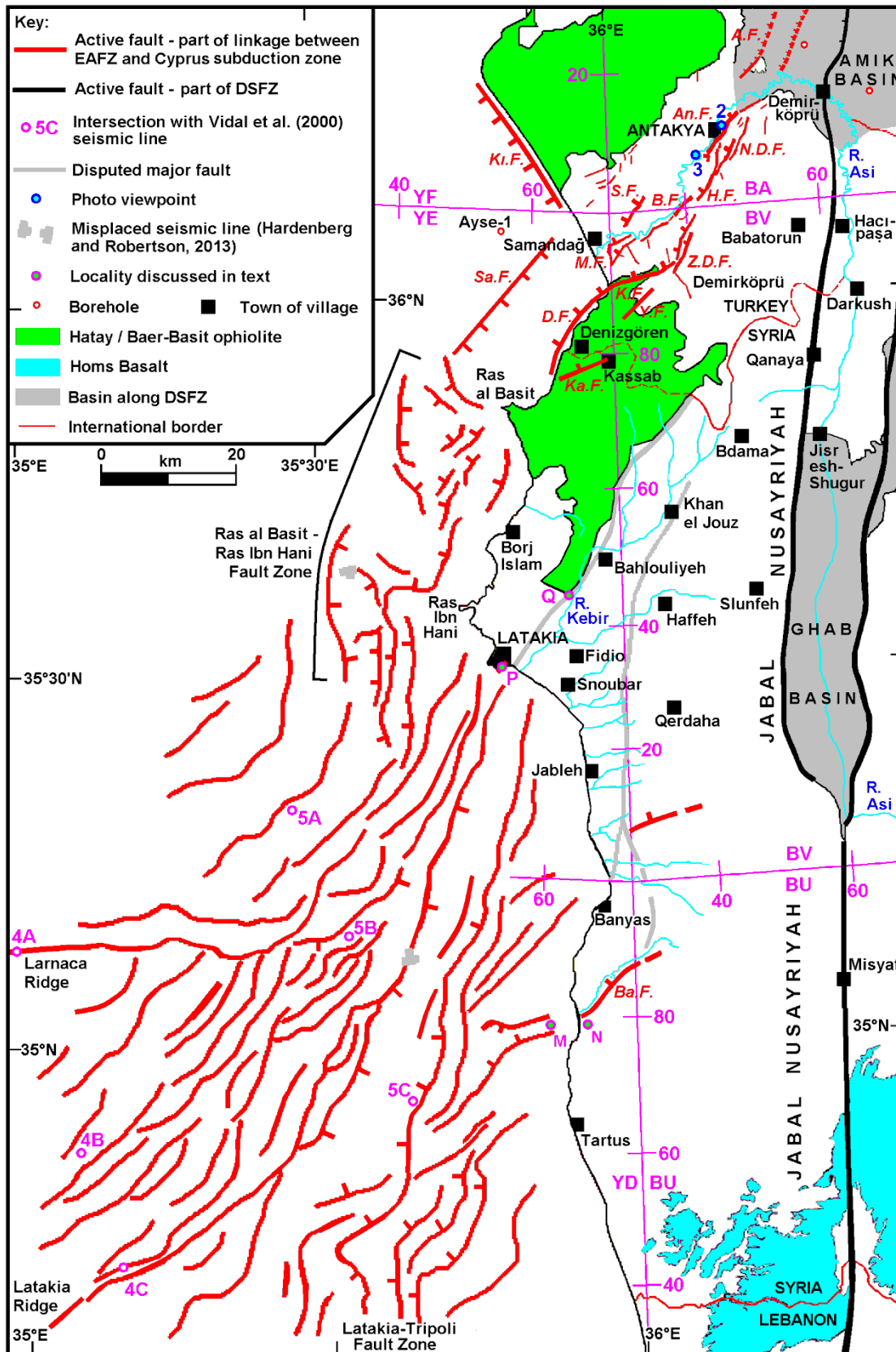
Evidence such as that reported above leads to the notion that between ~6 Ma and ~4 or ~3.5 Ma a phase of transcurrent faulting occurred in northern Arabia and eastern Turkey but with a different geometry to that active at present; Westaway et al. (2008) called this the 'Latest Miocene – Mid-Pliocene' or LMMP deformation phase. Maps of the regional geometry of faulting envisaged during the LMMP phase have been published before (e.g., by Westaway et al., 2008, and Demir et al., 2012) and so are not repeated here, although some of the faults that appear to have been active during this phase are depicted on Fig. 1. Conversely, in other parts of the study region the same faults seem to have been active during both the LMMP and present phases of deformation, albeit with different senses and rates of slip. Thus, for example, the DSFZ south of the Ghab Basin already existed during the LMMP phase in the same place as at present, given the aforementioned chronology and disposition of the Homs Basalt. Farther north, now-inactive fault strands have been recognised east of the Karasu Valley (e.g., Coşkun and Coşkun, 2000), including the Afrin Fault (Fig. 1), and are thought (e.g., Westaway et al., 2008) to represent the northward continuation of the western boundary of the Arabian Plate at this time (see, also, Demir et al., 2012). Trifonov et al. (2011) have resolved both the LMMP and the present phase of deformation from earlier motions and have summarised the evidence distinguishing each of these phases for the DSFZ and other localities within the Arabian Plate. Kinnaird and Robertson (2013) have subsequently recognised a phase of crustal deformation in Cyprus that spanned the latter part of the Messinian and the Early Pliocene, with a deformation sense that was distinct from the phases occurring both before and after, apparently the local equivalent of the LMMP phase recognized elsewhere.

Concurrently with these developments, offshore seismic reflection studies have revealed clear evidence for significant active (i.e., post-Early Pliocene) crustal deformation between NW Syria and Cyprus (e.g., Hall et al., 2005; Bowman, 2011), a region that had not been clearly documented beforehand. This complex picture is represented schematically in Fig. 1 in terms of the Larnaca

Ridge, which links the Latakia area of NW Syria with the Larnaca area of SE Cyprus, and the Latakia Ridge, which links the Latakia area to the active subduction zone SW of Cyprus. The eastern parts of these zones are regarded as having accommodated relative motions consistent with NE-SW-directed distributed left-lateral simple shear and transtension since the Early Pliocene (e.g., Hall et al., 2005). Westaway et al. (2008) estimated that the relative motion between the Turkish and Arabian plates was much less during the LMMP phase than at present; if so, rates of crustal deformation in the present study region were also much less than at present (potentially explaining the lack of evidence of crustal deformation in offshore areas between the start of the MSC and the Early Pliocene; e.g., Hall et al., 2005) such that most of the crustal deformation since the end of the NW-SE crustal shortening has occurred during the present phase of deformation, rather than during the LMMP phase.

However, the occurrence of two changes in the regional kinematics, at the start of the LMMP and present phases of deformation, is not universally recognised, although many authors have noted some sort of plate reorganisation in the region in the recent geological past. For example, Allen et al. (2004) lumped both phases together as a single generalised plate reorganisation that occurred diachronously during ~5±2 Ma. Likewise, following Freund et al. (1970), many investigators have recognised a major change in the kinematics of the southern DSFZ during the Late Miocene but have not resolved the greater detail now evident farther north. The occurrence of these plate reorganisations means (as Allen et al., 2004, already pointed out) that GPS measurements of rates of motion cannot be reliably extrapolated beyond ~3.5 Ma for comparison with observations (cf. ArRajehi et al., 2010).

The causes of these changes are not well established. Nonetheless, Westaway (2003) suggested that the start of the LMMP phase might have been triggered by the change in the regional state of stress that accompanied the fall in Mediterranean sea level due to the MSC. The start of the present phase

might, analogously, have been triggered by the changed state of stress accompanying the rise in the level of the Caspian Sea in the Mid Pliocene, at the start of its Akchagyl transgression, although there is uncertainty in the timing of this event (e.g., ~4.2 Ma, Steininger et al., 1996; ~3.4 Ma; Hall et al., 2009; ~3.2 Ma, Van Baak et al., 2013), making this idea difficult to test. Others have argued that change in the regional kinematics might have been driven by stresses associated with the development of high topography in the Anatolian / Iranian plateau (e.g., Austermann and Iaffaldano, 2013), or associated with subduction beneath the Aegean Sea (e.g., Royden and Papanikolaou, 2011), although neither of these mechanisms can explain the precise timings of the observed changes. As a final alternative, Kinnaird and Robertson (2013) have proposed that the onset of the present phase of deformation has been a consequence of the 'collision' between the Erastothenes Seamount (Fig. 1), which is underlain by continental crust, and the continental crust of Cyprus, which resulted in the termination of subduction beneath southern Cyprus; however, these authors favour a nominal timing of this change of ~3 Ma rather than the somewhat earlier ages indicated by other forms of evidence.

3. Linkage between active faulting offshore of northern Syria and onshore in southern Turkey

3.1 The Antakya-Samandağ Fault Zone

The Amik Basin depocentre (to be discussed in section 6) at the southern end of the Karasu Valley (Figs. 1 and 4) is linked to the Mediterranean coast at Samandağ via a lowland corridor along which the River Orontes flows and in which the city of Antakya is located. Like the Ceyhan valley farther north (section 4.1), this lowland corridor is uplifting, as is indicated by the staircase of Orontes terraces (Erol, 1963; Bridgland et al., 2012); the terrace correlation and age model of Erol (1963) suggests an uplift rate of ~0.2 mm a^{-1}. Downstream of the Amik Basin to the coast, the Orontes falls by ~75 m in ~30 km at a mean longitudinal gradient of ~2.5 m km^{-1}; conversely, in the ~50 km distance upstream of the Amik Basin from Jisr esh-Shugur in Syria to Demirköprü (Fig. 4) it falls by ~40 m (from ~130 to ~90 m a.s.l.), at a mean gradient of ~0.8 m km^{-1}. As Bridgland et al. (2012)

noted, the steeper gradient evidently reflects the adjustment of the river to develop greater erosional power to keep pace with the uplift occurring downstream of the Amik Basin. Furthermore, the Orontes terrace deposits downstream of the Amik Basin are formed almost entirely of clasts of local provenance, indicating that the Amik Basin has acted as a sediment trap for material transported from farther upstream (Bridgland et al., 2012).

Following early studies such as those by Muehlberger and Gordon (1987) and Perinçek and Çemen (1990), many authors have proposed that this corridor is bounded by active faults; some workers, most recently Over et al. (2002), have inferred that both its NW and SE margins are active-fault-bounded, whereas others (e.g., Rojay et al., 2001) have inferred that its NW margin is active-fault-bounded, and such a feature continues to be included on regional summary maps in publications that are not specific to the locality, such as those by Trifonov et al. (2011) and Mahmoud et al. (2013). More recently, others (e.g., Boulton et al., 2006, 2007; Boulton and Whittaker, 2009) have argued that although its NW margin is not an active fault zone, its SE margin is bounded by active oblique normal faults. The evidence of northwest-dipping active faulting along the SE margin of this zone indeed seems compelling (Figs 2, 3), some of these faults having been recognized many years ago, for example by Tolun and Erentöz (1963) or Erol (1963).

This fault zone has recently been designated by others (e.g., Boulton et al., 2006, 2007; Boulton and Whittaker, 2009) as the 'Hatay Graben'. However, it is apparent from the published descriptions of the faulting and from the motions of adjoining GPS points (DORT-SENK and ULUC-SENK; Table 1), which suggest rates of left-lateral slip and extension across this zone of ~4-5 mm a^{-1} and ~3-4 mm a^{-1}, respectively, that it is not a simple zone of extension as the term 'graben' would imply. We thus suggest that a better name for it is the Antakya-Samandağ Fault Zone (ASFZ); Emre et al. (2012a) have called it the Antakya Fault Zone. To facilitate future discussion, we have also named some of the more important active faults recognized within this zone (Fig. 4). The footwall escarpments of these faults dominate the local topography; for example, the land surface rises abruptly from near

sea level to ~400 m a.s.l. across the Antakya Fault (Fig. 2), then by a further ~200 m across the subparallel Nagar Dağı Fault ~2 km to the southeast (Fig. 4). Some ~10 km south of Antakya, the footwall escarpment of the Harbiye Fault rises to ~600 m a.s.l. (Fig. 3) forming another prominent landform that extends for >5 km past the suburb of Harbiye (c. BA 44103 03428) and the village of Döver (c. BV 40494 99352). Another ~10 km farther SSW, the summit of Ziyaret Dağı (c. BV 39200 91700) rises to 1235 m a.s.l. in the footwall of another fault within this zone, which we name the Ziyaret Dağı Fault (Fig. 4). The river terrace evidence demonstrates that localities in the hanging-walls of these faults are uplifting, indicating the effect of erosional isostasy on the vertical crustal motions (Bridgland et al., 2012; see, also, Seyrek et al., 2008). Nearer the coast, the River Orontes flows along a gorge within the footwall of the Sutaşı Fault before emerging through its footwall escarpment, as Erol (1963) noted and Bridgland et al. (2012) have discussed in detail.

However, as already noted, Karabacak et al. (2010) and Karabacak and Altunel (2013) have disputed that this is an active fault zone. They indeed noted that one fault within it (the one which we call the Antakya Fault; Fig, 4) passes through St Peter's Church (Sanpiyer Kilisesi) in Antakya, the oldest extant Christian church (built in the first century A.D.), which is an underground excavation in the limestone forming the footwall (Fig. 2). They pointed out that no earthquake has ruptured this segment of fault for the last ~2000 years, and concluded that the fault is no longer active; however, this might represent an interseismic interval or the deformation on this timescale might have been accommodated on the subparallel Nagar Dağı Fault ~2 km to the southeast (Fig. 4). Many historical earthquakes are indeed known to have affected Antakya, ancient Antioch; Boulton and Robertson (2008) compiled a list, although none has been definitively associated with any particular active fault (but c.f. section 3.2). The geomorphological evidence of young normal faulting in this locality (including landforms such as wineglass canyons where tributaries of the Orontes flow through the footwall escarpment) is indeed very clear, as Bridgland et al. (2012) also noted.

3.2 Active faulting in the coastal sector of the Turkey-Syria border area

In recent years, offshore seismic reflection studies have revealed clear evidence for significant active (i.e., post-Early Pliocene) crustal deformation between NW Syria and Cyprus (e.g., Vidal et al., 2000a, 2000b; Hall et al., 2005; Bowman, 2011), a region that had not been clearly documented beforehand. Figure 4 illustrates the Bowman (2011) dataset, along with (for comparison) the points where the Vidal et al. (2000a, 2000b) seismic lines were interpreted as crossing active fault zones. The complex picture thus indicated (e.g., Hall et al., 2005) is represented schematically in Fig. 1 in terms of the Larnaca Ridge and the Latakia Ridge, as already discussed.

Bowman (2011) also reported a NNE-trending zone of active transtension offshore of northernmost Syria; this zone is ~50 km long, extending from SW of Latakia to west of the Ras al Basit headland, and persisting for up to ~20 km offshore. This zone, not previously clearly recognized, which we call the Ras al Basit – Ras Ibn Hani Fault Zone (RRFZ; Fig. 1), evidently accommodates a northward continuation of the left lateral transtensional relative motion evident (Hall et al., 2005) on the Latakia Ridge and Larnaca Ridge fault systems. The northern end of this fault zone is ~25 km SW of the coastal area around Samandağ to which the faulting that we have grouped within the ASFZ was mapped by Boulton and Whittaker (2009). A SE-dipping normal fault (which we call the Samandağ Fault (Fig. 4) was depicted in this intervening area, ~10 km offshore, by Aksu et al. (2005), but any local faulting has not been mapped in detail.

The land surface along this most southerly part of the Turkish coastline rises to the summit of Keldağ, at 1729 m a.s.l. (c. YE 67500 83000), some 3.5 km inland (Fig. 5). Erol (1963) noted the rise to ~700 m a.s.l. in the immediate vicinity of the coastline, across a facetted escarpment that we regard as the footwall of another active normal fault; we call this the Denizgören Fault (Fig. 5). The coastal morphology in this area was investigated by Pirazzoli et al. (1991), who noted an abundance of Holocene raised shoreline features, up to ~2 m above modern sea-level, one of which yielded a radiocarbon date of ~2900 years. This coastline is thus uplifting, presumably in part as a result of

regional-scale uplift (Bridgland et al., 2012) and in part due to the local effect of active normal faulting. The abrupt coastal morphology continues southward into Syria for a few kilometres, dying out around Badrusiyeh (c. YE 60275 74632), where we interpret the SW end of the Denizgören Fault, its total length being thus ~15 km.

Figure 5 : Denizgören Fault imagery
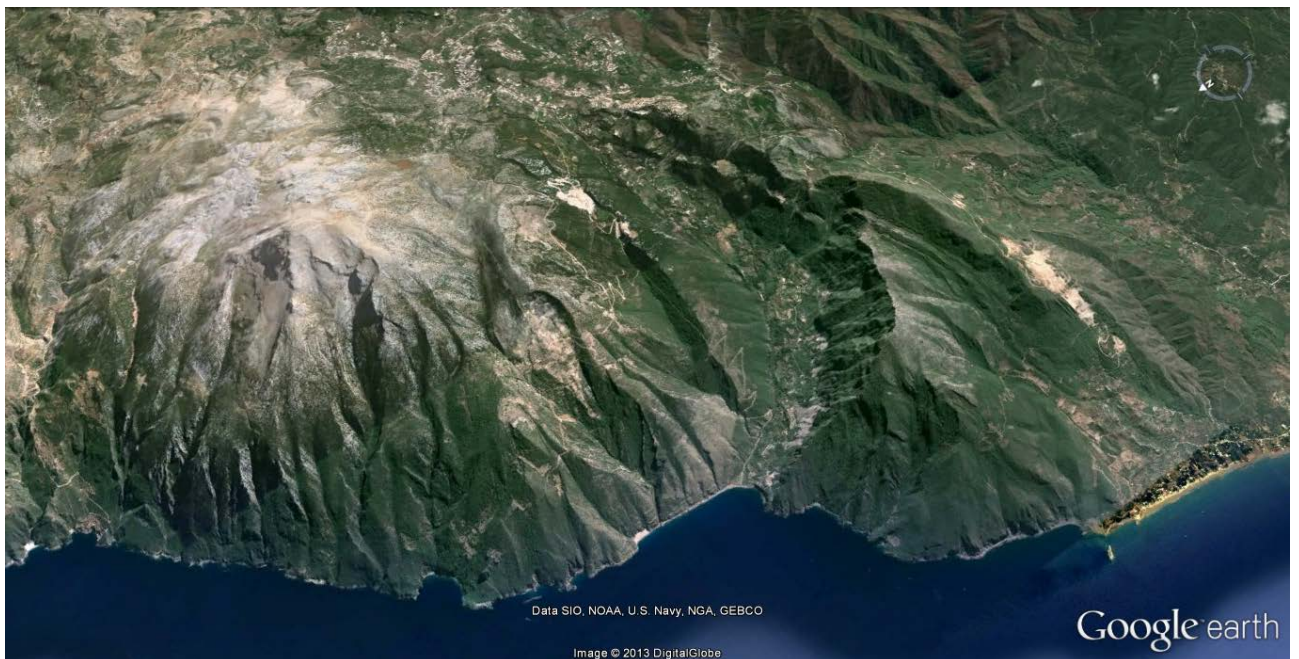
The straight NW-SE-trending coastline NW of Samandağ was interpreted as another active normal fault by Aksu et al. (2005); we call this the Kızıldağ Fault. This coastline is rather less spectacular than that to the south, the coastal facets (which we interpret as forming the footwall escarpment of the Kızıldağ Fault) typically rise no higher than ~200 m a.s.l. However, Pirazzoli et al. (1991) reported a Holocene palaeoshoreline ~3 m above the modern sea-level, dating to ~2.6 ka, indicating faster uplift than in the footwall of the Denizgören Fault. By comparison of several sites, Pirazzoli et al. (1991) attributed ~0.8 m of this uplift to slip during a major earthquake on 9 July 551 A.D., which might thus have occurred on the Kızıldağ Fault. The Roman port of Seleucia Pieria, near modern Samandağ, was abandoned after this event, as Bridgland et al. (2012) have also discussed.

Inland of the Denizgören Fault, a smaller (no more than ~200 m high and ~6 km long) NNW-facing escarpment is evident between Kasab (c. YE 68268 79086) and Badrusiyeh (c. YE 63279 76400). This is shown as a normal fault on the local geological map (Ponikarov et al., 1963) as offsetting Mesozoic limestone that is dipping steeply to the SSE; we call it the Kasab Fault. The abruptness of the local landscape morphology suggests that it may well be an active normal fault. Emre et al. (2012a) depicted a ~5 km long, SW-striking, left-lateral fault farther northeast, near Yeşiltepe (between c. BV 33400 88000 and c. BV 29500 84800), and Emre et al. (2011) illustrated its continuation for ~4 km to the Syrian border (c. YE 68500 81400); a fault in this position would link the Ziyaret Dağı Fault to the Kasab Fault (Fig. 4).

Overall, we conclude that the faulting in this area, including the offshore RRFZ and the onshore active faults adjoining the Turkey-Syria border, links the Latakia Ridge / Larnaca Ridge fault system to the ASFZ. The faulting in this area has previously not been fully recognized, in part because this sensitive border area has been relatively little studied and in part because of the necessity to integrate onshore and offshore data. The Kızıldağ Fault might link northward to the onshore faulting

east of Karataş (Fig. 1), as Aksu et al. (2005) tentatively suggested, or might instead link to normal faulting along the coastline around İskenderun, reported by Emre et al. (2012a). Regardless of its precise geometry, the recognition of the zone of active faulting depicted in Fig. 4 means that the region farther north cannot be regarded as forming a 'promontory' of the African Plate, confirming it as part of the overall deforming zone between the Turkish and Arabian plates, as is also evident from the GPS data (Table 1).

3.3 Faulting offshore of the Syrian coast.

In the 1990s some workers proposed that the principal continuation of the DSFZ northward from the Jordan Valley region lay offshore of Syria. Thus, for example, Girdler (1990) proposed that this fault zone continues NNW from the Beirut area to merge, ~50 km west of Latakia, with a hypothetical NE-trending plate boundary linking the Famagusta area of eastern Cyprus to the İskenderun area of southern Turkey. Butler et al. (1997) suggested, instead, that the DSFZ continues NNW from the coastline near the Syria-Lebanon border to merge, ~20 km west of Banyas, with a continuation of the Latakia Ridge. However, these hypotheses have been widely criticized (e.g., Yurtmen et al., 2002), given that they were not evidence-based.

The first evidence that an active fault zone (schematically depicted as the 'Latakia-Tripoli Fault Zone' or LTFZ in Fig. 1) runs SSW, offshore from the Latakia area to the vicinity of Tripoli in northern Lebanon, was reported by Trifonov et al. (1991) after a Russian research ship mapped the offshore bathymetry of this area (as described by Hall, 2005), revealing sea-floor relief that was interpreted as evidence of active faulting involving components of normal and left-lateral slip. This fault zone has since been depicted by Trifonov (2000), Rukieh et al. (2005), Trifonov et al. (2011), and others; the Trifonov (2000) and Rukieh et al. (2005) depictions show two subparallel WNW-dipping oblique normal faults that pass ~23 km and ~12 km west of the Syrian coast at Tartus. Subsequent investigations (e.g., Elias et al., 2007) have strengthened the evidence for active left-lateral and

reverse faulting offshore of Lebanon; however, in the view of these authors this faulting merges with the DSFZ both southward, near the Lebanon-Israel border (via the Roum Fault), and northward, near the Lebanon-Syria border, rather than having any continuation farther north offshore of Syria. Vidal et al. (2000b) published an interpretation of a seismic section (their profile 5, at locality 5C in Fig. 1) showing a component of normal faulting offsetting the Pliocene and Quaternary sediments within a ~300 m high bathymentic escarpment offshore of Syria in roughly the position of the LTFZ, but did not comment on this observation or illustrate the seismic section that revealed it. Hardenberg and Robertson (2013) re-published (in their Fig. 5) seismic profile 5 of Vidal et al. (2000b), clearly showing the normal fault offset at point 5C, although they located this seismic line in the wrong place (see Fig. 4 and its caption). Bowman (2011) published another seismic section across this putative fault zone (his Fig. 14), which shows that the principal bathymetric relief is caused by submarine canyons, but the evaporite sequence dating from the MSC has nonetheless also experienced deformation consistent with a component of normal faulting.

Support for the idea that an active fault zone is located in this offshore area is provided by GPS (Table 1): points RSHM, BATH and DOHA (Fig. 1) are moving southward at ~1.5 mm a^{-1} relative to points (located north of the Carmel Fault; Sadeh et al., 2012) in NW Israel. It would therefore appear that this component of relative motion passes southward from the Latakia Ridge onto the LTFZ (Figs 1, 4) and then rejoins the DSFZ in southern Lebanon via the system of faults already known in that area (e.g., Elias et al., 2007), which include the Roum Fault (Fig. 1). For comparison, Nemer and Meghraoui (2006) estimated a slip rate of ~0.95±0.10 mm a^{-1} on the Roum Fault from palaeoseismicity and estimated its total slip to be 8.5 km from the left-lateral offset of the River Litani in southern Lebanon. Butler et al. (1998) inferred that the Roum Fault became active around the time of the MSC, consistent with its activity having spanned both the LMMP and present phases of crustal deformation. This amount of total slip would indicate a slip rate of ~1.4 mm a^{-1} if time-averaged since 6 Ma, or ~2.4 mm a^{-1} time-averaged since 3.6 Ma. Some of this slip has evidently been

absorbed by crustal shortening in Lebanon (e.g., Griffiths et al., 2000; Nemer and Meghraoui, 2006); we suggest that part of it passes northward onto the LTFZ as indicated schematically in Fig. 1.

Another deduction from the GPS data (Table 1), which at first sight seems surprising, is that point LAUG in coastal Lebanon is moving SSW relative to the points (RSHM, BATH and DOHA) in western Syria at ~2 mm a^{-1}. One might instead expect, from the west-east-striking reverse fault zone (represented by the 'Aakkar Thrust') interpreted in the Syria-Lebanon border area (Fig. 1) by Elias et al. (2007), that LAUG would be moving northward relative to these points in western Syria. We suggest that the westward component of the observed motion of LAUG is accommodated by the Mount Lebanon Thrust system just offshore (Fig. 1), and the southward component is due to a component of left-lateral slip being also taken up on this offshore structure, which we envisage as continuing southward the component of relative motion across the LTFZ. The proximity of point LAUG to this offshore fault zone means that this southward component of motion arises as a result of the east-west velocity gradient expected due to the interseismic accumulation of strain (cf. equation (1)). We presume that these components of relative motion outweigh any N-S crustal shortening on the Aakkar Thrust and related structures. This interpretation could be tested by future elastic modelling, including the effect of this offshore faulting, but such analysis is beyond the scope of the present study.

One of the more important normal faults, recognized offshore of western Syria by Bowman (2011), corresponds to the normal fault depicted by Vidal et al (2000b) at locality 5C (Fig. 4) and also coincides with the more westerly of the offshore normal faults recognized by Trifonov (2000); the more easterly offshore normal fault recognized by Trifonov (2000) coincides with other normal faults closer inshore, recognized by Bowman (2011). Each of the studies that has gathered data from this area has thus made a consistent interpretation. Furthermore, the seismic evidence indicates that the more easterly of these faults continues northeastward to within ~2 km of the coast south of Banyas

(M in Fig. 4), in close proximity to a normal fault that has been mapped onshore (N in Fig. 4; Ponikarov et al., 1963). Dodonov et al. (2008) have shown that this latter fault offsets the Last Interglacial (MIS 5e; ~125 ka) marine terrace, which declines from ~20 m a.s.l. in its footwall to ~7 m a.s.l. in its hanging-wall, indicating a vertical slip rate of ~0.1 mm a^{-1}. The offshore faulting has also been traced using seismic reflection to within ~1 km of the coastline off Latakia. Hardenberg and Robertson (2013) reported evidence of minor Quaternary faulting in the coastal section at Latakia (between YE 52082 31640 and YE 52494 32742; P in Fig. 4) suggesting that this faulting also affects the onshore area. Hardenberg and Robertson (2007) proposed that there is a component of active normal faulting in this area given different heights of Holocene marine terraces on either side this stretch of coastline, although Dalongueville et al. (1993) did not recognise any such height variation along the coast of NW Syria. Dodonov et al. (2008) reported that the Last Interglacial marine terrace declines from ~35 m a.s.l. at Latakia to ~30 m a.s.l. ~20 km farther southeast at Snoubar, which they thought might relate to a component of downthrow to the southeast on a fault in the Latakia area; however, Bridgland et al. (2008), who surveyed this marine terrace very accurately using differential GPS, found no evidence for such a variation. The older marine terraces inland of Latakia and the fluvial terraces of the Nahr el Kebir River likewise indicate uplift at ~0.4 mm a^{-1} (Bridgland et al., 2008), with no evidence of any differential movement that might indicate any active fault with a significant vertical slip rate in the vicinity.

We thus regard the idea that the LTFZ accommodates a (small) part of the present-day relative motion between the African and Arabian plates as tenable. Figure 4 illustrates the nature of the linkage between active fault zones offshore of Syria, which thus accommodate part of the relative motion between the Turkish and Arabian plates. Moving northward, a broad zone of active crustal deformation, encompassing many faults associated with the Larnaca Ridge, Latakia Ridge, and LTFZ, becomes localized into the much narrower RRFZ and continues northward into the ASFZ. Until the ASFZ is reached the bulk of this zone of deformation is offshore, although its easternmost

extremities pass onshore for short distances, with evidence of onshore active normal faulting in the Banyas, Latakia and Kasab areas (Fig. 4).

3.4 Relative motion of Cyprus

The Reilinger et al. (2006) block model based on GPS envisaged that Cyprus is part of the Turkish plate, to the north of its SW-trending offshore boundary with the African plate (their 'Sinai' plate), across which mainly left-lateral relative motion is occurring at ~8 mm a^{-1}. Kinnaird and Robertson (2013) have subsequently proposed on the basis of geological evidence that since ~3 Ma Cyprus has been likewise 'coupled' to the Turkish plate, moving westward relative to the African and Arabian plates. However, the GPS data now available (Table 1) indicate that point NICO in central Cyprus is moving eastward relative to points on the adjacent Turkish mainland (SEKI and MERS) at ~5 mm a^{-1}, this motion being probably accompanied by a component of N-S shortening. This relative motion is presumably partitioned across active faults in northern Cyprus, such as the left-lateral Ovgros Fault Zone and the Kythrea reverse fault zone (Fig. 1; cf. Kinnaird and Robertson, 2013). Components of left-lateral and reverse slip are also evident offshore within the SW part of the MKFZ as is swings towards a west-east orientation, approaching Cyprus from the northeast (e.g., Hall et al., 2005). NICO is also moving southward at ~3 mm a^{-1} relative to points in NW Israel (CSAR and AREL; Table 1). This indicates that the east-west-trending western part of the Latakia Ridge to the south of Cyprus mainly accommodates a component of crustal shortening, likewise consistent with the offshore seismic evidence (e.g., Hall et al., 2005).

Many workers have established that the relative plate motion west of Cyprus is localized on the Florence Rise, beneath which the African plate (formed in oceanic crust) is subducting northeastward below the Turkish plate (e.g., Woodside et al., 2002; Wdowinski et al., 2006). We envisage that the relative motions occurring across northern Cyprus and across the western Latakia Ridge south of Cyprus merge across SW Cyprus into the localized relative motion evident farther

west. Given the data in Table 1, the relative motion between the African and Turkish plates in the vicinity of NICO can thus be estimated by adding the components identified above (~5 mm a^{-1} of E-W left-lateral slip plus a small amount of N-S shortening across the Kyrenia Range plus ~3 mm a^{-1} of N-S shortening across the Latakia Ridge); one may thus estimate an overall rate of ~6-7 mm a^{-1} in a direction between ~SW and ~S60°W. The Wdowinski et al. (2006) Euler vector (with pole at 31.58°N, 35.40°E) predicts relative motion towards S64°W but their rate of relative rotation (1.171° Myr^{-1}) gives a relative velocity of ~8.9 mm a^{-1}. The consistency between these independent estimates is reasonable, but a lower rotation rate (say, 0.85° Myr^{-1}) would give better agreement.

3.5 Disputed onshore faulting in northwestern Syria

Some authors (e.g., Rukieh et al., 2005; Hardenberg and Robertson, 2007, 2013; Trifonov et al., 2011) have proposed that another major left-lateral fault zone (which they call the 'Nahr el Kebir Fault Zone') runs onshore at Latakia and continues northeastward. Hardenberg and Robertson (2013) have also proposed that active normal faulting continues northward from the Banyas area for ~70 km to Khan el Jouz (Fig. 4); in the view of these latter authors this greatly prolonged 'Banyas Fault' and the 'Nahr el Kebir Fault Zone' bound the 'Nahr el Kebir Graben', a hypothetical zone of active oblique extension associated with left-lateral slip on the 'Nahr el Kebir Fault Zone'.

A major NE-trending lineation, formed by the SE margin of the latest Cretaceous Baer-Basit ophiolite, follows the line of the 'Nahr el Kebir Fault Zone' for most of its length (Fig. 4). However, several lines of evidence suggest that the throughgoing 'Nahr el Kebir Fault Zone', accommodating active left-lateral and normal slip, is a mistaken concept. First, as noted above, the marine terraces and fluvial terraces of the Nahr el Kebir River show no evidence of tilting towards this structure (Bridgland et al., 2008); indeed, according to Dodonov et al (2008) the Last Interglacial marine terrace tilts gently away from it. Second, Bridgland et al. (2008) examined the SE margin of the latest Cretaceous Baer-Basit ophiolite at one locality (Khorafy Quarry: YE 63808 45068; Q in Fig. 4) where it

was well exposed as a result of quarrying of a terrace deposit of the Nahr el Kebir, but found no evidence of active faulting. Third, according to Trifonov et al. (2011) the 'Nahr el Kebir Fault Zone' joins the Qanaya-Babatorun Fault in southernmost Turkey (c. BV 62500 95600, near Hacıpaşa; Fig. 4). We have investigated this area, but found no evidence for such a fault junction, nor did others who have worked in that area (e.g., Perinçek and Eren, 1990; Karabacak et al., 2010). Fourth, except where cut by minor faults such as south of Banyas (Fig. 4), the contact between Pliocene marine sediments within the 'Nahr el Kebir Graben' and older rocks both NW of the 'Nahr el Kebir Fault Zone' and east of the putative northward prolongation of the 'Banyas Fault' has been mapped as an onlapping, rather than a faulted contact (Ponikarov et al., 1963). Fifth, the GPS evidence, including the lack of significant relative motion between points RSHM and DOHA (Fig. 1; Table 1) also suggests that no significant slip is being accommodated on the 'Nahr el Kebir Fault Zone' (or, indeed, the putative northward prolongation of the 'Banyas Fault'). Sixth, Al Abdalla et al. (2010), have interpreted the 'Nahr el Kebir Fault Zone' as marking the line of a northwest-dipping thrust or reverse fault that was active until the Late Miocene, before the present geometry of plate motions developed, suggesting that the associated lineation has nothing to do with the active crustal deformation. Finally, the recent discovery by seismic survey of actively-developing transtensional basins offshore of northernmost Syria (Bowman, 2011), forming the RRFZ (Figs 1, 4), obviates any need to postulate activity on the 'Nahr el Kebir Fault Zone' to link the Latakia Ridge and Larnaca Ridge to localities farther northeast.

Hardenberg and Robertson (2013) also noted evidence (from ~5 km east of Bahlouliyeh; c. BV 500 350) of debris-flow activity affecting Messinian evaporates, which they suggested might be associated with contemporaneous faulting, which would fall within the LMMP phase rather than the present phase of crustal deformation. The 'Nahr el Kebir Fault Zone' might conceivably have been active at this time as part of a linkage between the Latakia Ridge / Larnaca Ridge and the Afrin Fault (Fig. 1), which (following Westaway et al., 2008) we envisage as marking the contemporaneous

northward continuation of the DSFZ. Such a linkage would have been superseded by the RRFZ, ASFZ and KVFZ when the modern geometry of faulting came into being at ~4 Ma. Sites are, indeed, known elsewhere, where debris flows were triggered by the combination of active faulting and climatic conditions during the MSC (e.g., Westaway, 2006). However, other sites are known where debris flow activity occurred at this time without any connection with active faulting (e.g., Suc et al., 2013). Whether the 'Nahr el Kebir Fault Zone' was a significant active fault zone uring the LMMP phase or not must thus remain an open question; it is tentatively included as such in Fig. 1.

4. Investigations of the Amanos Mountains and their western foothills

The Amanos Mountains form the NW extremity of the Arabian Platform, their SSW-NNE orientation following the line of the suture of the former southern Neotethys Ocean (Fig. 1). The core of this range consists of Palaeozoic and possible Precambrian rocks, overlain by Mesozoic limestone and the latest Cretaceous Hatay ophiolite (e.g., Schwan, 1971; Dean and Monod, 1985), the local counterpart of the Baer-Basit ophiolite in Syria. In the western foothills of the range (Fig. 6) the Mesozoic limestone is overlain by limestone and clastic sediments, emplaced during the phase of Cenozoic NW-SE convergence and identified as the 'subduction / accretion complex' in Fig. 6, overlain by younger sandstone and conglomerate of the Kadirli Formation and Erzin Formation. Significant recent developments in understanding of the kinematics of onshore parts of the study region have concerned this mountain range and its surroundings.

Figure 6 : Amanos western foothills map
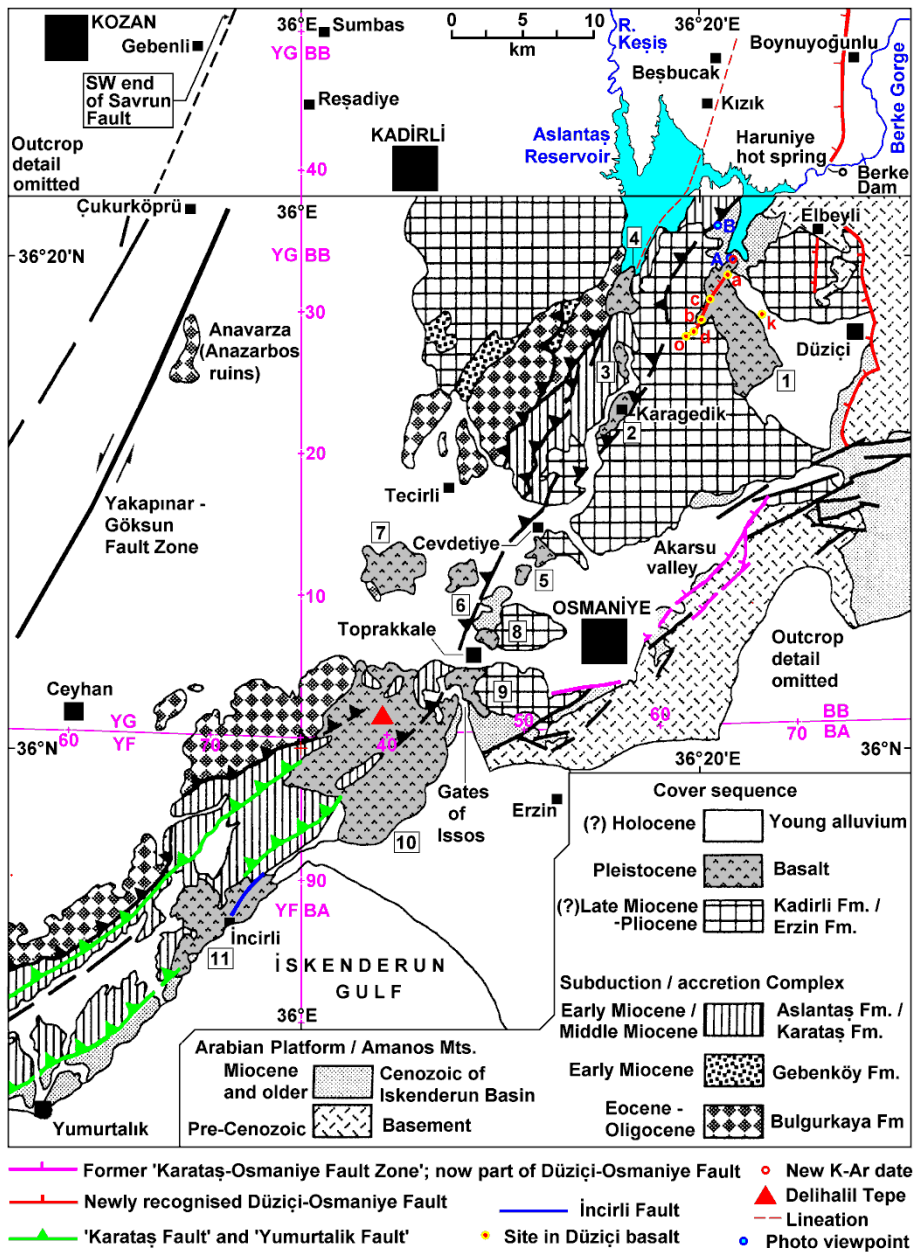
As Seyrek et al. (2007, 2008) have discussed, for decades the topography and structure of the Amanos Mountains were regarded as relics of ancient crustal deformation. For example, the McKenzie (1976) scheme projected the EAFZ obliquely across this mountain range between Türkoğlu and Osmaniye (Fig. 1), the development of the mountain range being considered unrelated to the active crustal deformation that was inferred to be occurring. As already noted (section 2), in contrast with the earlier view, the Amanos Mountains are nowadays envisaged as actively developing within

a complex zone of distributed crustal deformation. Recent key observations, summarised here, include: the documentation of regional uplift within the western foothills of this mountain range (Seyrek et al., 2008); the inference from modelling the landscape development and from biogeography that the topography of this mountain range has developed while the present phase of crustal deformation has been active (i.e., since ~4 Ma); and the reports (Emre and Duman, 2011; Emre et al., 2012b; Duman and Emre 2013) of active faulting within and beyond the western foothills of this mountain range and along the western margin of the highest part of the range, the latter interpreted as a previously unrecognized major active normal fault (Figs. 1 and 6).

The Amanos Mountains are transected by the River Ceyhan (Figs 1, 6), which is entrenched within the ~2 km deep Berke Gorge in the core of the range, evidently an example of antecedent drainage from before the time when this high topography developed (Seyrek et al., 2008). The Ceyhan valley through the western footwalls is inset by river terraces indicating rates of fluvial incision and uplift that taper downstream from ~0.35-0.4 mm a^{-1} in the reach now flooded by the Aslantaş Reservoir to ~0.25 mm a^{-1} at Cevdetiye (Seyrek et al., 2008; Fig. 6). The first objective of this section will be to strengthen the latter conclusion with new dating evidence. Modelling of the landscape development by Seyrek et al. (2008) led to the conclusion that the high topography and entrenched drainage within the Amanos Mountains have developed on the timescale of the present phase of crustal deformation (i.e., since ~4 Ma), primarily as the isostatic response to erosion. Other information pertaining to the crustal deformation in this region is derived from molecular genetics; frog populations in the Cilician Plain (west of the Amanos Mountains) have evidently been isolated from those in the Türkoğlu / Narlı Plain (east of the mountains) for more than three million years (Akın et al., 2010; Plötner et al., 2010), even though both regions are drained by the River Ceyhan (Fig. 1). Substantial topography, requiring entrenchment of the Berke Gorge, evidently began to develop around this time, roughly synchronous with the start of the present phase of crustal deformation, consistent with the earlier inference (section 2.2) that deformation rates during the LMMP phase

were relatively low. Subsequently, Emre et al. (2012b) and Duman and Emre (2013) have included this region in their inventory of active faults associated with the EAFZ. They did not cite Seyrek et al. (2008), but have argued for active faults transecting the landscape, passing through sites that the latter study investigated in detail. On the other hand, they have proposed that the highest topography within the Amanos Mountains has developed as a result of localized footwall uplift adjacent to a previously unrecognized active normal fault zone, thus implying that the uplift in this area is fault-related, not regional. The second objective of this section is to revisit key aspects of the Duman and Emre (2013) scheme; we shall do this in two parts, first for the area northeast of Osmaniye and second for the area farther southwest. We shall conclude this section with a synthesis of the active crustal deformation in this part of our study region.

4.1 Regional uplift in the western Amanos foothills

As noted above, by dating basalt flows (from the Karagedik and Pınarözü flow units, 2 and 4 in Fig. 6) and surveying the heights of terrace deposits of the River Ceyhan, some of which underlie these basalts, Seyrek et al. (2008) deduced rates of fluvial incision and uplift that taper downstream from ~0.35-0.4 mm a^{-1} in the reach now flooded by the Aslantaş Reservoir to ~0.25 mm a^{-1} at Cevdetiye (Fig. 6). All dates from both these basalt flow units were close to 280 ka, suggesting a brief episode of Quaternary volcanism during the latter part of the Middle Pleistocene. However, the larger Düziçi basalt flow unit (1 in Fig. 6) was not dated; Seyrek et al. (2008) assumed the same age as for other basalts in the vicinity. The Düziçi basalt flowed northward down the Sabun Suyu tributary valley, dying out at ~200 m a.s.l. between the villages of Abacılar and Gümüş near the point where this tributary enters the Aslantaş Reservoir (Fig. 6). As described by Seyrek et al. (2008), a Ceyhan terrace deposit at ~185 m a.s.l., ~85 m above the flooded Ceyhan valley floor, is banked against the bluff at the tip of this basalt flow. Seyrek et al. (2008) assumed that this basalt dates from ~280 ka and thus inferred that this ~85 m terrace dates from MIS 8, indicating an uplift rate of ~85 m / ~240 ka or ~0.35 mm a^{-1}.

To verify this interpretation, a ~1 kg sample of the basalt was collected from this locality (sample 06TR43, from BB 65791 33417, adjoining Boyalı farmstead near Abacılar), which was crushed and from which groundmass was separated and dated at the Laboratoire des Sciences du Climat et de l'Environnement at Gif-sur-Yvette, France, using the unspiked (or Cassignol) variant of the K-Ar method. Details of the preparation and analysis procedure, together with an explanation of how technique can give results for very young samples of basalt groundmass that are both accurate and precise, have been explained before (e.g., by Demir et al., 2009, 2012, and in references cited therein) and so are not repeated here. The age thus obtained, 282±9 ka (±2σ) (Table 2), is concordant with the dating by Seyrek et al. (2008) of the Karagedik and Pınarözü basalts and supportive both of their inference that there was a single abrupt episode of Quaternary volcanism in this area circa 280 ka and with their interpretation of the uplift history.

4.2 Active faulting to the northeast of Osmaniye

Emre et al. (2012b) and Duman and Emre (2013) have proposed a geometry of active faulting in the area to the northeast of Osmaniye that represents a radical departure from previous thinking. In their view (see, e.g., Fig. 10 of Duman and Emre, 2013) this area contains a zone of NE-SW- or NNE-SSW-striking normal and left-lateral faults. In their view, the principal normal fault in the area, their Düziçi-Osmaniye Fault, runs for ~45 km along the SE margin of the Akarsu valley and the eastern margin of the Düziçi plain, as indicated in Fig. 6. They depicted a second, subparallel, ~5 km long normal fault ~3-4 km west of the northern end of the Düziçi-Osmaniye fault, south of the village of Elbeyli; we call this structure the Elbeyli Fault. They also inferred two left-lateral faults: their 'Toprakkale Fault', which they traced for >50 km between Toprakkale, Cevdetiye, Karagedik and Boynuyoğunlu, crossing the Ceyhan valley (flooded by the Aslantaş Reservoir) west of the Sabun Suyu confluence. In addition, they reported a second left-lateral fault, ~2-3 km farther SE, some 15 km long, extending between Oluklu (~8 km NE of Karagedik; o in Fig. 6) and a point on the north side

of the flooded Ceyhan valley, ~5 km NNW of Elbeyli. We call this structure the Celiler Fault after a village that lies on it (c in Fig. 6).

The southern part of the Düziçi-Osmaniye normal fault, around Osmaniye, had previously been regarded as part of the 'Karataş-Osmaniye Fault Zone', the hypothetical in-line ENE continuation of the active laft-lateral faulting in the Karataş area to the EAFZ at Türkoğlu (Fig. 1), which is now considered a mistaken concept (see above; section 2). The footwall escarpment of this fault, rising to the southeast of Osmaniye, has ~1 km of relief. The northern part of this fault around Düziçi was recognised as a normal fault, downthrown to the west, by Pamir and Erentöz (1975), although not as an active normal fault. It has some 2 km of footwall relief, between the hanging-wall around Düziçi at ~300 m a.s.l. and the ~2300 m high mountain summits in its footwall (Fig. 7); however, this relief underestimates the throw as former equivalents of the several hundred metres of Cenozoic sediment present in its hanging-wall (Pamir and Erentöz, 1975) have evidently been eroded from the footwall, along with part of the thickness of Mesozoic limestone. This footwall escarpment exhibits planar facets and 'wineglass canyons', where tributaries of the Ceyhan have incised much more rapidly into the footwall than into the hanging-wall that is itself uplifting at ~0.4 mm a^{-1} (see above).

Figure 7 : Amanos Mountains field photographs

Duman and Emre (2013) also reported evidence of tilting of the hanging-wall towards this fault, but did not indicate what the evidence was or where it was located. In our view, the clearest evidence for such tilting is provided by the disposition of the Düziçi basalt. As already noted, this flowed northward towards the Ceyhan along the general line of the Sabun Suyu tributary valley (Fig. 6). This basalt is tilted gently eastward, towards the Düziçi-Osmaniye Fault, as would be expected in the hanging-wall of an active normal fault. Thus, for example, near its western margin near Oluklu (site d in Fig. 6, at BB 63024 28320) the top of the basalt is at ~275 m a.s.l., whereas ~5 km farther east near Kaşobası (site k in Fig. 6, at BB 67866 29669) the eastern margin of the basalt is exposed in bluffs overlooking the Sabun Suyu at ~245 m a.s.l. This tilt seems to continue farther east, but nearer the fault the basalt is buried beneath the young alluvium of the Düziçi plain (Fig. 6). The landscape and structure adjoining the Düziçi-Osmaniye fault indeed have many characteristics of an active normal fault; it is thus surprising that prior to Emre et al. (2012b) and Duman and Emre (2013) no-one had proposed this interpretation.

In the view of Emre et al. (2012b) and Duman and Emre (2013) the Düziçi-Osmaniye Fault dies out northward, just south of the point near the Haruniye hot springs (BB 73466 38830; Fig. 6) where the Ceyhan exits from the Berke Gorge. They envisaged that their NE-striking left-lateral 'Toprakkale Fault' (see below) intersects the frontal escarpment of the core of the Amanos Mountains north of this point, near Boynuoğunlu, beyond which the range front develops a component of reverse slip.

However, this interpretation makes no kinematic sense, as the geometry which they envisage would require a component of extension, not shortening, at a leftward step in left-lateral faulting. The frontal escarpment maintains similar morphology and the same sense of down-to-the-west stratigraphic offset north of the Berke Gorge as farther south (Fig. 7), albeit in more subdued form, suggesting to us that a component of normal slip and extension is present throughout. We thus infer that the Düziçi-Osmaniye Fault continues northward for an additional ~20 km, beyond the extent envisaged by Emre et al. (2012b) and Duman and Emre (2013), as depicted schematically in Figs 1 and 6.

Emre et al. (2012b) and Duman and Emre (2013) also reported the subsidiary ~5 km long Elbeyli normal fault, which strikes southward, ~4 km west of the main Düziçi-Osmaniye fault, between the villages of Elbeyli and Alibozlu, northeast of the outcrop of Düziçi basalt. We can confirm this structure, which can be traced in the field (between c. BB 71873 31811 and c. BB 71622 34432), but the ~20 m maximum height of its footwall escarpment reveals it to be a minor feature.

As already noted, the Celiler Fault farther west was also noted by Emre et al. (2012b) and Duman and Emre (2013); its western part crosses the distal part of the Düziçi basalt with a general S35ºW-N35ºE orientation between Oluklu (site o in Fig. 6, c. BB 62465 27982) and Abacılar (c. BB 65401 32323), passing through the villages of Böcekli (c. BB 63573 29121) and Celiler (c. BB 64151 30572). Along this line the basalt surface drops down to the NW by between ~5 and ~10 m, suggesting a component of downthrow in that direction. Duman and Emre (2013) reported no evidence of left-lateral slip and we know of none, either; we thus infer that this is another minor normal fault, not a left-lateral fault as these authors suggested.

At site d, the fault-line scarp created by the component of downthrow on the Celiler Fault exposes Pleistocene gravel emplaced by the River Ceyhan, its top at ~270 m a.s.l., which facilitated the

interpretation of the Ceyhan terrace staircase by Seyrek et al. (2008). In the view of these authors, the river subsequently migrated northward and westward to its modern course, in part because of the erosion-resistance of the basalt; allowing for this course lengthening, the ~168 m of subsequent fluvial incision indicates ~176 m of uplift. The probable age of this terrace deposit is MIS 12 (~425 ka), indicating a time-averaged uplift rate of ~0.41 mm a^{-1}. This is slightly higher than the ~0.35 mm a^{-1} estimated for the fluvial gravel near the basalt sampling site north of Abacılar, providing further evidence for the component of eastward tilting in the hanging-wall of the Düziçi-Osmaniye Fault.

The area under discussion includes several other topographic lineations with trend similar to the active normal faults already discussed, as is apparent from detailed topographic maps (such as that published as Fig. 4(b) of Seyrek et al., 2008). An example is the lineation formed by the relatively straight eastern side of the wide part of the Aslantaş Reservoir, which also continues in-line to the NNE beyond the reservoir for ~8 km to the vicinity of Beşbucak (c. BB 64900 47500; Fig. 6). Across this lineation the Miocene marine sediments drop down from east to west, so that another alluvial plain, ~5 km wide from west to east, occurs in the Kızık / Beşbucak area just above the level of the reservoir. This ~20 km long lineation has not previously been mapped as an active normal fault but in the light of the reassessment of adjoining structures can be considered another candidate as such.

The final active fault interpreted in this area by Emre et al. (2012b) and Duman and Emre (2013), their 'Toprakkale Fault', warrants some thought. The line of this structure (SSW-NNE through Toprakkale, Cevdetiye and Karagedik to the Ceyhan – Sabun Suyu confluence area then on to Boynuyoğunlu) has hitherto been regarded (Parlak et al. 1997; Seyrek et al., 2008; Fig. 6) as an ancient reverse fault, pre-dating the neotectonic phase. However, Emre et al. (2012b) and Duman and Emre (2013) have reinterpreted it as an active left-lateral fault. They indeed described its slip as having offset tributaries of the Ceyhan left-laterally by 20-30 m during the Holocene and also having offset the Karagedik basalt, although Seyrek et al. (2008) did not notice any such tributary offsets or

any disruption of this ~280 ka basalt during the course of their detailed study of the area. One would indeed expect to find the basalt offset left-laterally by ~600-800 m if this fault has maintained the Holocene slip rate that Duman and Emre (2013) suggested, which it clearly is not; no offset, even by a few metres, is evident. We thus infer that, as an important active left-lateral fault, the 'Toprakkale Fault' is a mistaken concept; Emre et al. (2012b) and Duman and Emre (2013) have evidently mistaken an ancient fault for an active one. A possible reason for this error, evident in the field (for example, around Güzelyurt near the Aslantaş Reservoir, where the field photo in Fig. 7(b) was taken), is that the outcropping Miocene marine sediments typically have steep dips subperpendicular to the strike of this old reverse fault; the differential erosion-resistence between more- and less-lithified beds creates linear trends in the topography that might on casual inspection be mistaken for relief related to active faulting.

4.3 Active faulting to the southwest of Osmaniye

Emre and Duman (2011) and Duman and Emre (2013) also considered the active faulting that extends southwestward from Osmaniye to the coast at Yumurtalık (Fig. 6) and onward to the Karataş area (Fig. 1). In their view the Karataş and Yumurtalık faults in this area (Figs 1 and 6) are active left-lateral faults; Duman and Emre (2013) reported left-lateral offsets of Late Pleistocene drainage of up to 50 m and inferred left-lateral slip rates on each of ~1 mm a^{-1}, but provided no clear location details.

This is another locality where the nature of any active faulting has long been contentious. McKenzie (1976) noted scarps along the lines of what are now known as the Karataş and Yumurtalık faults on satellite imagery and inferred these to be the in-line continuation to the SW of the EAFZ from the Türkoğlu area (Fig. 1). Subsequently, Kelling et al. (1987) noted field evidence of left-lateral slip on the Karataş Fault but Karig and Kozlu (1990) regarded it as a young reverse fault. Reinterpretation of seismic sections by Aksu et al. (2005) led to the conclusion that both faults follow the line of a

reverse fault zone that was active prior to the LMMP phase of deformation but they show components of subsequent normal and left-lateral slip.

Duman and Emre (2013) also stated that the Yumurtalık Fault offsets Pleistocene basalt near its NE end (although again providing no clear location details) but, as was noted by Seyrek et al. (2008), the undated but very young (on account of its fresh appearance; possibly Holocene) Delihalil Tepe Basalt crosses both faults with no observable offset (Fig. 6). The Yumurtalık Fault also crosses the older Botaş Basalt near İncirli; this basalt was dated to 630±180 ka (±2σ; whole-rock unspiked K-Ar) by Arger et al. (2000) and was shown by Gürsoy et al. (2003) to be reverse-magnetised, so its probable age is ~800 ka, late in the Matuyama chron. Seyrek et al. (2008) reported no clear evidence of any offset of this basalt by the Yumurtalık Fault, although much of the land surface in this area is covered by a pediment of basalt blocks that makes identification of margins of in situ outcrop difficult; furthermore, much of this area now forms a port, so the natural landscape has been obliterated and parts of it are inaccessible. Duman and Emre (2013) reported offsets of this basalt by strands of the Yumurtalık Fault, the most important of which was depicted on their Fig. 11 as trending circa N35°E and offsetting the NE margin of the outcrop by ~400 m along a bluff indicative of downthrow to the SE by ~50 m. In-situ basalt is evident on the NW side of this fault (c. YF 64169 89705) and on its SE side (c. YF 64576 89986), at points that are ~500 m apart, but the area in between has been obliterated to build a motorway to serve the port, so it is hard to say whether this is a true left-lateral offset. Nonetheless, if this evidence is taken at face value it suggests a time-averaged left-lateral slip rate of ~0.5-0.6 mm a^{-1} with a minor component of normal slip.

4.4 Summary and synthesis

Seyrek et al. (2008) deduced that the isostatic response to erosion provides the principal mechanism for the development of the topography of the Amanos Mountains since ~4 Ma. They envisaged that active faulting that came into being at the start of the present phase of deformation resulted in the

initial development of topography, but feedback associated with the the isostatic response to erosion subsequently took over, facilitated by the high local runoff that results from orographic precipitation on this topography. The subsequent realization that this region has been affected by both active normal faulting and regional uplift means that uplift varies laterally in a much more complex way than Seyrek et al. (2008) envisaged; in particular, uplift rates have been significantly higher in the core of this mountain range than in its western foothills, as a result of the component of vertical slip on the Düziçi-Osmaniye Fault and the smaller normal faults in the surrounding area. We thus presume that the localised uplift of localities in the footwall of the Düziçi-Osmaniye Fault facilitated rapid erosion of the former Cenozoic sedimentary cover and contributed to sustaining the uplift of these areas; conversely, the wider regional uplift, including the uplift of the western foothills, located as they are in the hanging-wall of this fault, is not explicable in terms of the regional tectonics and is presumably climate-driven, mediated by erosional isostasy, like in many other parts of the region (e.g., Bridgland et al., 2012; Demir et al., 2012).

If it is assumed that the estimated ~3 km of vertical slip on the Düziçi-Osmaniye Fault around Düziçi has developed since 3.6 Ma, the vertical slip rate has been ~0.8 mm a^{-1}, so the uplift rate in the footwall has been ~1.2 mm a^{-1}, given the ~0.4 mm a^{-1} rate near the hanging-wall cutoff (Seyrek et al., 2008). Assuming a ~45° dip, the extension rate across this fault has also been ~0.8 mm a^{-1}, and some 3 km of extension across this fault can thus be estimated. Conversely, the GPS data (Table 1) indicate that extension at ~4 mm a^{-1} is expected across the zone containing this fault. Some of this is evidently occurring on the other normal faults (or candidates) in the region; for example, ~10 m of extension on the Celiler Fault can be estimated since ~280 ka, the age of the Düziçi basalt, indicating a time-averaged rate of ~0.04 mm a^{-1}. However, the normal faults currently known in this region can account for only a small proportion of the ~14 km of extension (~4 mm a^{-1} x ~3.6 Ma) during the inferred age of this deforming zone.

Farther southwest, we infer that a component of left-lateral slip has been accommodated on the Karataş and Yumurtalık faults, to link the offshore MKFZ to the zone of extension that includes the Düziçi-Osmaniye Fault (Fig. 1). The apparent offset of the late Early Pleistocene Botaş Basalt near İncirli by the Yumurtalık Fault suggests a time-averaged left-lateral slip rate of ~0.5-0.6 mm a^{-1} along with a minor component of normal slip; such an interpretation, of components of left-lateral and normal slip, on the basis of field geology, would be consistent with that obtained by Aksu et al. (2005) for both the Karataş and Yumurtalık faults from seismic reflection evidence.

The GPS data (e.g., the relative motions between points MERS and DORT; Table 1) indicate a left-lateral slip rate of ~4 mm a^{-1} for the SMFZ. Although the evidence suggests that part (apparently, a small proportion) of this is accommodated on the Karataş and Yumurtalık faults, these have evidently not slipped since the eruption of Delihalil Tepe; the bulk of this relative motion is presumably taken up on the subparallel Yakapınar-Göksun Fault (Fig. 1), part of which slipped most recently in the magnitude ~6 Ceyhan earthquake of 27 June 1998 (e.g., Aktar et al., 2000).

5. Investigations in the Karasu Valley

As already noted, previous studies have recognised the Amanos Fault and the East Hatay Fault along the western and eastern sides of the Karasu Valley; we now regard all fault strands within this zone as parts of the KVFZ. Previous studies have identified multiple localities where slip on the Amanos Fault offsets Pleistocene basalt flows. Although many localities exhibit components of down-to-the-east slip, consistent with a component of normal faulting, the principal effect is left-lateral slip, at rates of several millimetres per year (Yurtmen et al., 2002; Seyrek et al., 2007). We first review the evidence pertaining to the East Hatay Fault, which is located a short distance inside Syria at the margin of the southern part of the valley but passes into Turkey farther north (Fig. 1). We then re-examine the active or Quaternary faulting at the western margin of the Karasu Valley near Aktepe

(Fig. 8), where new field and geochronological evidence provides evidence for faster left-lateral slip than previously envisaged.

Figure 8 : SRTM imagery of Aktepe area
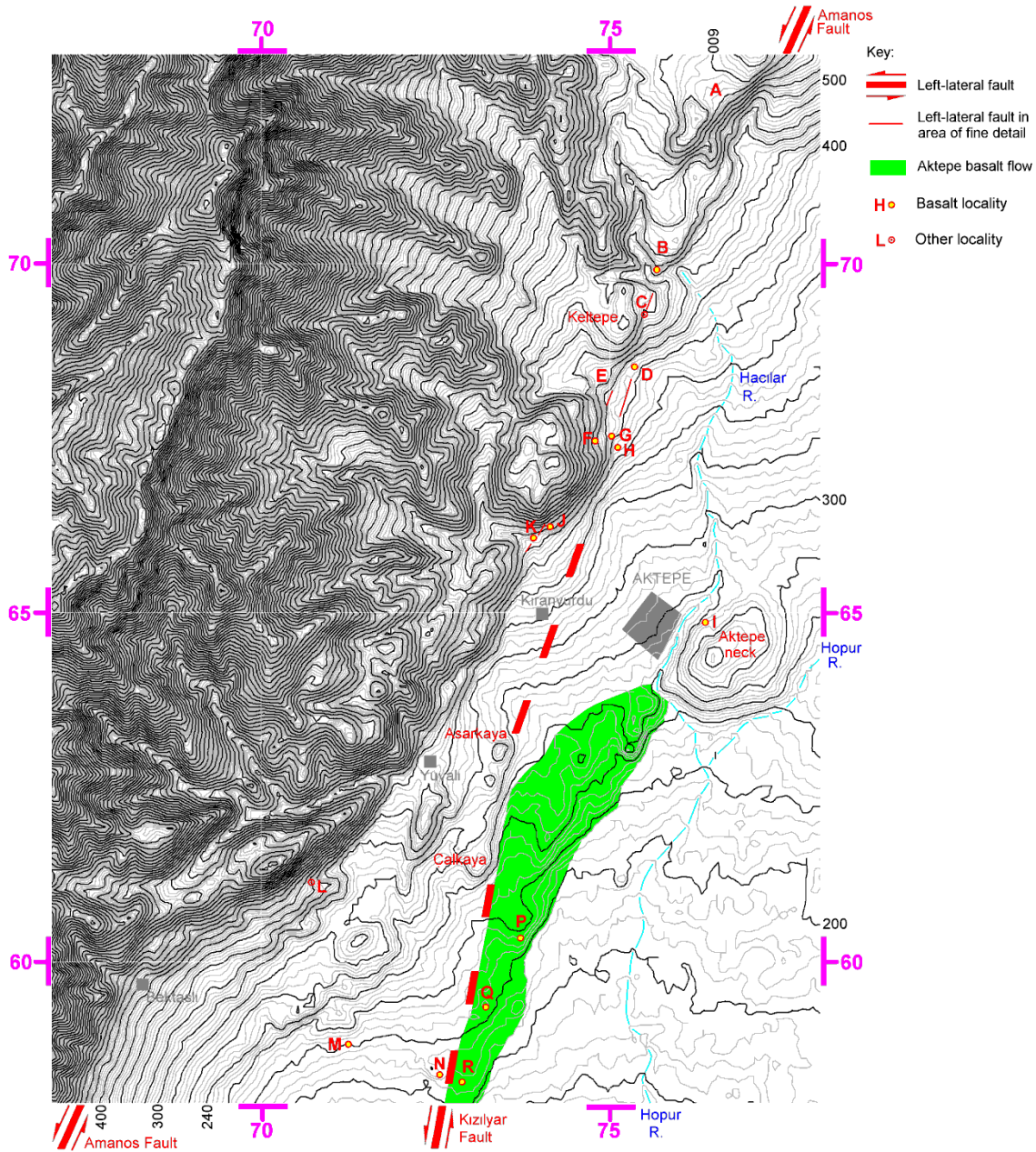
5.1 The East Hatay Fault

Westaway (2004) suggested that the East Hatay Fault might have slipped left-laterally by ~10 km, based on offsets of the Hatay ophiolite mapped independently on the Turkish and Syrian sides of the

border. However, given the history of Cenozoic crustal deformation in this region there can be no certainty that all this offset developed during the present phase of crustal deformation. More recently, Karabacak et al. (2010) and Karabacak and Altunel (2013) have proposed that this fault is not active at present. Conversely, as well as suggesting a new name for this fault, the Yesemek Fault, Duman and Emre (2013) reported a number of indicators of Quaternary left-lateral slip. Most of these were described too vaguely to be identifiable to any particular locality, and so cannot be verified. However, one of their sites was illustrated in a field photograph (their Fig. 22(b)); although no co-ordinates were provided, we have located the precise site (Fig. 9), ~500 m north of the village of Karakaya, some 20 km north of the point where the fault enters Turkey (Fig. 1).

Figure 9 : Karakaya Google Earth image

At this site (Fig. 9) a small stream flows down a bluff within the Hatay ophiolite, crossing the fault from the southeast. The stream, incised into a young alluvial fan, is offset leftward (between points CA 03441 94841 and CA 03413 94817) in line with the foot of the bluff, providing evidence (equivalent in character to similar evidence documented at sites along the Amanos Fault by Karabacak et al., 2010) of a component left-lateral slip. The left-lateral offset between these points is

37 m, consistent with the ~40 m estimated by Duman and Emre (2013), oriented subparallel to the ~N30^{o}E trend of the bluff.

As with similar measurements by Karabacak et al. (2010), one requires a timescale for such observations of fluvial incision to determine a slip rate. There is abundant evidence within Turkey for phases of fluvial incision in response to climate change (e.g., Bridgland et al., 2012; Demir et al., 2012). Rivers in this region typically incise when the climate becomes warmer and/or wetter, as a result of the increased flow and tendency for the more abundant vegetation to restrict movement of sediment from hillslopes into rivers. The climate of Turkey is known to have been cold and arid around the Last Glacial Maximum, becoming warmer and wetter around the start of the Lateglacial Interstadial (or Bolling-Allerod Interstadial), at ~15 ka, then colder and dryer again during the Younger Dryas Stadial, then wetter again at the start of the Holocene, at ~11 ka (e.g., Roberts et al., 2001; Jones et al., 2007). The strongest of these transitions was at the start of the Lateglacial Interstadial, making this the preferred candidate event, although other timings, such as the start of the Holocene (or, indeed, earlier times of climate instability), cannot be ruled out. Subject to this assumption, the ~37 m left-lateral offset at Karakaya indicates a left-lateral slip rate on the East Hatay Fault of ~2.5 mm a^{-1}.

However, an additional complicating factor is that slip rate estimates over such timescales are often unrepresentative of longer-timescale motions. This has been clearly demonstrated on the northern DSFZ in western Syria where palaeoseismic studies spanning the past ~2000 years indicate a ~7 mm a^{-1} slip rate (Meghraoui et al., 2003) but elastic modelling of GPS data indicates a rate of no more than ~3 mm a^{-1} (Alchalbi et al., 2010). Likewise, Altunel et al. (2009) have estimated a slip rate of ~6 mm a^{-1} at the northern end of the Qanaya-Babatorun Fault where it enters the Amik Basin from offset archaeological features, where GPS data (e.g., the SENK-HARM relative velocity in Table 1) indicate a much lower rate. As already noted (see above; section 4), the Karataş and Yumurtalık

faults may conversely have Holocene slip rates of zero even though there is evidence of significant Pleistocene left-lateral slip on them. Such effects have been documented on other strike-slip fault zones elsewhere (e.g., Blisniuk et al., 2010; Ferry et al., 2011) and seem to arise because of complexities in the manner in which interseismic elastic strain becomes converted into permanent deformation. In effect, a fault may slip slowly during a span of time then later accelerate to 'catch up' with the expected long-timescale slip rate, this effect being possibly influenced by changes in crustal rheology during the course of the faulting (e.g., Cowie et al., 2007).

As previously noted (e.g., Westaway, 2004; Seyrek et al., 2007), comparison of Turkish and Syrian geological maps covering the northern part of the reach of the Karasu River that forms the international border (~25 km SSW of Karakaya; Fig. 1) indicates apparent offsets of outcrop boundaries within the Cretaceous succession of ~10 km. However, the sensitivity of the border area has prevented any fieldwork aimed at verifying this mapped offset. Nonetheless, given the age of the faulting, a 10±1 km offset is consistent with a constant slip rate of ~2.7±0.5 mm a^{-1}, in agreement with the estimate for the slip rate since the Late Pleistocene at Karakaya. In the absence of stronger evidence, our 'best estimate' of the slip rate on the East Hatay Fault is the above ~2.5 mm a^{-1}.

Moving farther south, the East Hatay Fault passes end-on into the Armanaz Fault in NW Syria (Fig. 1; see, also section 5.3). However, the GPS data (Table 1) indicate that the slip rate is rather less on the Armanaz Fault than on the East Hatay Fault; the relative velocities of points SENK-HOWR and SENK-GAZI are ~3 mm a^{-1} and that for SENK-HARM is <2 mm a^{-1}. However, HARM is too close to the Armanaz Fault to represent its full slip rate given the manner in which interseismic strain is partitioned (cf. equation (1)). We tentatively estimate on this basis slip rates of ~2 mm a^{-1} on the Qanaya-Babatorun Fault and Armanaz Fault are each no more than ~1 mm a^{-1} in the area immediately south of the Amik Basin. Farther south, elastic modelling by Mahmoud et al. (2013)

indicates that the overall slip rate at the latitude of the Ghab Basin (combining the faults on its eastern and western sides; Fig. 1) is only ~2 mm a^{-1}.

5.2 The Aktepe area

The first detailed mapping of the area west opf the town of Aktepe, by Atan (1969), depicted what is now known as the Amanos Fault running across the flank of the hill, Yünlü Tepe, to the north of the Küreci valley (Fig. 8) along which the River Olucak debouches from the Amanos Mountains. Pleistocene basalt is juxtaposed against the ESE side of this fault; Seyrek et al. (2007) inferred that this basalt originally formed part of the flow unit that was erupted within the Küreci valley, and was translocated NNE to its present position by left-lateral slip on the Amanos Fault. Our expectation (which turned out to be correct) was therefore that this basalt would be of the same age as the oldest part of the Küreci valley flow unit, for which Yurtmen et al. (2002) obtained a date of 553±20 ka (unspiked K-Ar; ±2σ), thus confirming this aspect of the Seyrek et al. (2007) interpretation.

Figure 10 : Atan's map
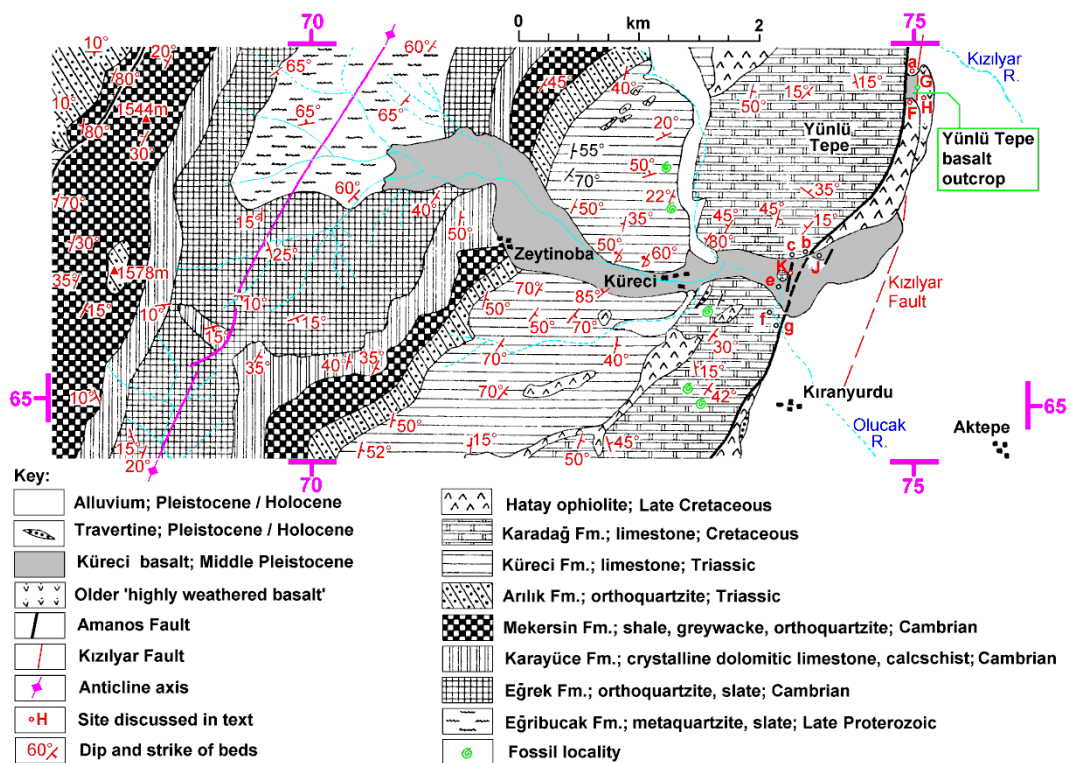
The basalt mapped by Atan (1969) was depicted by him to the north of a narrow (~150 m wide) outcrop of the latest Cretaceous Hatay Ophiolite, on the ESE side of the Amanos Fault. An excerpt from this map covering this area was re-published as Fig. 12 of Seyrek et al. (2007) and is repeated here (Fig. 10) to facilitate discussion. This map shows the basalt outcrop extending eastward beyond the ophiolite and southward around its eastern margin for short distances. As previously noted (e.g., Yurtmen et al., 2002; Seyrek et al., 2007), exposures of bedrock in this part of the Karasu Valley are quite limited, due to widespread cover of colluvial deposits and pervasive vegetation (cf. Fig. 11); furthermore, we noted evidence of significant disturbance to the area including levelling of part of it, possibly from a past attempt to mine the adjacent ophiolite, chromite mining having been undertaken within this ophiolite elsewhere in the region (e.g., Tolun and Pamir, 1975).

We found that the single basalt outcrop mapped by Atan (1969) consists of two distinct basalts that are juxtaposed. An outcrop of relatively fresh (and, thus, relatively young) basalt, which we call the Yünlü Tepe Basalt, some ~250 m long (SSW-NNE) and ~150 m wide (WNW-ESE) terminates at a bluff up to ~30 m high (Fig. 11), trending SSW-NNE and in-line with the ESE edge of the ophiolite 'sliver' (in and around point G in Figs 8, 10 and 12). The northern end of this basalt is difficult to locate precisely due to colluvium and vegetation, but its cutoff at the Amanos Fault is circa BA 74900 67700, at point a in Fig. 10. This basalt has its maximum thickness roughly midway along this outcrop, where the full height of the bluff consists of basalt; at its SSW end (c. BA 75000 67450) the basalt can be seen to be banked against the adjacent ophiolite (Fig. 11). Below this bluff and extending to the east of the ophiolite 'sliver' (before being buried beneath the widespread colluvium) highly weathered, and thus, presumably, significantly older, basalt (H in Fig. 8) is seen.

Figure 11 : field photograph looking west at the Yünlü Tepe Basalt

Figure 12 : Google Earth image

We sampled both basalts for geochronology; however, the basalt to the ESE proved unsuitable due to its highly weathered state. Sample 06TR27, consisting of ~1 kg of the fresher Yünlü Tepe Basalt and collected near the base of the bluff at the point where it was thickest (at BA 75032 67528; site G in Figs 8, 10, and 12; see also Fig. 11), was dated using the procedure described previously (Table 2). The numerical age thus obtained, 566±18 ka (±2σ), is concordant with that of 533±20 ka (±2σ) reported by Yurtmen et al. (2002) for the oldest basalt within the Küreçi valley (circa site K in Figs 8 and 10), consistent with our initial working hypothesis regarding the origin of the Yünlü Tepe Basalt. The cross-sectional profile of this basalt, exposed in the bluff (Fig. 11), evidently reflects that of the Küreci valley floor at the time of emplacement.

Roughly 1 km NNE of the site where our sample was collected, in line with the aforementioned bluff, is another outcrop of basalt, truncated at is WNW flank by a more subdued bluff, less than 10 m high (Site D in Figs 8 and 12). This outcrop extends SSW-NNE for almost 300 m (from c. BA 75283 68334 to BA 75356 68610) but its width is no more than ~80 m, before it, too, plunges eastward beneath the widespread colluvium; this basalt appears thickest near its mid-point, circa BA 75327 68499. The length (SSW-NNE) of this outcrop is similar to that of the outcrop of the Yünlü Tepe Basalt at our sampling site. We have not sampled this more northerly outcrop of basalt, but suggest that it is offset left-laterally from the Yünlü Tepe Basalt and is indeed the continuation of the latter towards the Karasu Valley interior. To facilitate discussion we name the left-lateral fault thus indicated the Kızılyar Fault, after the river that crosses it north of our sampling site (Figs 8, 10). Restoring this northern end to the cutoff of the Yünlü Tepe Basalt by the Kızılyar Fault near point a (c. BA 75050 67700) gives an offset of ~866 m towards a UTM azimuth of N21°E, whereas restoring the southern end to the cutoff near point F (circa BA 75000 67450) gives an offset of ~928 m towards a UTM azimuth of N18°E. We thus estimate that the Kızılyar Fault has slipped by ~900±50 m towards a UTM azimuth of circa N19°E (D-G in Figs 8 and 12) since the eruption of the Yünlü Tepe Basalt, indicating a time-averaged slip rate of ~1.6 mm a^{-1} since ~566 ka. Moreover, the projection of this fault NNE

from our sampling site at a geographical azimuth of circa N17⁰E predicts that it merges with the

Amanos Fault circa BA 75500 69300 (C in Figs 8 and 12), ~2 km NNE of our sampling site.

Figure 13 : View of the fault escarpment along Yünlü Tepe

Immediately SSW of our sampling site, the bluff along which the Yünlü Tepe Basalt is truncated by

the Kızılyar Fault is in line with the base of the escarpment along the ESE margin of the 'ophiolite

sliver' flanking Yünlü Tepe (Fig. 13). This bluff evidently marks the continuation of the Kızılyar Fault

to the SSW. Moving farther SSW, the same fault can be projected along the ESE margin of the

ophiolite 'sliver', passing near Kıranyurdu, ~2 km WNW of Aktepe. Some 6 km SSW of our sampling

site, or ~4 km SW of Aktepe, and in-line with this projection, is the linear ridge formed by the low

hills Asarkaya Tepe and Çalkaya Tepe, which form an outcrop of Palaeocene limestone of the

Eşmişek Formation of Atan (1969), abruptly truncated to the ESE by a ~20 m high bluff (Fig. 8). This

linear bluff was tentatively interpreted as fault-bounded by Seyrek et al. (2007) (it is thus marked

with dashed 'fault' ornament in their Fig. 3). However, farther SSW there are no landforms that can

plausibly be correlated with an in-line continuation of this fault; any continuation in that direction

(as well as any interpolation between the sites we have mentioned) is evidently obscured by the

pervasive colluvium and, farther SSW, by the alluvial fill along the axis of the Karasu Valley. Nonetheless, to the west of this line (c. site G in Fig. 14) a linear bluff oriented ~S30°W-S40°W has been interpreted by Yurtmen et al. (2002), Seyrek et al. (2007) and others as marking the active Güzelce Fault; this may link the Kızılyar Fault to the Amanos Fault at the western margin of the Karasu Valley in the Karacağıl-Kırıkhan area, as depicted schematically in Fig. 14. Any relief across such a fault is of course a consequence not of the predominant left-lateral slip but of the occurrence of a minor component of vertical slip, which is not necessarily present in all localities. Another possibility, first tentatively suggested by Rojay et al. (2001), is that a component of the active faulting continues SSW along the Karasu Valley interior to the Amik Basin. This possibility is depicted in Fig. 14 by inclusion of the Danaahmetli Fault, which we have named – again, to facilitate discussion – after a village in the area, circa BA 69372 46432. Karabacak and Altunel (2013) depicted active faulting along this line but offered no supporting evidence. One potential form of evidence that might demonstrate the existence of such a fault is the disposition of the Karasu Valley basalt; as indicated by the borehole evidence (Fig. 14) basalt is present in the subsurface along the eastern side of the southernmost Karasu Valley but not along its western side, raising the possibility that its emplacement has been constrained by relief along this fault line (cf. Fig. 8).

Figure 14 here: Schematic map of Amik Basin faulting
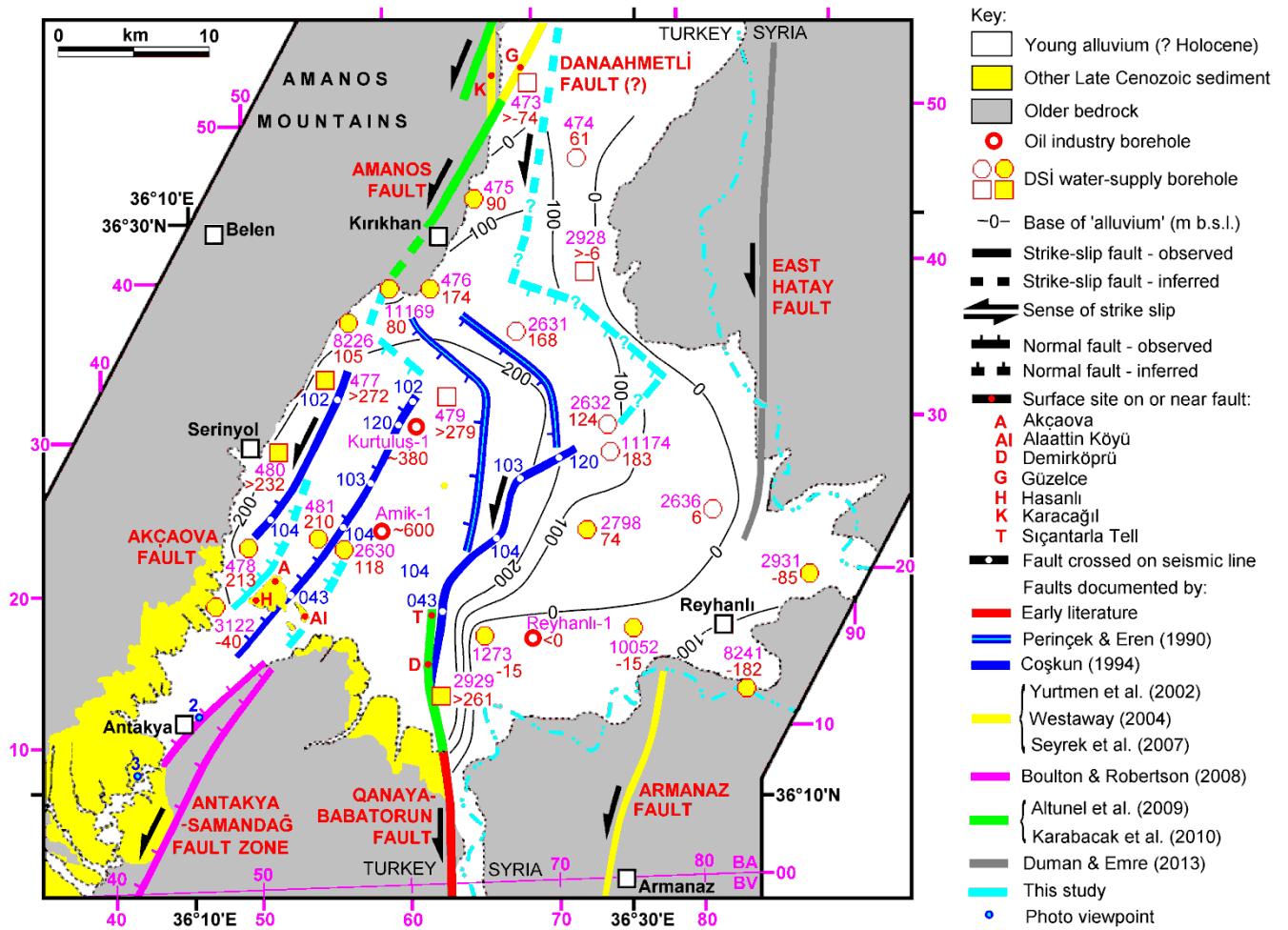
The closest basalt outcrop mapped by Atan (1969) on the WNW side of the inferred SSW continuation of the Kızılyar Fault, which may be the offset counterpart of the highly weathered basalt at our sampling site, is ~8 km SW of Aktepe (c. BA 71330 58730; M in Fig. 8; Atan's map of this area was re-published by Yurtmen et al., 2002, so is not repeated here). East of Atan's (1969) map area, outcrop of basalt persists to where we envisage the line of the Kızılyar Fault (N in Fig. 8; c. BA 72574 58323); the left-lateral offset thus apparent (H-N in Fig. 8) is ~9 km. The young basaltic volcanism in the Karasu Valley began circa 3 Ma (the oldest reported K-Ar date being ~2.7 Ma, from Çapan et al., 1987; see, also, the review of the geochronological evidence by Yurtmen et al., 2002). If this is the age of our 'highly weathered basalt' and its correct correlation, the subsequent time-averaged slip rate on the Kızılyar Fault has been ~3 mm a^{-1}, somewhat higher than the post-early

Middle Pleistocene estimate. However, shallow drilling (DSİ, 1975) indicates that basalt is much more extensive in the subsurface that at outcrop in the southern Karasu Valley; nonetheless, there is no information from such drilling on which to propose a unique counterpart on the WNW side of the Kızılyar Fault of our 'highly weathered basalt'. Likewise, no counterpart of the aforementioned outcrop of Eşmişek Formation has been mapped on the ESE side of this fault, which could also provide an indication of the total slip; any such counterpart is presumably buried beneath the Quaternary colluvium and basalt somewhere farther north.

We estimate the position of the southern margin of the Yünlü Tepe Basalt where it is cut off by the Amanos Fault as circa BA 74850 67450 (F in Figs 8 and 10) and also infer that the southern margin of the counterpart of this basalt in the Küreçi valley at the time of eruption as circa BA 73850 66050 (K in Figs 8 and 10). Both these estimates are difficult to ascertain precisely: the former due to limited exposure and the latter due to the fact that the Olucak River within the Küreci valley has subsequently incised around the southern margin of this basalt and the associated erosion may well have reduced the width of the basalt flow unit. As was noted by Seyrek et al. (2007), the northern edge of the basalt where cut off by the laft-lateral faulting at the mouth of the Küreçi valley is well defined (it is at BA 73872 66180; c in Fig. 10, some ~100 m west of the point – b in Fig. 10, circa BA 74000 66200 – where this cutoff was located by Atan, 1969) and can serve as a piercing point, but the northern edge of the basalt east of Yünlü Tepe (mapped by Atan, 1969, at a in Fig. 10, and c. BA 74900 67700) is less easy to establish, as already noted. We estimate, however, that the southern edge of the basalt at the mouth of the Küreci valley is ~130 m south of its northern edge, thus obtaining the co-ordinates of BA 73850 66050 (point K in Figs 8 and 10). The distance F-K is ~1720 m, whereas the distance a-c is ~1835 m, both offset measurements being oriented circa N35°E (UTM); averaging these values gives a 'best-estimate' of the slip on this part of the Amanos Fault since ~566 ka of ~1800 m, in agreement with the estimate by Seyrek et al. (2007). When added to the ~900 m of estimated slip on the Kızılyar Fault, gives a total slip of ~2700 m. We estimate the uncertainty in this

value (taking into account all the uncertainties in the measurements for both faults) as ±200 m (±2σ). Dividing 2700±200 m by 566±18 ka gives an estimate for the overall left-lateral slip rate, assuming the uncertainties in age and distance measurements are uncorrelated, of 4.77±0.38 mm a[-1] (±2σ); the overall azimuth of this relative motion is ~N30°E (UTM) or ~N28°E (geographical).

As Seyrek et al. (2007) discussed, after the earliest basalt in the Küreci valley 'escaped' across the Amanos Fault, later eruptions became ponded within this valley as the Yünlü Tepe ophiolite sliver became juxtaposed across the mouth of the valley due to the continuing left-lateral slip. The youngest part of this ponded basalt flow unit within the Küreci valley was dated by Yurtmen et al. (2002) to 325±14 ka (unspiked K-Ar; ±2σ) whereas basalt (from BA 74151 66226; point J in Figs 8 and 10) that is banked against the southern margin of the ophiolite sliver (thus representing the southern edge of the first flow unit after this outcrop of ophiolite cleared the valley mouth) was dated by Seyrek et al. (2007) to 385±13 ka (Ar-Ar; ±2σ). These two dates can be presumed to represent the same span of time, but differ due to some unknown source of systematic error affecting either or both dates. As Seyrek et al. (2007) noted, the Amanos Fault cuts the southern margin of the Küreci valley at point g in Fig. 10 (c. BA 73800 65600), which is ~700 m SSW of this basalt outcrop, indicating a ~700 m upper bound to the slip on the Amanos Fault since the basalt was emplaced, consistent with an associated time-averaged slip rate of ~2 mm a[-1]. However, the basalt on the southern side of this valley is inset below, and younger than, the thicker basalt on the north side of the valley and so was evidently emplaced at a later stage; this is confirmed by an date for the basalt close to river level at point e (BA 73857 65985) of 253±14 ka (unspiked K-Ar; ±2σ) (Yurtmen et al., 2002). As already noted, the southern edge of the thicker and older basalt on the north side of the Küreci valley is circa BA 73850 66050 (point K in Figs 8 and 10), and if the basalt at site J is restored to this point a left-lateral offset of ~350 m is indicated, consistent with a slip rate of ~1 mm a[-1], these estimates being lower bounds to the true offset and slip rate. The time-averaged slip rate on this part of the Amanos Fault since the eruption of this ~385 ka / ~325 ka basalt has thus

been somewhere within the range ~1-2 mm a^{-1}, rather less than the ~3 mm a^{-1} time-averaged rate

time-averaged since the eruption of the ~566 ka / ~533 ka basalt flow, during which the fault has

slipped by ~1800 m. Indeed, taking as the lower bound to the difference in age between these two

basalt flows 533 ka minus 385 ka or 148 thousand years, the ~1450 m of contemporaneous left-

lateral slip (the difference between the left-lateral offsets of ~1800 m for the Yünlü Tepe basalt and

~350 m for its younger counterpart) gives an estimated slip rate of ~10 mm a^{-1}, roughly equal to the

overall relative motion between the Turkish and Arabian plates (see above; section 2). Conversely,

taking this difference in age as flows 566 ka minus 325 ka or 241 thousand years, the slip rate

estimate decreases to ~5.6 mm a^{-1}, slightly more than the ~4.8 mm a^{-1} rate, time-averaged since 566

ka, for the Amanos and Kızılyar faults combined. These observations raise the possibility that

between ~566 and ~325 ka the Kızılyar Fault was not active in this locality and the transcurrent

component of plate motion was accommodated entirely on the Amanos Fault, whereas since ~325

ka the time-averaged slip rate on the Amanos Fault has been only ~1.1 mm a^{-1} (~350 m / ~325 ka)

with a slip rate of ~2.8 mm a^{-1} (~900 m / ~325 ka) on the Kızılyar Fault.

Furthermore, since the eruption of the 253±14 ka (±2σ) basalt in the Küreci valley floor, adjacent to

the present River Olucak and directly west of the Amanos Fault (at point f in Fig. 10), there has been

minimal fluvial downcutting and no obvious vertical or left-lateral fault offset (this locality is

illustrated in a field photograph taken from BA 73728 65812, point f in Fig. 10, by Seyrek et al.,

2007). We are thus led to infer that this fault has not been active here since this time, in which case

its most recent ~350 m of slip must have occurred between ~325 ka and ~253 ka at a rate of ~4.9

mm a^{-1}. During the most recent geological past the left-lateral faulting in this part of the Karasu

Valley might well thus have been accommodated only on the Kızılyar Fault. Dividing its 900±50 m of

post-Middle Pleistocene slip by the age of this basalt thus gives a slip rate on the Kızılyar Fault of

3.56±0.28 mm a^{-1} since 253±14 ka; the estimated ~1800 m of slip would then imply that the time-

averaged slip rate on the Amanos Fault between ~566 and ~253 ka had been ~5.8 mm a^{-1}. These

deductions are complicated further by the possibility of systematic errors in the basalt dates, as are evident from the mismatches already discussed for independent datings of what appear to be equivalent basalt flows, and other examples indicative of systematic error discussed by Seyrek et al. (2007). Nonetheless, the evidence suggests variations over time in the partitioning of left-lateral slip between different faults within the Karasu Valley and possibly also variations over time in the overall left-lateral slip rate. Duman and Emre (2013) have suggested that the less fresh morphology of the Amanos Fault compared with the East Hatay Fault suggests that recent slip has been concentrated on the latter. We deduce, instead, that in the Aktepe area the most recent slip has been concentrated on the Kızılyar Fault, within the Karasu Valley interior, rather than on the Amanos Fault at the western valley margin.

The Emre et al. (2012a) map of active faults in this part of Turkey depicts the geometry that we envisage for the splaying of the Kızılyar Fault from the Amanos Fault, but offers no indication as to the basis for this depiction which – to the best of our knowledge – has not been published before. The above summary of evidence indicates the basis for such an interpretation. The principal difference between their interpretation and ours is that they envisage the Kızılyar Fault as dying out ~3 km south of the splay point, roughly where it crosses the River Olucak (Fig. 8), whereas we infer that it is many kilometres longer.

Farther south, left-laterally offset basalt at the western margin of the Karasu Valley is also evident in the vicinity of Karacağıl (e.g., Parlak et al., 2001; Yurtmen et al., 2002; Seyrek et al., 2007). One strand of the Amanos Fault thus identified offsets ~428±14 ka (unspiked K-Ar; ±2σ) basalt by ~400 m and ~1 Ma basalt by ~1000 m, suggesting to Seyrek et al. (2007) a steady left-lateral slip rate of ~1 mm a^{-1}. On the other hand, if this fault segment became inactive circa 253 ka (see above), its slip rate between 428 and 253 ka would have been ~2.3 mm a^{-1}. Boulton (2013) has estimated that ~700 m of left-lateral slip has occurred at this locality since the ~428 ka basalt eruption; if so, the

subsequent time-averaged slip rate has been ~1.6 mm a^{-1}, and would have been ~4 mm a^{-1} if all this slip occurred between 428 ka and the inferred change in the geometry of faulting circa 253 ka. Karabacak et al. (2010) have suggested that another strand runs some 2 km farther west, being revealed by aligned left-laterally offset stream channels. However, none of these offsets are dated, so the slip rate on this lineation is unknown. Yurtmen et al. (2002) and Seyrek et al. (2007) also inferred that the aforementioned Güzelce Fault (at G in Fig. 14) splays NNE from the Amanos Fault near Karacağıl; as already noted, we envisage that at its NNE end this Güzelce Fault links into the Kızılyar Fault to the SSW of Aktepe.

North of the Yünlü Tepe area, Seyrek et al. (2007) noted three additional localities where they tentatively estimated slip rates of ~3 mm a^{-1} on the Amanos Fault, at Hassa, Kısık Tepe, and Hacılar, whereas our present analysis indicates somewhat higher slip rates north of the Kızılyar Fault splay: ~4.9 mm a^{-1}, time-averaged since ~556 ka, and ~4.5 mm a^{-1}, time-averaged since ~325 ka. The calculations for Hassa and Kısık Tepe divide measured offsets of basalt landforms by estimates, based on the available geochronological evidence, of the age of these landforms. However, in neither case was the youngest basalt in the vicinity dated, so (as Seyrek et al., 2007, indeed noted) the resulting slip calculations may well underestimate the true slip rate. We thus see no difficulty in reconciling the ~3 mm a^{-1} slip rate estimates obtained by Seyrek et al. (2007) with the higher rates suggested in the present study.

Conversely, at Hacılar the gorge of the Hacılar River was plugged by several tens of metres of basalt, which Seyrek et al. (2007) dated to 159±15 ka (Ar-Ar; ±2σ), superseding an 80±100 ka (spiked K-Ar; ±2σ) date for the same basalt by Rojay et al. (2001); the river subsequently incised through this basalt and its gorge has since become offset left-laterally by a distance that Seyrek et al. (2007) measured as 450±25 m and Karabacak et al. (2010) re-measured as ~430 m. Seyrek et al. (2007) thus estimated the local left-lateral slip rate on the Amanos Fault as ~450 m / ~159 ka or ~2.8 mm a^{-1}.

However, this calculation does not take into account the time required for this small river to re-incise through the basalt; the present-day offset of this gorge only reflects the slip since the river cut down through the basalt and its gorge has become 'locked' in the resistant rock. Farther downstream near Aktepe, just before its confluence with the larger Hopur River, the Hacılar River cuts through another basalt flow unit, which flowed SW from the nearby Aktepe volcanic neck, (Fig. 8). The basalt from this neck was dated to 260±80 ka (±2σ), ka (at site I in Fig. 8; c. BA 76420 64850) by Rojay et al. (2001), making it probably somewhat older than the basalt at Hacılar. The course of the Hacılar River was evidently blocked by this Aktepe basalt flow and the requirement for it to cut down into this basalt may have delayed the start of its incision into the Hacılar basalt flow farther upstream. For these various reasons the slip rate estimated by Seyrek et al. (2007) from the offset of the gorge at Hacılar should be regarded as a minimum. Nonetheless, if this estimate of ~2.8 mm a^{-1} is not a serious underestimation in might be a further reflection of the reduction in slip rate evident from our analysis of the disposition of basalt flows in the Küreci valley (see above), being in approximate agreement with our estimate of ~3.6 mm a^{-1} for the slip rate on the Kızılyar Fault, taking all of its most recent ~900 m of slip to have occurred since ~253 ka. Thus, ~450 m of slip on this fault at a time-averaged rate of ~2.8 mm a^{-1} since ~159 ka may have been preceded by ~450 m of slip at a time-averaged rate of ~4.8 mm a^{-1} between ~253 ka and ~159 ka.

6. The Amik Basin

The Amik Basin adjoins the SSW end of the Karasu Valley and the northern end of the DSFZ (Figs 1. 14). Past interpretations of this area have been extremely diverse; early studies (e.g., Perinçek and Çemen, 1990) envisaged this basin and the adjoining Karasu Valley as a graben, which they called the 'Hatay Graben' or 'Hatay Karasu Graben'. Subsequently, many authors have envisaged this basin as marking a leftward step in the left-lateral faulting as it transfers from the Amanos Fault onto the Qanaya-Babatorun Fault, a point of view that has hitherto been adopted in our own publications (e.g., Yurtmen et al., 2002; Westaway, 2003, 2004; Seyrek et al., 2007). Others (e.g., Reilinger et al.,

2006; Boulton and Robertson, 2008; Boulton, 2013) have envisaged it as marking a southward splay of the left-lateral faulting along the Karasu Valley into two zones of deformation, one heading southward to the DSFZ and the other (which we call the ASFZ; section 3) heading southwestward through Antakya before continuing offshore. Finally, Karabacak et al. (2010) and Karabacak and Altunel (2013) have proposed that the principal fault in the area is a left-lateral fault that heads SSW along the Karasu Valley interior (in roughly the location we now envisage for the Danaahmetli Fault; Fig. 14) before continuing in-line onto the Qanaya-Babatorun Fault, with no leftward step and no transfer of any component of relative motion onto faults that continue to the southwest. Furthermore, in their view the Amik Basin depocentre is a relic of an earlier phase of deformation, the eastern and western halves of which have been translocated by the most recent phase of left-lateral slip, rather than an actively-developing sedimentary basin. The GPS data suggest that the Amik Basin currently accommodates ~5 mm a^{-1} of left-lateral slip and ~2 mm a^{-1} of extension (vectors ULUC-HOWR and ULUC-HARM in Table 1, with calculations assuming a nominal N35^{o}E orientation of the basin; although given the location of point HARM in Fig. 1 the ULUC-HARM vector may understate any contribution from slip on the Armanaz Fault / East Hatay Fault).

Perinçek and Çemen (1990) and Perinçek and Eren (1990) justified their interpretation on the basis of seismic reflection evidence that they interpreted in terms of major normal faults with downthrow to the WNW beneath the Amik Basin, with thick 'Plio-Quaternary' sedimentary successions in their hanging-walls (Fig. 15); they were unspecific as to the timing of this component of extension, but the logic underlying their interpretation required it to be active at present. However, Coşkun (1994) and Coşkun and Coşkun (2000) reinterpreted the same seismic dataset very differently (Fig. 16); in their view the lateral variations in thickness of Cenozoic sediment beneath the Amik Basin were primarily due to irregular post-emplacement relief of the surface of the Hatay Ophiolite, subsequently modified by effects of crustal shortening during the Cenozoic convergence phase. During this phase this relief was infilled and buried by Cenozoic marine sediment; this carbonate-dominated

succession is overlain by clastic marine sediments, known as the Samandağ Formation, which represent the marine re-flooding of the area in the Early Pliocene following the MSC (e.g., Boulton et al., 2007). These marine sediments give way later in the Pliocene to fluvial and lacustrine sediments in the basin interior, interbedded with basalt flows and colluvial input near its margins, emplacement of which has continued to the present day (e.g., Bridgland et al., 2012). Until it was artificially drained in the twentieth century, this was indeed an active fluvio-lacustrine depocentre (e.g., Kiliç et al., 2006; Çalışkan, 2008; Ozelkan et al., 2011; Bridgland et al., 2012), the sediments being dominated by silt or sandy silt in the basin interior, giving way to coarser alluvial fan deposits near the basin margins (e.g., Rojay et al., 2001).
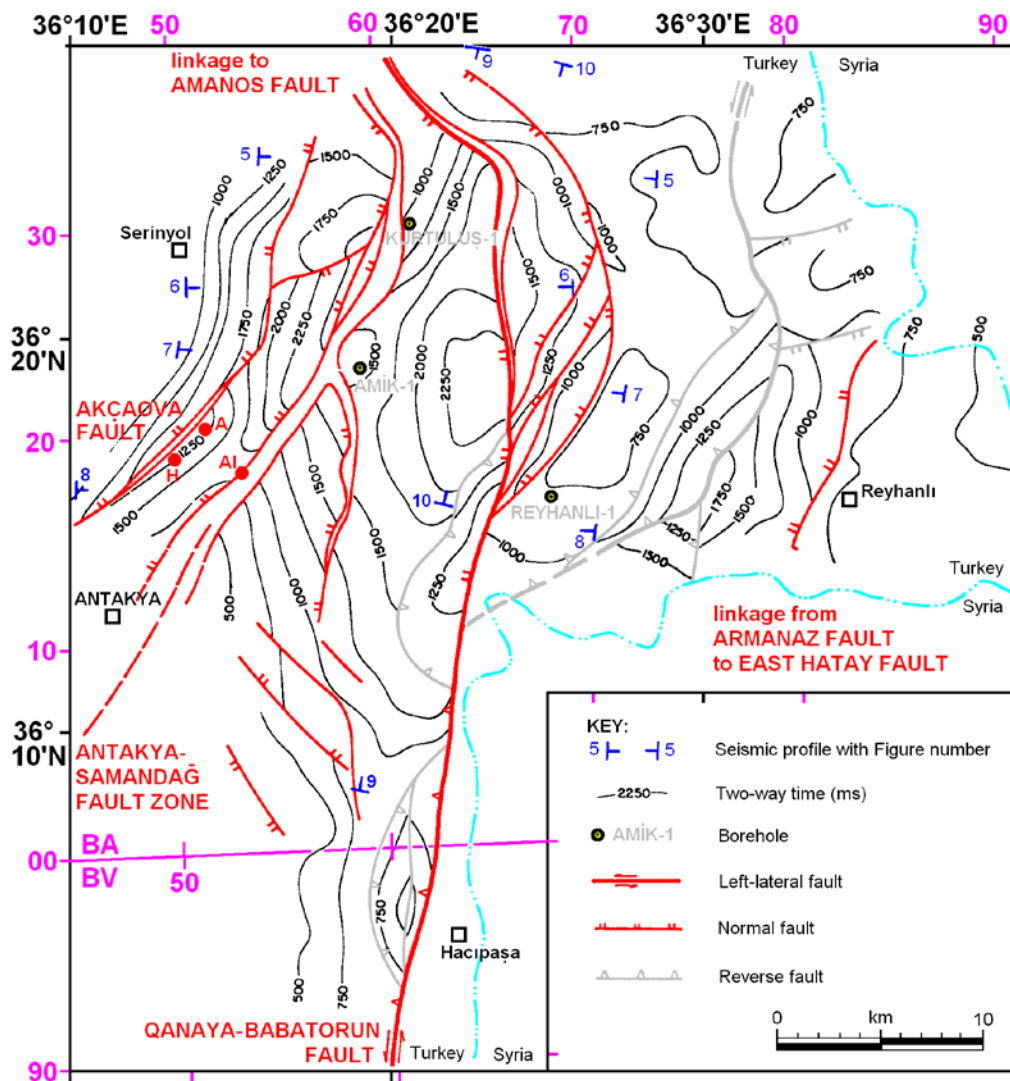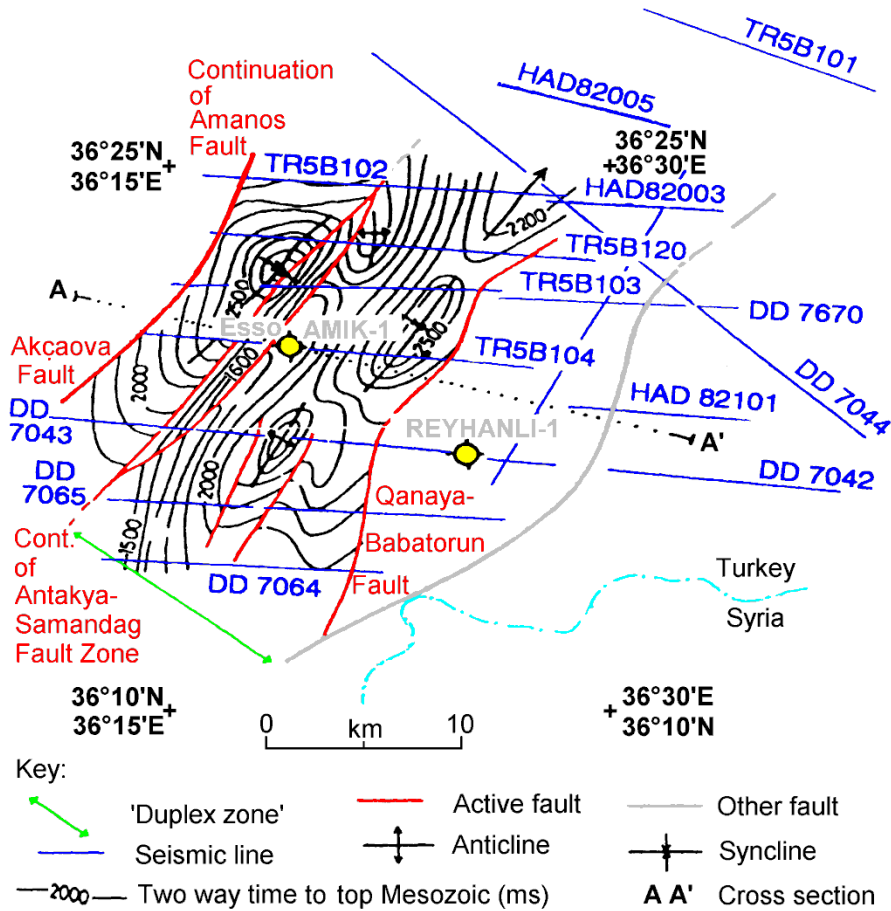
Fig. 15

Fig. 16

The disposition of the sedimentary fill within the Amik Basin has been determined using many water-supply boreholes (DSİ, 1975); results of this study are summarised in Fig. 14, this dataset having also previously been utilised by Rojay et al. (2001), Yurtmen et al. (2002) and Karabacak et al. (2010). The thickness of this sedimentary fill was thus shown to exceed 360 m in boreholes that did not reach any older rocks (Fig. 14); its thickness generally increases towards the centre of the Amik Basin but shows abrupt variations indicative of intra-basinal dip-slip faulting (Rojay et al., 2001). However, the dataset is not logged in great detail and includes no geochronological evidence, which has caused uncertainty as to what timescale is actually represented. Thus, Rojay et al. (2001) variously referred to this sediment as 'Quaternary' or 'Plio-Quaternary' and seem to have regarded the start of its emplacement as following the end of the Early Pliocene marine inundation. On the

other hand, Karabacak et al. (2010) considered this sediment to be Quaternary, inferring an age of 1.6 Ma for its base from a nominal age for the start of the Pleistocene and, furthermore, envisaging it as overlying Pliocene lacustrine sediment, even though in the original DSİ (1975) dataset the succession was depicted as overlying 'pre-Pliocene basement'. Also, the interpreted shape of the Amik Basin changes significantly from that depicted by Karabacak et al. (2010) if boreholes that did not reach the base of the 'Plio-Quaternary' sediment are included and if the boreholes are plotted at their published co-ordinates, as has been done in Fig. 14; Karabacak et al. (2010) neither noted nor explained why many of these boreholes were plotted kilometres away from these published co-ordinates and also at different sites from where Rojay et al. (2001) had previously plotted them. In addition, the seismic reflection dataset of Coşkun and Coşkun (2000) depicted marine limestone of the Teknepınar Formation (Middle Miocene; now known as the Sofular Formation; Boulton et al., 2007) at two-way times of ~0.2-0.3 s beneath the central part of the basin, which would imply (assuming a seismic velocity of 1700 m s^{-1}, after Hall et al., 2005) upper bounds to the Plio-Pleistocene sediment thickness of less than 200-300 m (i.e., less than the thicknesses indicated in many of the DSİ boreholes; Fig. 14). On the other hand, Perinçek and Çemen (1990) and Perinçek and Eren (1990) interpreted the seismic reflection dataset for the same area (Fig. 15) in terms of dramatic lateral variations in the thickness of the 'Plio-Quaternary' succession; in their view this varies in the basin interior between ~1.5 and ~0.3 s two-way time, or between ~1300 and ~250 m, between sites in hanging-walls and in footwalls of normal faults (Fig. 15). Perinçek and Eren (1990) reported the thickness of this succession as 465 m in the Kurtuluş-1 borehole, placing its base ~380 m below sea-level, and depicted it at a two-way time of ~0.8 s in the Amik-1 borehole, corresponding to a base ~600 m below sea-level, although noting that the this deposit was much thinner (<50 m thick) in the Reyhanlı-1 borehole near the SE margin of the basin (Fig. 14). Assuming this sedimentation began at ~3.6 Ma, the ~250-1300 m thickness indicates time-averaged deposition rates between ~0.07 and ~0.36 mm a^{-1}.

To shed light on the geometry of the active strike-slip faulting beneath the Amik Basin, in particular the location of the northward continuation of the Qanaya-Babatorum Fault, we have revisited the seismic reflection dataset for the area. Only the Perinçek and Eren (1990) and Coşkun (1994) interpretations provide accurate locations of seismic lines and borehole control (Figs 15 and 16). However, both Coşkun (1994) and Coşkun and Coşkun (2000) report west-east or WNW-ESE oriented seismic sections that show a SW-NE- or SSW-NNE-trending bedrock high, formed in the Hatay Ophiolite, penetrated by the Amik-1 borehole. The DSFZ (i.e., the Qanaya-Babatorun Fault) was thus envisaged as forming a flower structure within the thicker Cenozoic succession to the east, its main strand being interpreted as passing ~6 km ESE of the borehole with the southern end of the Amanos Fault roughly the same distance WNW of the same borehole (Fig. 14). The Amik-1 borehole is located at 36°19'24.4''N 36°19'11.3''E (Hemer et al., 1988), which corresponds to UTM co-ordinates BA 59404 23159. Seismic line TR5B104, which passes through this borehole, is oriented at an azimuth of S85°E (geographical) or S87°E (UTM), and crosses the Qanaya-Babatorun Fault at a distance of ~8.2 km (Fig. 14). The co-ordinates of this crossing point, near which the structural trend in the bedrock is circa S40°W-N40°E, can thus be determined as circa BA 67540 22160. The Qanaya-Babatorun Fault was traced northward to this point from Demirköprü at the southern edge of the basin by Altunel et al. (2009), this fault transects Sıçantarla Tell circa BA 62590 17990 (~3 km north of Demirköprü, circa BA 62500 15000) where its trend is N-S. The point where the Qanaya-Babatorun Fault crosses the seismic line through the Amik-1 borehole is thus ~6.5 km northeast of this tell, suggesting that (rather than continuing northward across the basin, as proposed by Karabacak and Altunel, 2013) this fault swings to a northeastward orientation a short distance north of the tell, as it enters the region with very strong SW-NE structural fabric inherited from the ophiolite obduction and Cenozoic crustal shortening (Fig. 16). Similar calculations enable determination of the points where other seismic lines in Fig. 16 cross the Qanaya-Babatorun and Amanos faults; these, too, have been plotted on Fig. 14.

Conversely, the interpretation of the seismic data by Perinçek and Eren (1990) (Fig. 15) depicts greater complexity, despite being noncommittal as to the age of any of the faulting. We have therefore ornamented Fig. 15 to emphasize those faults that appear (from deformation of sediments depicted in the seismic sections) to have been active during the present phase of deformation, guided by the fact (evident from earlier discussion) that normal faulting would not be expected in this area prior to the present phase of deformation (or the LMMP phase, if any faults in the area had significant slip rates then; cf. section 2). This dataset thus suggests that the ASFZ continues northeastward or NNE beneath the western Amik Basin before stepping to the left, apparently linking to the Amanos Fault near Kırıkhan (Fig. 14). Likewise, the Qanaya-Babatorun Fault continues NNE beneath the central Amik Basin, seemingly splaying into several strands, before also stepping leftward to link to the Amanos Fault near Kırıkhan. Farther east, another fault strand depicted in Fig. 15 appears to link the Armanaz Fault with the East Hatay Fault (Fig. 14), but was not illustrated by any of the seismic sections reported by Perinçek and Eren (1990).

Although the Perinçek and Eren (1990) (Fig. 15) and Coşkun (1994) (Fig. 16) interpretations of the Amik Basin differ markedly, regarding details such as the thickness variations of the 'Plio-Quaternary' sediment and the magnitude of components of normal slip on faults within the basin, they have sufficient points in common to indicate the overall geometry of the basin. One difference is that active faulting persists farther northeast in the Coşkun (1994) scheme than in the Perinçek and Eren (1990) version; this continuation of the faulting may account for abrupt variations in the thickness of the 'Plio-Quaternary' sediment in this part of the basin (boreholes 2632 and 11174; Fig. 14). Rojay et al (2001) noted evidence of a SW-dipping active normal fault at the NE margin of the basin in a position consistent with linkage between this faulting and the southern end of the Danaahmetli Fault; this linkage is tentatively depicted in Fig. 14, but it appears that most of the active deformation has been concentrated west of this line. None of the seismic evidence supports the suggestion (Karabacak and Altunel, 2013) that the Qanaya-Babatorun Fault links end-on, north of the

Amik Basin, with a fault in the position of our Danaahmetli Fault. On the contrary, the evidence supports the view that the Amik Basin is associated with a leftward step in the faulting; it can thus be validly classified as a pull-apart basin. Moreover, this leftward step coincides with the part of the Amik Basin with relatively thick Pleistocene sediment (Fig. 14), indicating that the deposition of this sediment has accompanied localised subsidence, presumably reflecting in part the local sediment loading and in part the local component of active extension. Furthermore, maps of palaeo-environments prior to the Amik Basin being drained in the mid twentieth century (published, for example, by Yener et al., 2000; Çalışkan, 2008; Eger, 2011; and Bridgland et al., 2012) show lacustrine and wetland environments in roughly the same location as this leftward step in the faulting, confirming the proposed causal connection between surface environments and active crustal deformation.

In the SW Amik Basin around Alaattin Köyü (Fig. 14) an inlier of older sediment rises above the general ~85 m a.s.l. surface of the Holocene alluvial plain to a maximum height of 159 m a.s.l. This outcrop was mapped as Pliocene marine deposits by Tolun and Erentöz (1962), implying that it forms part of the aforementioned Samandağ Formation. The sediments have since been mapped as marine limestone of Middle Miocene age (e.g., Boulton et al., 2007; Boulton and Whittaker, 2009); quarry exposures reveal, however, that they consist of laminated sands and silts that Bridgland et al. (2012) regarded as of fluvio-lacustrine origin. In one quarry exposure (at BA 52626 16772) the shell of a large gastropod that resembled *Apamaeus apamea* (known from the Pleistocene of the Ghab and Hula basins; Bridgland et al., 2012), was observed, but disintegrated before definitive identification was possible. The residue of the sample, sieved with a 500 μm mesh, has yielded ostracods, other molluscan material, fish teeth and otoliths, and oogonia of charophytes (non-marine aquatic plants), but no evidence of any marine detritus (e.g., barnacle plates, foraminifera, or marine ostracods). The ostracod remains include very abundant carapaces of *Cyprideis torosa*, all of which are smooth, and small numbers of other freshwater taxa; the molluscs include abundant

shells of the small brackish-water gastropod *Hydrobia acuta*, indeterminate shell fragments, and opercula of the gastropod *Bithynia* sp. The assemblage is similar to others documented in the Karkour area of the Ghab Basin by Bridgland et al. (2012) and in that locality is indicative of a brackish lake. *Apamaeus apamea* lived in the Hula Basin between circa MIS 21 and MIS 7 (or ~850-200 ka) according to the synthesis of evidence by Bridgland et al. (2012); pending definitive confirmation of the presence of this taxon, an age within this time span (i.e., latest Early Pleistocene to late Middle Pleistocene) is therefore tentatively inferred for the deposit at Alaattin Köyü. The salinity of the water in which these sediments were deposited is constrained because the lower bound for whole populations of *C. torosa* to develop with smooth carapaces (~7‰ according to Frenzel et al., 2012) is similar to the upper bound for survival of *Bithynia*. The common European species *B. tentaculata* is normally considered unable to tolerate salinity beyond ~6-7‰ (e.g., Järvekülg, 1979), although it has been reported in a brackish lake in Croatia where the salinity reaches ~8‰ (Beran et al., 2013). However, a different, eastern Mediterranean, species, *B. phialensis*, lives at present in the Amik Basin (Şereflişan et al., 2009), although other taxa are found elsewhere in Turkey (e.g., Yıldırım, 1999; Glöer and Yıldırım, 2006) and in the Orontes catchment in Syria and Lebanon (e.g., Schütt, 1983; Bössneck, 2011; Glöer et al., 2012). Although the *Bithynia* opercula from Alaattin Köyü are not identified to species level, *B. phialensis* has been reported in an estuary in Israel that intermittently experiences salinity up to 8.5‰ (Reinhardt et al., 2003). Taking all the evidence into account, we envisage that when these sediments were laid down the Amik Basin contained a brackish lake, rather than forming an estuary (and certainly not a marine depocentre), presumably with an outlet to the sea via an ancestral lower Orontes valley.

Several authors (e.g., Rojay et al., 2001; Bridgland et al., 2012; Emre et al., 2012a) have suggested that the Alaattin Köyü inlier might be locally uplifted in the footwall of a NE-dipping normal fault. However, the highest topography in this inlier adjoins its NW margin, which forms a linear escarpment oriented NE-SW that is ~3 km long and up to ~75 m high, between the villages of

Akçaova (c. BA 51314 19563) and Hasanlı (c. BA 49560 18715). Moreover, the location of this escarpment is consistent with the footwall of one of the faults recognised on the seismic profiles (Figs 16, 15), which is evidently an oblique normal fault; we name this the Akçaova Fault. Around Akçaova this fault has a throw of ~500 ms two-way time from the offset of the Miocene horizon depicted in Fig. 15, which equates to ~400 m assuming the difference in travel time is due to variable thickness of the 'Plio-Quaternary' sediment with a seismic velocity of ~1.7 km s^{-1}. The local record indicates a switch from deposition to localised uplift, which suggests that the Akçaova Fault has not been active with its present slip sense throughout the present phase of deformation, but instead became active (or developed a component of normal slip) at a relatively late stage. A minimum age for the onset of its normal slip can be determined if all the ~2 mm a^{-1} of extension across the Amik Basin, measured geodetically (Table 1), is assumed to be accommodated on this fault; if the fault is assumed to dip at 45° then its ~400 m of estimated heave implies an age of ~200 ka (~400 m / ~2 mm a^{-1}). An age in the latest Early Pleistocene or earlier Middle Pleistocene for the sediments exposed in the footwall of the Akçaova Fault is thus tenable, even if only a small proportion of the extension across the Amik Basin is accommodated on this fault. Conversely, the northeastward continuation of the ASFZ passes near Alaattin Köyü, ~3 km SE of the Akçaova Fault (Fig. 15); although it has much more throw (~1000 ms two-way time, or ~900 m) is has no clear expression in the local landscape in this vicinity (unlike farther SW; Figs 2, 3). Likewise, the main strand of the northward continuation of the Qanaya-Babatorun Fault has downthrow to the west of up to (~1000 ms two-way time, or ~900 m (Fig. 15). Assuming 45° dips for these normal fault segments, some ~2200 m (i.e., 400 m + 900 m + 900 m) of total heave (i.e., extension) can be estimated on these faults, which indicates a time-averaged extension rate since ~3.6 Ma of ~0.6 mm a^{-1}, much less than the rate expected geodetically (Table 1).

In addition to geological investigations, the Amik Basin been the subject of archaeological studies (e.g., Wilkinson, 1997; Yener and Wilkinson, 1999; Yener et al., 2000; Wilkinson et al., 2001; Yener,

2005; Casana, 2008; Eger, 2011), which demonstrate significant human alteration of the environment in antiquity. Thus, although lakes had developed in this basin in the Early Holocene, the large 'Lake of Antioch' that existed from the first millennium B.C. onward appears to have formed because human activity (agriculture and mining) destabilised hillslopes causing large fluxes of sediment into the basin, which raised the land surface near its margins, blocking the former outlet of the combined Karasu and Afrin rivers and inundating the basin interior. The effect of mining of the Hatay ophiolite is evident from chromium and nickel contamination of the sediments (e.g., Friedman et al., 2000), whereas the general magnitude of slope processes is evident from the depths of up to 6 m by which older features, including archaeological sites and the former land surface, have been buried (e.g., Yener et al., 2000; Casana, 2008). The former outlet of the combined Karasu and Afrin rivers was located in the hanging-wall of the Akçaova Fault (Fig. 14) and evidently became blocked by alluvial fans emanating from the Amanos Mountains ~5 km farther northwest. During antiquity, like at present, the River Orontes flowed SE of the uplifted footwall block beside the Akçaova Fault, along the line of the ASFZ (Fig. 14), although it is known to have avulsed when in flood into the 'Lake of Antioch' farther north, this intermittent flooding evidently contributing to sustaining the lake, as beds of sand (of Orontes provenence) are interbedded with the lacustrine silt at some sites within the former lake basin (e.g., Yener et al., 2000; Eger, 2011). In contrast, the present course of the Orontes is quite stable, having become entrenched up to ~10 m below the land surface in the southern Amik Basin (Bridgland et al., 2012), possibly in response to the downstream shortening of its channel that has resulted in recent decades from its canalization through the centre of Antakya. The lacustrine silts of recent millennia were emplaced at typical rates of ~0.5 mm a^{-1} and give way below depths of several metres to fluvial sands (e.g., Yener et al., 2000), which indicate that no lake existed in the Amik Basin immediately beforehand. Thus, although the 'Lake of Antioch' roughly delinated the relatively deep part of the Amik Basin with significant rates of sedimentation and subsidence, it reflected an artificially modified environment, rather than indicating the depocentre in its natural state.

Overall, we conclude that the Amik Basin is a pull-apart basin located at a leftward step in left-lateral transtensional faulting where this faulting splays from the KVFZ to the ASFZ and northern DSFZ. This basin receives fluvial sediment from a large surrounding region and is, in effect, a sediment trap; the loading effect of this sediment evidently combines with the isostatic adjustment to the crustal thinning that accompanies the local component of extension to cause subsidence that persists well outside the zone where the active faulting has been concentrated, creating a depocentre of unusual shape that has no doubt hindered interpretation. Although the basin has a drainage outlet, via the lower River Orontes, uplift is occurring at a significant rate in this reach, contributing to the development of the sediment trap farther upstream; as Bridgland et al. (2012) noted, the vertical crustal motions in this region are not explicable solely in terms of plate motions but also reflect contributions from isostatic effects of surface processes.

7. Discussion

The present analysis indicates that the relative motion between the Turkish and Arabian plates is partitioned in a quite complex and time-dependent manner between the individual active faults within this deforming zone (Fig. 1). Like Duman and Emre (2013), we envisage that maybe two thirds of the relative plate motion, say ~6-7 mm a^{-1}, occurs on the KVFZ. The other third, or ~3-4 mm a^{-1}, occurs farther NW on the MKFZ; a substantial part of this, maybe ~1 mm a^{-1}, seems to splay onto the Karataş and Yumurtalık Faults before stepping leftward via the extension across the Düziçi-Osmaniye Fault; the remainder, some 2-3 mm a^{-1}, as envisaged by Westaway (2004), appears to continue northeastward on other strands of the SMFZ (Fig. 1). As regards nomenclature, we agree with Duman and Emre (2013) that the whole of this deforming zone north of the Turkish coastline near Karataş (i.e., the SMFZ) and north of the Amik Basin in Hatay (i.e., the KVFZ) should be considered as the SW part of the East Anatolian Fault Zone, reflecting its location at the boundary zone between the Turkish and Arabian plates. In the Karasu Valley, our best estimate of the left-lateral slip rate on

the East Hatay Fault is ~2.5 mm a^{-1}, but this is derived only from a relatively short timescale (post-latest Pleistocene) offset. The bulk of the left-lateral relative motion, some 4-5 mm a^{-1}, is accommodated on fault segments at the western margin of the Karasu Valley and in the valley interior, including the newly-recognised Kızılyar Fault. We estimate that ~1-2 mm a^{-1} of this left-lateral slip steps leftward across the NE Amik Basin onto the Qanaya-Babatorun Fault; the remainder, some 3-5 mm a^{-1}, steps leftward across the SW Amik Basin onto the ASFZ (Fig. 14). The latter component of left-lateral slip passes southwestward onto the RRFZ, then is partitioned between the Larnaca Ridge and Latakia Ridge, with maybe 1.5 mm a^{-1} of this motion taken up on the LTFZ (Fig. 1) and thus passed into the southern DSFZ.

We thus envisage that the ~5 mm a^{-1} left-lateral slip rate on the southern DSFZ is partitioned farther north with maybe ~0.5 mm a^{-1} of slip 'absorbed' by oblique extension on the Carmel Fault in northern Israel (Table 1; cf. Sadeh et al., 2012) and ~1 mm a^{-1} 'absorbed' by the oblique crustal shortening in the western part of the Palmyra Fold Belt in Syria (Abou Romieh et al., 2009, 2012; Alchalbi et al., 2010), leaving ~3.5 mm a^{-1}, accommodated maybe at ~2 mm a^{-1} on the onshore northern DSFZ and ~1.5 mm a^{-1} transferred via the Roum Fault onto the LTFZ. However, the Carmel Fault crosses the coastline near Haifa in the extreme north of Israel; the nature of its northward continuation, offshore of Lebanon, is unclear. Conceivably, it may also link northward into the LTFZ, making the slip rate on that higher (~2 mm a^{-1}), comparable to the slip rate on the onshore northern DSFZ (compare the relative motions between GPS points in western Syria and those north and south of the Carmel Fault in northern Israel; Table 1). The component of left-lateral slip on the LTFZ is thus the principal reason why the slip rate on the northern DSFZ is rather less than that on the southern DSFZ (cf. Alchalbi et al., 2010; ArRajehi et al., 2010).

In some parts of this deforming zone it is now possible to see how the expected relative motion has been accommodated on individual faults. Notably, we have shown for the first time how the ~5 mm

a^{-1} of left-lateral slip expected across the interior and western margin of the Karasu Valley in the vicinity of Aktepe has been accommodated on the Amanos and Kızılyar faults. However, the available evidence cannot account for more than ~3 mm a^{-1} of this slip during the Late Pleistocene; evidently, either the slip rate on the East Hatay Fault has increased on this time scale to balance a decrease in the slip rate on these other faults or one or more additional active left-lateral faults remains to be discovered. Likewise, the left-lateral slip rate now envisaged on the ASFZ requires some 14-18 km (~4-5 mm a^{-1} x 3.6 Ma) of left-lateral slip to have occurred during the present phase of deformation. However, there is no indication that the various faults currently recognised have accommodated anything like this much relative motion. Furthermore, restoration of slip of this magnitude in the reference frame of the block to the southeast would place the city centre of Antakya in the western part of the Amik Basin interior, raising the possibility that this component of crustal motion has caused a significant change in the shape of this part of the study region. On the other hand, it is possible that much of this relative motion has been accommodated by distributed deformation (or slip on many smaller-scale faults than those considered in this study; cf. Boulton and Robertson, 2008) rather than on the limited number of major faults recognised; the Antakya area indeed experiences frequent moderate-sized earthquakes (magnitudes ~4-5; e.g., Ergin et al., 2004), consistent with slip on relatively minor structures, but has not experienced a major earthquake for centuries. Likewise, notwithstanding the recognition of the Düziçi-Osmaniye Fault (Figs 1 and 7), the known normal faults within and adjoining the Amanos Mountains are insufficient to account for the several millimetres per year of extension that is predicted from the GPS data (Table 1). Here, too, evidently either more as-yet-unrecognised active normal faults exist or distributed extension (or slip on large numbers of mesoscale faults) is significant.

Many workers have attempted to relate active faults in the study region to known historical earthquakes, the most thorough analysis of this type being by Duman and Emre (2013). Direct confirmation by palaeoseismic studies is, however, relatively limited attempt; notable examples

being by Akyuz et al. (2006) on the Qanaya-Babatorun Fault and by Emre et al. (2009) on the northward continuation of this fault into the southern Amik Basin. There are nonetheless many active (or potentially active) fault segments in the region on which the timing of the last significant earthquake is essentially unknown; hence the debate, for example, as to whether the long interval since any large earthquake on the fault at St Peter's Church in Antakya (Fig. 2) indicates inactivity or highlights a 'seismic gap' potentially indicative of imminent recurrence. Several of the active faults newly recognised or re-emphasised in the present study, such as the Düziçi-Osmaniye, Kızılyar and Akçaova faults, are of large enough dimensions that they may potentially rupture in damaging earthquakes, and warrant more thorough investigation. Pending detailed documentation of every active or potentially active fault in the region, integration of diverse geodetic and geological data, as is attempted in the present study, can bear upon the assessment of earthquake hazard by determining slip rates on known faults and suggesting sites of suspected active faulting.

8. Conclusions

A great deal of new information has developed in recent years regarding senses and rates of crustal deformation in the boundary zone between the Turkish, African and Arabian plates in central-southern Turkey, NW Syria, and adjacent offshore areas. This study has set out to synthesize this evidence, attempting to resolve some of the contradictory interpretations of key localities by different teams, along with new investigations targeted at key areas of uncertainty. We have thus identified or inferred some hitherto unrecognised active faults and have clarified the roles of other structures within the framework of plate motions provided by the GPS studies. As suggested by Duman and Emre (2013), roughly one third of the relative motion between the Turkish and Arabian plates is accommodated on the Misis-Kyrenia Fault Zone, which links to the region from the Kyrenia mountain range of northern Cyprus, and farther northeast on the Sürgü-Misis Fault Zone. Much of this motion passes NNE then eastward around the northern limit of the Amanos Mountains, as previously thought (e.g., Westaway, 2004), but some of it splays northeastward to link into newly-

recognized normal faulting within the Amanos Mountains. The remaining two thirds of the relative motion is accommodated by the Karasu Valley Fault Zone; some of this component steps leftward across the Amik Basin before passing southward onto the northern Dead Sea Fault Zone but much of it continues southwestward past the city of Antakya (as suggested, for example, by Boulton and Robertson, 2008), then onto offshore structures, ultimately linking to the subduction zone bounding the Turkish and African plates to the southwest of Cyprus. However, some of this offshore component of motion splays southward and continues west of the Syrian coast before linking onshore into the southern DSFZ (as suggested by Trifonov et al., 2011), this component of relative motion being the main reason why the slip rate on the northern DSFZ, measured geodetically, is so much lower than that on its southern counterpart. In some parts of this region, notably in the Karasu Valley, it is now clear how the expected relative plate motion has been accommodated on active faults during much of the Quaternary; quite complex changes in the partitioning of this motion on timescales of hundreds of thousands of years are indicated by offsets of dated Pleistocene basalt flows, rather than constant slip rates on individual faults. However, in other parts of the region it remains unclear whether additional major active faults remain unrecognised or whether significant relative motions are accommodated by distributed deformation or on large numbers of smaller-scale structures.

References
Abou Romieh, M., Westaway, R., Daoud, M., Radwan Y., Yassminh, R., Khalil, A., al-Ashkar, A., Loughlin, S., Arrell, K., Bridgland, D., 2009. Active crustal shortening in NE Syria revealed by deformed terraces of the River Euphrates. Terra Nova 27, 427–437.

Abou Romieh, M., Westaway, R., Daoud, M., Bridgland, D.R., 2012. First indications of high slip rates on active reverse faults NW of Damascus, Syria, from observations of deformed Quaternary sediments: Implications for the partitioning of crustal deformation in the Middle Eastern region. Tectonophysics 538–540, 86–104.

Akın, Ç, Bilgin, C.C., Beerli, P., Westaway, R., Ohst, T., Litvinchuk, S.N., Uzzell, T., Bilgin, M., Hotz, H., Guex, G.-D., Plötner, J., 2010. Phylogeographic patterns of genetic diversity in eastern

Mediterranean water frogs have been determined by geological processes and climate change in the Late Cenozoic. Journal of Biogeography, doi: 10.1111\j.1365-2699.2010.02368.x, 14 pp.

Aktar, M., Ergin, M., Özalaybey, S., Tapirdamaz, C., 2000. A lower-crustal event in the northeastern Mediterranean: the 1998 Adana Earthquake (M_w=6.2) and its aftershocks. Geophysical Research Letters, 27, 2361–2364.

Aksu, A.E., Calon, T.J., Hall, J., Yaşar, D., 2005. Origin and evolution of the Neogene İskenderun Basin, northeastern Mediterranean Sea. Marine Geology, 221, 161-187.

Aksu, A.E., Calon, T.J., Piper, D.J.W., Turgut, S., Izdar, E.K., 1992. Architecture of late orogenic basins in the eastern Mediterranean Sea. Tectonophysics 210, 191– 213.

Aktaş, G., Robertson, A.H.F., 1984. The Maden Complex, SE Turkey: Evolution of a Neotethyan active margin. In: Dixon, J.E., Robertson, A.H.F. (Eds.), The Geological Evolution of the Eastern Mediterranean. Geological Society, London, Special Publications, 17, 375-402.

Akyuz, H.S., Altunel, E., Karabacak, V., Yalciner, C.C., 2006. Historical earthquake activity of the northern part of the Dead Sea Fault Zone, southern Turkey. Tectonophysics, 426, 281-293.

Al Abdalla, A., Barrier, E., Matar, A., Muller, C. 2010. Late Cretaceous to Cenozoic tectonic evolution of the NW Arabian platform in NW Syria. In: Homberg, C., Bachmann, M. (Eds.), Evolution of the Levant Margin and Western Arabia Platform since the Mesozoic. Geological Society, London, Special Publications, 341, 305–327.

Alchalbi, A., Daoud, M., Gomez, F., McClusky, S., Reilinger, R., Abu Romeyeh, M., Alsouod, A., Yassminh, R., Ballani, B., Darawcheh, R., Sbeinati, R., Radwan, Y., Al Masri, R., Bayerly, M., Al Ghazzi, R., Barazangi, M., 2010. Crustal deformation in northwestern Arabia from GPS measurements in Syria: slow slip rate along the northern Dead Sea Fault. Geophysical Journal International 180, 125–135.

Allen, M.B., Armstrong, H.A., 2008. Arabia–Eurasia collision and the forcing of mid-Cenozoic global cooling. Palaeogeography, Palaeoclimatology, Palaeoecology 265, 52–58.

Allen, M.B., Jackson, J., Walker, R., 2004. Late Cenozoic reorganization of the Arabia-Eurasia collision and the comparison of short-term and long-term deformation rates. Tectonics, 23, TC2008, doi: 10.1029/2003TC001530.

Altunel, E., Meghraoui, M., Karabacak, V., Akyüz, H.S., Ferry, M., Yalcıner, C.C., Munschy, M., 2009. Archeological sites (tell and road) offset by the Dead Sea Fault in the Amik Basin, southern Turkey. Geophysical Journal International 179, 1313–1329.

Ambraseys, N.N., Jackson, J.A., 1998. Faulting associated with historical and recent eathquakes in the Eastern Mediterranean region. Geophysical Journal International, 133, 390-406.

ArRajehi, A., McClusky, S., Reilinger, R., Daoud, M., Alchalbi, A., Ergintav, S., Gomez, F., Sholan, J., Bou-Rabee, F., Ogubazghi, G., Haileab, B., Fisseha, S., Asfaw, L., Mahmoud, S., Rayan, A., Bendik, R., Kogan, L., 2010. Geodetic constraints on present-day motion of the Arabian Plate: implications for Red Sea and Gulf of Aden rifting. Tectonics 29, TC3011, doi: 10.1029/2009TC002482.

Atan, O.R., 1969. Eğribucak – Karacaören (Hassa) – Ceylânlı – Dazevleri (Kırıkhan) arasındaki Amanos Dağlarının jeolojisi. Report no. 139. General Directorate of Mineral Research and Exploration, Ankara, 85 pp.

Austermann, J., Iaffaldano, G., 2013. The role of the Zagros orogeny in slowing down Arabia-Eurasia convergence since ~5 Ma. Tectonics, 32, doi: 10.1002/tect.20027, 13 pp.

Beran, L., Lajtner, J., Crnčan, P., 2013. Aquatic molluscan fauna (Mollusca: Gastropoda, Bivalvia) of Vrana Lake Nature Park (Croatia). Natura Croatica, 22, 15–27.

Blisniuk, K., Rockwell, T., Owen, L.A., Oskin, M., Lippincott, C., Caffee, M.W., Dortch, J., 2010. Late Quaternary slip rate gradient defined using high-resolution topography and [10]Be dating of offset landforms on the southern San Jacinto Fault Zone, California. Journal of Geophysical Research, 115, B08401, 11 pp., doi: 10.1029/2009JB006346.

Bössneck, U., 2011. New records of freshwater and land molluscs from Lebanon (Mollusca: Gastropoda & Bivalvia). Zoology in the Middle East 54, 35–52.

Boulton, S.J., 2013. Tectonic development of the southern Karasu Valley, Turkey: successive structural events during basin formation. In: Robertson, A.H.F., Parlak, O., Ünlügenç, U.C. (Eds), Geological Development of Anatolia and the Easternmost Mediterranean Region. Geological Society, London, Special Publications, 372, 531-546.

Boulton, S.J., Robertson, A.H.F., 2008. The Neogene–Recent Hatay Graben, South Central Turkey: graben formation in a setting of oblique extension (transtension) related to post-collisional tectonic escape. Geological Magazine, 145, 800–821.

Boulton, S.J., Robertson, A.H.F., Ellam, R.M., Safak, U., Unlügenç, U.C., 2007. Strontium isotopic and micropalaeontological dating used to help redefine the stratigraphy of the Neotectonic Hatay Graben, southern Turkey. Turkish Journal of Earth Sciences 16, 1–39.

Boulton, S.J., Robertson, A.H.F., Ünlügenç, U.C., 2006. Tectonic and sedimentary evolution of the Cenozoic Hatay Graben, southern Turkey: a two-phase model for graben formation. In: Robertson, A.H.F., Mountrakis, D. (Eds.), Tectonic development of the Eastern Mediterranean: Geological Society, London, Special Publication, 260, pp. 613–634.

Boulton, S.J., Whittaker, A.C., 2009. Quantifying the slip rates, spatial distribution and evolution of active normal faults from geomorphic analysis: field examples from an oblique-extensional graben, southern Turkey. Geomorphology 104, 299–316.

Bowman, S.A., 2011. Regional seismic interpretation of the hydrocarbon prospectivity of offshore Syria. GeoArabia, 16, 95-124.

Brew, G., Lupa, J., Barazangi, M., Sawaf, T., Al-Imam, A., Zaza, T., 2001. Structure and tectonic development of the Ghab Basin and the Dead Sea fault system, Syria. Journal of the Geological Society, London, 158, 665-674.

Bridgland, D.R., Westaway, R., 2008. Preservation patterns of Late Cenozoic fluvial deposits and their implications: results from IGCP 449. Quaternary International 189, 5–38.

Butler, R.W.H., Spencer, S., Griffiths, H.M., 1997. Transcurrent fault activity on the Dead Sea Transform in Lebanon and its implications for plate tectonics and seismic hazard. Journal of the Geological Society, 154, 757-760.

Butler, R.W.H., Spencer, S., Griffiths, H.M., 1998. The structural response to evolving plate kinematics during transpression: evolution of the Lebanese restraining bend of the Dead Sea Transform. In: Dewey, J.F., Holdsworth, R.E., Strachan, R.A. (eds.), Transpression and transtension zones. Geological Society, London, Special Publications, 135, 81-106.

Çalışkan, V., 2008. Human-Induced wetland degradation: a case study of Lake Amik (southern Turkey). Balwois (Ohrid, Republic of Macedonia) 27, 1–10.

Çapan, U.Z., Vidal, P., Cantagrel, J.M., 1987. K–Ar, Nd, Sr and Pb isotopic study of the Quaternary volcanism in Karasu Rift (Hatay) N-end of Dead Sea rift zone in SE Turkey. Hacettepe University Earth Science Journal 14, 165–178.

Casana, J., 2008. Mediterranean valleys revisited: linking soil erosion, land use, and climate variability in the northern Levant. Geomorphology 101, 429-442.

Chorowicz, J., Dhont, D., Ammar, O., Rukieh, M., Bilal, A., 2005. Tectonics of the Pliocene Homs basalts (Syria) and implications for the Dead Sea Fault Zone activity. Journal of the Geological Society, London, 162, 259-271.

Coşkun, B., 1994. Oil possibilities of duplex structures in the Amik–Reyhanlı basin, SE Turkey. Journal of Petroleum Geology 17, 461–472.

Coşkun, B., Coşkun, B., 2000. The Dead Sea Fault and related subsurface structures, Gaziantep Basin, southeast Turkey. Geological Magazine 137, 175–192.

Cowie, P.A., Roberts, G.P., Mortimer, E., 2007. Strain localization within fault arrays over timescales of 10^0–10^7 years: observations, explanations, and debates In: Handy, M.R., Hirth, G., Hovius, N. (eds.), Tectonic Faults: Agents of Change on a Dynamic Earth. Dahlem Workshop Report 95. Massachusetts Institute of Technology Press, Cambridge, Massachusetts, pp. 47-77.

Dalongueville, R., Laborel, J., Pirazzoli, P., Sanlaville, P., Arnold, M., Bernier, P., Evin, J., Montaggioni, L.-F., 1993. Les variations recentes de la ligne de rivage sur le littoral Syrien. Quaternaire, 4, 45-53.

Dean, W.T., Monod, O., 1985. A new interpretation of Ordovician stratigraphy in the Bahçe area, northern Amanos Mountains, south central Turkey. Geological Magazine, 122, 15-25.

Demir, T., Seyrek, A., Guillou, H., Scaillet, S., Westaway, R., Bridgland, D., 2009. Preservation by basalt of a staircase of latest Pliocene terraces of the River Murat in eastern Turkey: evidence for rapid uplift of the eastern Anatolian Plateau. Global and Planetary Change, 68, 254-269.

Demir, T., Seyrek, A., Westaway, R., Bridgland, D., Beck, A., 2008. Late Cenozoic surface uplift revealed by incision by the River Euphrates at Birecik, southeast Turkey. Quaternary International, 186, 132-163.

Demir, T., Seyrek, A., Westaway, R., Guillou, H., Scaillet, S., Beck, A., Bridgland, D.R., 2012. Late Cenozoic regional uplift and localised crustal deformation within the northern Arabian Platform in southeast Turkey: investigation of the Euphrates terrace staircase using multidisciplinary techniques. Geomorphology, 165-166, 7-24.

Devyatkin, E.V., Dodonov, A.E., Gablina, S.S., Golovina, L.A., Kurenkova, V.G., Simakova, A.N., Trubikhin, V.M., Yasamanov, N.A., Khatib, K., Nseir, H., 1996. Upper Pliocene–Lower Pleistocene marine deposits of western Syria: stratigraphy and paleogeography. Stratigriraphy and Geological Correlation, 4 (1), 67–77.

Devyatkin, E.V., Dodonov, A.E., Sharkov, E.V., Zykin, V.S., Simakova, A.N., Khatib, K., Nseir, H., 1997. The El-Ghab rift depression in Syria: its structure, stratigraphy and history of development. Stratigraphy and Geological Correlation 5, 362–374.

Dodonov, A.E., Trifonov, V.G., Ivanova, T.P., Kuznetsov, V.Y., Maksimov, F.E., Bachmanov, D.M., Sadchikova, T.A., Simakova, A.N., Minini, H., Al-Kafri, A.-M., Ali, O., 2008. Late Quaternary marine terraces in the Mediterranean coastal area of Syria: Geochronology and neotectonics. Quaternary International, 190, 158-170.

Domas, J. 1994. The Late Cenozoic of the Al Ghab Rift, NW Syria. Sbornik Geologickych Ved, Antropozoikum 21, 57–73.

DSİ, 1975. Asi havzası hidrojeolojik etüt raporu (Asi Basin hydrogeological study report). Devlet Su İşleri Genel Müdürlüğü (General Directorate of State Water Works), Ankara.

Dubertret, L., 1962. Carte géologique du Liban, Syrie et bordure de pays voisins, 1:1,000,000 scale. Musée d'Histoire Naturelle, Paris.

Duman, T.Y., Emre, Ö., 2013. The East Anatolian Fault: geometry, segmentation and jog characteristics. In: Robertson, A.H.F., Parlak, O., Ünlügenç, U.C. (Eds), Geological Development of Anatolia and the Easternmost Mediterranean Region. Geological Society, London, Special Publications, 372, 495-529.

Eger, A.A., 2011. The swamps of home: marsh formation and settlement in the early medieval Near East. Journal of Near Eastern Studies, 70, 55-79.

Elias, A., Tapponnier, P., Singh, S.C., King, G.C.P., Briais, A., Daeron, M., Carton, H., Sursock, A., Jacques, E., Jomaa, R., Klinger, Y., 2007. Active thrusting offshore Mount Lebanon: source of the tsunamigenic A.D. 551 Beirut-Tripoli earthquake. Geology, 35, 755-758.

Emre, Ö., Duman, T.Y., 2011. Active Fault Map series of Turkey, 1:250,000 scale, Mersin (NJ 36-16) quadrangle, sheet number 34. General Directorate of Mineral Research and Exploration, Ankara.

Emre, Ö., Duman, T.Y., Olgun, Ş., 2012a. Active Fault Map series of Turkey, 1:250,000 scale, Antakya (NJ 37-13) quadrangle, sheet number 39. General Directorate of Mineral Research and Exploration, Ankara.

Emre, Ö., Duman, T.Y., Olgun, Ş., Elmacı, H., Özalp, S., 2012b. Active Fault Map series of Turkey, 1:250,000 scale, Gaziantep (NJ 37-9) quadrangle, sheet number 38. General Directorate of Mineral Research and Exploration, Ankara.

Emre, Ö., Duman, T.Y., Özalp, S., Elmacı, H., Olgun, Ş., 2011. Active Fault Map series of Turkey, 1:250,000 scale, Adana (NJ 36-12) quadrangle, sheet number 33. General Directorate of Mineral Research and Exploration, Ankara.

Ergin, M., Aktar, M., Eyidoğan, H. 2004. Present-day seismicity and seismotectonics of the Cilician basin: Eastern Mediterranean Region of Turkey. Bulletin of the Seismological Society of America, 94, 930–939.

Erol, O. 1963. Asi Nehri deltasının jeomorfolojisi ve dördüncü zaman denizakarsu şekilleri (Die Geomorphologie des Orontes-deltas und der anschliessenden pleistozänen Strand- und Fluss terrassen, Provinz Hatay, Türkei). İstanbul Universitesi Dil ve Tarih-Coğrafya Fakültesi Yayınları [Publications of the Faculty of Language and History-Geography of İstanbul University] 148, 1–110 [in Turkish and German].

Ferry, M., Meghraoui, M., Abou Karaki, N., Al-Taj, M., Khalil, L., 2011. Episodic behavior of the Jordan Valley section of the Dead Sea Fault inferred from a 14-ka-long integrated catalog of large earthquakes. Bulletin of the Seismological Society of America, 101, 39–67.

Frenzel, P., Schulze, I., Pint, A., 2012 Noding of *Cyprideis torosa* valves (Ostracoda) – a proxy for salinity? New data from field observations and a long-term microcosm experiment. International Review of Hydrobiology 97, 314–329.

Freund, R., Garfunkel, Z., Zak, I., Goldberg, M., Weissbrod, T., Derin, B., Bender, F., Wellings, F.E., Girdler, R.W., 1970. The shear along the Dead Sea Rift [and Discussion]. Philosophical Transactions of the Royal Society of London, Series A, 267, 107-130.

Friedman, E.S., Sato, Y., Alataş, A., Johnson, C.E., Wilkinson, T.J., Yener, K.A., Lai, B., Jennings, G., Mini, S.M., Alp, E.E., 2000. An x-ray fluorescence study of lake sediments from ancient Turkey using synchrotron radiation. In: Proceedings of the 47th Annual Denver X-ray Conference, Colorado Springs, Colorado, 3-7 August 1998. Advances in X-ray Analysis, 42, 151-160.

Girdler, R.W., 1990. The Dead Sea transform fault system. Tectonophysics, 180, 1-13.

Glöer, P., Dia, A., Falkner, G., 2012. The genus *Pseudobithynia* in Lebanon, with a redescription of three species and additional notes on its ecology (Mollusca: Bithyniidae). Zoology in the Middle East 57, 87-96.

Glöer, P. Yıldırım, M.Z., 2006. Some records of Bithyniidae from Turkey with the description of *Bithynia pesicii* n. sp. (Gastropoda: Bithyniidae). Malakologische Abhandlungen 24, 37–42.

Gomez, F., Khawlie, M., Tabet, C., Darkal, A.N., Khair, K., Barazangi, M., 2006. Late Cenozoic uplift along the northern Dead Sea transform in Lebanon and Syria. Earth and Planetary Science Letters 241, 913–931.

Green, T., Abdullayev, N.R., Hossack, J., Riley, G., Roberts, A.M., 2009. Sedimentation and subsidence in the South Caspian Basin, Azerbaijan. In: Brunet, M.-F., Wilmsen, M., Granath, J.W. (Eds), South Caspian to Central Iran Basins. Geological Society, London, Special Publications, 312, 241–260.

Griffiths, H.M., Clark, R.A., Thorp, K.M., Spencer, S., 2000. Strain accommodation at the lateral margin of an active transpressive zone: geological and seismological evidence from the Lebanese restraining bend. Journal of the Geological Society, London 157, 289-302.

Gürsoy, H., Tatar, O., Piper, J.D.A., Heimann, A., Mesci, L., 2003. Neotectonic deformation linking the east Anatolian and Karataş-Osmaniye intracontinental transform fault zones in the Gulf of İskenderun, southern Turkey, deduced from paleomagnetic study of the Ceyhan-Osmaniye volcanics. Tectonics, 22, 1067, 13 pp., doi: 10.1029/2003TC001524

Hall, J.K., 2005. Bathymetry and topography of the Syria-Lebanon continental margin In: Hall, J.K., Krasheninnikov, V.A., Hirsch, F., Benjamini, C., Flexer, A. (Eds.), Geological Framework of the Levant. Volume II: The Levantine Basin and Israel. Historical Productions-Hall, Jerusalem, Israel, pp. 149-180.

Hall, J., Aksu, A.E., Calon, T.J., Yaşar, D., 2005. Varying tectonic control on basin development at an active microplate margin: Latakia Basin, Eastern Mediterranean. Marine Geology, 221, 15-60.

Hardenberg, M.F., Robertson, A.H.F., 2007. Sedimentology of the NW margin of the Arabian plate and the SW–NE trending Nahr El-Kabir half-graben in northern Syria during the latest Cretaceous and Cenozoic. Sedimentary Geology, 201, 231-266.

Hardenberg, M.F., Robertson, A.H.F., 2013. Role of the Palaeogene–Recent sinistral El-Kabir Lineament and the associated transtensional Neogene–Recent El-Kabir Basin (northern Syria) in distributed deformation between the African and Eurasian plates. In: Robertson, A.H.F., Parlak, O., Ünlügenç, U.C. (Eds), Geological Development of Anatolia and the Easternmost Mediterranean Region. Geological Society, London, Special Publications, 372, 447–471.

Heimann, A., Steinitz, G., 1989. ^{40}Ar/^{39}Ar total gas ages of basalts from Notera 3 well, Hula Valley, Dead Sea Rift: stratigraphic and tectonic implications. Israel Journal of Earth Science 38, 173–184.

Heimann, A., Zilberman, E., Amit, R., Frieslander, U., 2009. Northward migration of the southern diagonal fault of the Hula pull-apart basin, Dead Sea Transform, northern Israel. Tectonophysics 476, 496–511.

Järvekülg, A., 1979. [The bottom sediments of the eastern part of the Baltic Sea]. Valgus, Tallinn, Estonia, 382 p. [in Russian].

Jones, M.D., Roberts, C.N., Leng, M.J., 2007. Quantifying climatic change through the last glacial–interglacial transition based on lake isotope palaeohydrology from central Turkey. Quaternary Research, 67, 463-473.

Hemer, D.O., Gohrbandt, K.H.A., Phillips, C.B., 1988. Oil and gas developments in the Middle East in 1987. American Association of Petroleum Geologists Bulletin, 72 (B 10), 294-312.

Karabacak, V., Altunel, E., 2013. Evolution of the northern Dead Sea Fault Zone in southern Turkey. Journal of Geodynamics 65, 282– 291.

Karabacak, V., Altunel, E., Meghraoui, M., Akyüz, H.S., 2010. Field evidences from northern Dead Sea Fault Zone (South Turkey): new findings for the initiation age and slip rate. Tectonophysics 480, 172–182.

Kiliç, S, Evrendilek, F., Berberoğlu, B., Demirkesen, A.C., 2006. Environmental monitoring of land-use and land-cover changes in Amik Plain, Turkey. Environmental Monitoring and Assessment 114, 157–168.

Kinnaird, T., Robertson, A.H.F., 2013. Tectonic and sedimentary response to subduction and incipient continental collision in southern Cyprus, easternmost Mediterranean region. In: Robertson, A.H.F., Parlak, O., Ünlügenç, U.C. (Eds), Geological Development of Anatolia and the Easternmost Mediterranean Region. Geological Society, London, Special Publications, 372, 585-614.

Krienitz, M.-S., Haase, K.M., Mezger, K., van den Bogaard, P., Thiemann, V., Shaikh-Mashail, M.A., 2009. Tectonic events, continental intraplate volcanism, and mantle plume activity in northern Arabia: constraints from geochemistry and Ar-Ar dating of Syrian lavas. Geochemistry, Geophysics, Geosystems 10, 26 pp. doi: 10.1029/2008GC002254.

Krijgsman, W., Hilgen, F.J., Raf, I., Sierro, F.J., Wilson, D.S., 1999. Chronology, causes and progression of the Messinian salinity crisis. Nature, 400, 652-655.

Ma, G. S.-K., Malpas, J., Xenophontos, C., Chan, G. H.-N., 2009. Petrogenesis of latest Miocene – Quaternary continental intraplate volcanism along the northern Dead Sea Fault System (Al Ghab – Homs Volcanic Field), western Syria: evidence for lithosphere-astnenosphere interaction. Journal of Petrology, 52, 401-430.

McCay, G.A., Robertson, A.H.F., 2013. Upper Miocene–Pleistocene deformation of the Girne (Kyrenia) Range and Dar Dere (Ovgos) lineaments, northern Cyprus: role in collision and tectonic escape in the easternmost Mediterranean region. In: Robertson, A.H.F., Parlak, O., Ünlügenç, U.C. (Eds), Geological Development of Anatolia and the Easternmost Mediterranean Region. Geological Society, London, Special Publications, 372, 421–445.

McClusky, S., Balassanian, S., Barka, A., Demir, C., Ergintav, S., Georgiev, I., Gurkan, O., Hamburger, M., Hurst, K., Kahle, H., Kastens, K., Kekelidze, G., King, R., Kotzev, V., Lenk, O., Mahmoud, S., Mishin, A., Nadariya, M., Ouzounis, A., Paradissis, D., Peter, Y., Prilepin, M., Reilinger, R., Sanli, I., Seeger, H., Tealeb, A., Toksöz, M.N., Veis, G., 2000. Global Positioning System constraints

on plate kinematics and dynamics in the eastern Mediterranean and Caucasus. Journal of Geophysical Research, 105, 5695-5719.

McKenzie, D.P. 1976. The East Anatolian Fault; a major structure in eastern Turkey. Earth and Planetary Science Letters, 29, 189–193.

Mahmoud, Y., 2012. Caractérisation géodesique de la deformation active du point triple d'Hatay (Syrie-Turquie) [Geodetic characterization of the active deformation at the Hatay triple junction (Syria, Turkey)]. Ph.D. thesis, University of Strasbourg, 192 pp. Available online: https://publication-heses.unistra.fr/public/theses_doctorat/Mahmoud_Yasser_2012_ED413.pdf

Mahmoud, Y., Masson, F., Meghraoui, M., Cakir, Z., Alchalbi, A., Yavasoglu, H., Yönlü, O., Daoud, M., Ergintav, S., Inan, S., 2013. Kinematic study at the junction of the East Anatolian fault and the Dead Sea fault from GPS measurements. Journal of Geodynamics, 67, 30-39.

Marco, S., Rockwell, T.K., Heimann, A., Frieslander, U., Agnon, A., 2005. Late Holocene activity of the Dead Sea Transform revealed in 3D palaeoseismic trenches on the Jordan Gorge segment. Earth and Planetary Science Letters 234, 189–205.

Meghraoui, M., Gomez, F., Sbeinati, R., Van Der Woerd, J., Mouty, M., Darkal, A. N., Radwan, Y., Layyous, I., Al-Najjar, H., Darawcheh, R., Hijazi, F., Al-Ghazzi, R., Barazangi, M. 2003. Evidence for 830 years of seismic quiescence from palaeoseismology, archaeoseismology and historical seismicity along the Dead Sea fault in Syria. Earth and Planetary Science Letters, 210, 35-52.

Maslin, M.A., Ridgwell, A.J., 2005. Mid-Pleistocene Revolution and the 'eccentricity myth'. In: Early-Middle Pleistocene Transitions: The Land-Ocean Evidence. Geological Society, London, Special Publications, 247, 19-34.

MTA, 2012. 14 Kasım 2012 Çöçelli (Pazarcık-K.Maraş) depremi bilgi notu. Available online: http://www.mta.gov.tr/v2.0/deprem/pdf/Deprem-Bilgi-Notu_2012-11-14_Cocelli-Pazarcik-Maras.pdf

Mudelsee, M., Schulz, M., 1997. The Mid-Pleistocene climate transition: onset of 100 ka cycle lags ice volume build up by 280 ka. Earth and Planetary Science Letters, 151, 117-123.

Muehlbenger, W.E., Gordon, M.B., 1987. Observations on the complexity of the East Anatolian Fault, Turkey. Journal of Structural Geology 9, 899–903.

Nemer, T., Meghraoui, M., 2006. Evidence of coseismic ruptures along the Roum fault (Lebanon): a possible source for the AD 1837 earthquake. Journal of Structural Geology 28, 1483-1495.

Over, S., Unlügenç, U.C., Bellier, O., 2002. Quaternary stress regime change in the Hatay region (SE Turkey). Geophysical Journal International 148, 649–662.

Ozelkan E., Uca Avci Z.D., Karaman M., 2011. Investigation on draining of the Lake Amik and the related environmental changes, by using RS technology In: Halounová, L. (ed.), Remote Sensing and Geoinformation not only for Scientific Cooperation. Proceedings of the 31st EARSeL http://www.earsel.org/symposia/2011-symposium-Prague/Proceedings/PDF/Coastal   Zones/4 ok25-a2531 Ozelkan Uca Damla.pdf

Palano, M., Imprescia, P., Gresta, S., 2013. Current stress and strain-rate fields across the Dead Sea Fault System: Constraints from seismological data and GPS observations. Earth and Planetary Science Letters, 369-370, 305–316.

Parlak, O., Kop, A., Unlügenç, U., Demirkol, C., 1998. Geochemistry and geochronology of basaltic rocks in the Karasu Graben near Kırıkhan (Hatay), Southern Turkey. Turkish Journal of Earth Sciences 7, 53–61.

Parlak, O., Kozlu, H., Demirkol, C., Delaloye, M., 1997. Intracontinental Plio-Quaternary volcanism along the African-Anatolian plate boundary, southern Turkey. Ofioliti, 22, 111-117.

Perinçek, D., Çemen, İ., 1990. The structural relationship between the East Anatolian and Dead Sea fault zones in southeastern Turkey. Tectonophysics 142, 331–340.

Perinçek, D., Eren, A.G., 1990. Dogrultu atımlı Dogu Anadolu Fayı ve Ölü Deniz Fay Zonları etki alanında gelişen Amik havzasının kökeni (The origin of Amik basin formed by the effect of East Anatolian Fault and Dead Sea Fault Zone). In Geology Proceedings of the 8th Petroleum Congress of Turkey, Ankara. Turkish Association of Petroleum Geologists, Ankara, pp. 180–192.

Perinçek, D., Kozlu, H., 1983. Stratigraphy and structural relations of the units if the Afşin-Elbistan-Doğanşehir region (eastern Taurus). In: Tekeli, O., Göncüoğlu, M.C. (Eds.), Geology of the Taurus Belt. Proceedings of the 1983 Ankara Symposium. General Directorate of Mineral Research and Exploration, Ankara, pp. 181-198.

Pirazzoli, P.A., Lael, J., Borel, J., Saliége, J.F., Erol, O., Kayan, I., Persol, A., 1991. Holocene raised shorelines on the Hatay coasts Turkey: palaeoecological and tectonic implications. Marine Geology 96, 295–311.

Plötner, J., Uzzell, T., Beerli, P., Akın, Ç., Bilgin, C.C., Haefeli, C., Ohst, T., Köhler, F., Schreiber, R., Guex, G.-D., Litvinchuk, A.N., Westaway, R., Reyer, H.-U., Hotz, H., 2010. Genetic divergence and evolution of reproductive isolation in eastern Mediterranean water frogs. In: Glaubrecht, M., Schneider, H. (Eds.) Evolution in action. Case studies in adaptive radiation and the origin of biodiversity. Special volume from the SPP 1127 of the Deutsche ForschungsGemeinschaft 'Radiations – Genesis of Biological Diversity'. Springer, Berlin, pp. 373-403.

Ponikarov, V.P. (Ed.), 1986. Geological Map of Syria (1: 1,000,000; 2nd Edition). Establishment of Geology and Mineral Resources (Ministry of Petroleum and Mineral Resources), Syrian Arab Republic.

Ponikarov, V.P., Kazmin, V.G., Mikhailov, I.A., Razvaliayev, A.V., Krasheninnikov, V.A., Kozlov, V.V., Soulidi-Kondratiyev, E.D., Faradzhev, V.A., 1966. The geological map of Syria, scale 1:1,000,000: Explanatory notes. Vsesoj. Exportno-Import Objed. Technoexport, Moscow, and Ministry of Industry, Syrian Arab Republic, Damascus.

Ponikarov, V.P., Shatsky, V., Kazmin, V.G., Mikhailov, I.A., Aistov, L., Kulakov, V., Shatskaya, M., Shirokov, V., 1963. Geological map of Syria, 1:200,000 scale, sheet I-36-XXIV and I-37-XIX, Latakia and Hama quadrangles. Technoexport, Moscow, and Ministry of Industry, Damascus.

Reilinger, R., McClusky, S., Vernant, P., Lawrence, S., Ergintav, S., Cakmak, R., Ozener, H., Kadirov, F., Guliev, I., Stepanyan, R., Nadariya, M., Hahubia, G., Mahmoud, S., Sakr, K., Ar Rajehi, A., Paradissis, D., Al-Aydrus, A., Prilepin, M., Guseva, T., Evren, E., Dmitrotsa, A., Filikov, S.V., Gomez, F., Al-Ghazzi, R., Karam, G., 2006. GPS constraints on continental deformation in the Africa–Arabia–Eurasia continental collision zone and implications for the dynamics of plate interactions. Journal of Geophysical Research 111, B05411, 26 pp, doi: 10.1029/2005JB004051.

Reinhardt, E.G., Fitton, R.J., Schwarcz, H.P., 2003. Isotopic (Sr, O, C) indicators of salinity and taphonomy in marginal marine systems. Journal of Foraminiferal Research, 33, 262-272.

Roberts, N., Reed, J.M., Leng, M.J., Kuzucuoğlu, C., Fontugne, M., Bertaux, J., Woldring, H., Bottema, S., Black, S., Hunt, E., Karabiyikoğlu, M., 2001. The tempo of Holocene climatic change in the eastern Mediterranean region: new high-resolution crater-lake sediment data from central Turkey. Holocene, 11, 721-736.

Robertson, A.H.F., 1998. Tectonic significance of the Eratosthenes Seamount: a continental fragment in the process of collision with a subduction zone in the eastern Mediterranean (Ocean Drilling Program Leg 160). Tectonophysics 298, 63–82.

Robertson, A.H.F., Unlügenç, U.C., Nurdan, I., Taşlı, K. 2004. The Misis-Andırın Complex: Mid-Tertiary subduction/accretion and melange formation related to closure and collision of the South Tethys in southern Turkey. Journal of Asian Earth Science, 22, 413–453.

Rojay, B., Heimann, A., Toprak, V., 2001. Neotectonic and volcanic characteristics of the Karasu fault zone (Anatolia Turkey): the transition zone between the Dead Sea transform and the East Anatolian fault zone. Geodinamica Acta 14, 197–212.

Royden, L.H., Papanikolaou, D.J., 2011. Slab segmentation and Late Cenozoic disruption of the Hellenic arc. Geochemistry, Geophysics, Geosystems, 12, Q03010, doi: 10.1029/2010GC003280, 24 pp.

Sadeh, M., Hamiel, Y., Ziv, A., Bock, Y., Fang, P., Wdowinski, S., 2012. Crustal deformation along the Dead Sea Transform and the Carmel Fault inferred from 12 years of GPS measurements. Journal of Geophysical Research 117, B08410, doi: 10.1029/2012JB009241.

Savage, J.C., Burford, R.O., 1973. Geodetic determination of relative plate motion in central California. Journal of Geophysical Research, 78, 832-845.

Sbeinati, M.R., Darawcheh, R., Mouty, M., 2005. The historical earthquakes of Syria: an analysis of large and moderate earthquakes from 1365 B.C. to 1900 A.D. Annals of Geophysics 48, 347–435.

Schütt, H., 1983. Die Molluskenfauna der Süßwässer im Einzugsgebiet des Orontes unter Berücksichtigung benachbarter Flußsysteme. Archiv für Molluskenkunde, 113, 17–91 and 225–228.

Schwan, W. 1971. Geology and tectonics of the central Amanos Mountains. In: Campbell, A.S. (ed.) Geology and History of Turkey. Petroleum Exploration Society of Libya, Tripoli, p. 283-303.

Sharkov, E.V., Chernyshev, I.V., Devyatkin, E.V., Dodonov, A.E., Ivanenko, V.V., Karpenko, M.I., Leonov, Y.G., Novikov, V.M., Hanna, S., Khatib, K., 1994. Geokhronologiya pozdnekaynozoyskikh bazal'tov Zapadnoy Sirii [Geochronology of late Cenozoic basalts in western Syria], Petrologiya, 2, 385–394.

Sharkov, E.V., Chernyshev, I.V., Devyatkin, E. V., Dodonov, A.E., Ivanenko, V.V., Karpenko, M.I., Lebedev, V.A., Novikov, V.M., Hanna, S., Khatib, K., 1998. New data on the geochronology of upper Cenozoic plateau basalts from the northeastern periphery of the Red Sea Rift area (northern Syria), Doklady of the Academy of Sciences of the USSR, Earth Science, English Translation, 358, 19–22.

Searle, M., Chung, S.-L., Lo, C.-H., 2010. Geological offsets and age constraints along the northern Dead Sea fault, Syria. Journal of the Geological Society, London 167, 1001-1008.

Şereflişan, H., Yıldırım, M.Z., Şereflişan, M., 2009. The gastropod fauna and their abundance, and some physicochemical parameters of Lake Gölbaşı (Hatay, Turkey). Turkish Journal of Zoology, 33, 287-296.

Seyrek, A., Demir, T., Pringle, M.S., Yurtmen, S., Westaway, R., Beck, A., Rowbotham, G., 2007. Kinematics of the Amanos Fault, southern Turkey, from Ar/Ar dating of offset Pleistocene basalt flows: Transpression between the African and Arabian plates. Geological Society, Special Publications, 290, London, pp. 255–284.

Seyrek, A., Demir, T., Pringle, M., Yurtmen, S., Westaway, R., Bridgland, D., Beck, A., Rowbotham, G., 2008. Late Cenozoic uplift of the Amanos Mountains and incision of the Middle Ceyhan river gorge, southern Turkey; Ar-Ar dating of the Düziçi basalt. Geomorphology, 97, 321-355.

Steiger, R.H., Jäger, E., 1977. Convention on the use of decay constants in geo- and cosmochronology. Earth and Planetary Science Letters 36, 359-363.

Steininger, F.F., Berggren, W.A., Kent, D.V., Bernor, R.L., Sen, S., Agustí, J., 1996. Circum-Mediterranean Neogene (Miocene and Pliocene) marine-continental chronologic correlations of European mammal units. In: Bernor, R.L., Fahlbusch, V., Mittmann, H.-W. (Eds), The Evolution of Western Eurasian Neogene Mammal Faunas. Columbia Univ Press, New York, pp. 7-46.

Suc, J.-P., Bache, F., Gorini, C., Do Couto, D., Jolivet, L., Rubino, J.-L., Mocochain, L., Popescu, S.-M., 2013. The Messinian Salinity Crisis: A perspective for reservoir exploration in the Mediterranean and adjacent basins. Search and Discovery, Article 30277, 35 pp. Available online: http://www.searchanddiscovery.com/documents/2013/30277suc/ndx_suc.pdf

Terlemez, H.Ç.İ., Şentürk, K., Ateş, Ş., Sümengen, M., Oral, A., 1997. Geological map of the Gaziantep – K24 quadrangle and accompanying 13 page explanatory guide. General Directorate of Mineral research and Exploration, Ankara (in Turkish).

Trifonov, V.G., Trubikhin, V.M., Adjamian, J., Jallad, Z., El Hair, Y., Ayed, H., 1991. Levant fault zone in the north-western Syria. Geotectonics 25 (2), 145–154.

Trifonov, V.G., Dodonov, A.E., Sharkov, E.V., Golovin, D.I., Chernyshev, I.V., Lebedev, V.A., Ivanova, T.P., Bachmanov, D.M., Rukieh, M., Ammar, O., Minini, H., Al Kafri, A.-M., Ali, O., 2011. New data on the Late Cenozoic basaltic volcanism in Syria, applied to its origin. Journal of Volcanology and Geothermal Research, 199, 177-192.

Tolun, N., Erentöz, C. 1962. Hatay sheet of the Geological Map of Turkey, 1:500,000 scale. General Directorate of Mineral Research and Exploration, Ankara.

Tolun, N., Pamir, H.N., 1975. Explanatory text of the 1:500,000 scale geological map of Turkey, Hatay sheet. General Directorate of Mineral Research and Exploration, Ankara, 99 pp.

Tüysüz, O., Tarı, U., Genç, Ş.C., İmren, C., Blackwell, B.A.B.; Wehmiller, J., Kaufman, D., Altıok, S., Beyhan, M., Fleitmann, D., Lom, N., Üsküplü, S., Tekeşin, Ö., Florentin, J.A., 2013. Geology and morphology of the Antakya Graben between the Amik Triple Junction and the Cyprus Arc. In: Abstract Volume, European Geosciences Union General Assembly 2013, Vienna, Austria, 7–12 April 2013. Available online: http://meetingorganizer.copernicus.org/EGU2013/EGU2013-2064-2.pdf

Van Baak, C.G.C., Vasiliev, I., Stoica, M., Kuiper, K.F., Forte, A.M., Aliyeva, E., Krijgsman, W., 2013. Paleomagnetic A magnetostratigraphic time frame for Plio-Pleistocene transgressions in the South Caspian Basin, Azerbaijan. Global and Planetary Change 103, 119–134.

Verberne, B.A., de Bresser, J.H.P., Niemeijer, A.R., Spiers, C.J., de Winter, D.A.M., Plümper, O., 2013. Nanocrystalline slip zones in calcite fault gouge show intense crystallographic preferred orientation: Crystal plasticity at sub-seismic slip rates at 18–150 °C. Geology, in press. Available online; doi: 10.1130/G34279.1.

Vidal, N., Alvarez-Marron, J., Klaeschen, D., 2000a. The structure of the Africa-Anatolia plate boundary in the Eastern Mediterranean. Tectonics, 19, 723-739.

Vidal, N., Klaeschen, D., Kopf, A., Docherty, C., Von Huene, R., Krashenninkov, V.A., 2000b. Seismic images at the convergence zone from south of Cyprus to the Syrian coast, eastern Mediterranean. Tectonophysics, 329, 157–170.

Walley, C. D., 1998. Some outstanding issues in the geology of Lebanon and their importance in the tectonic evolution of the Levantine region. Tectonophysics, 298, 37-62.

Wdowinski, S., Ben-Avraham, Z., Arvidsson, 1 R., Ekström, G., 2006. Seismotectonics of the Cyprian Arc. Geophysical Journal International 164, 176–181.

Westaway, R., 1994. Present-day kinematics of the Middle East and eastern Mediterranean. Journal of Geophysical Research, 99, 12071-12090.

Westaway, R., 1995. Deformation around stepovers in strike-slip fault zones, Journal of Structural Geology, 17, 831-846.

Westaway, R., 2003. Kinematics of the Middle East and Eastern Mediterranean updated. Turkish Journal of Earth Sciences 12, 5–46.

Westaway, R., 2004. Kinematic consistency between the Dead Sea Fault Zone and the Neogene and Quaternary left-lateral faulting in SE Turkey. Tectonophysics 391, 203–237.

Westaway, R., 2006. Late Cenozoic extension in southwest Bulgaria: a synthesis. In: Robertson, A.H.F., Mountrakis, D. (Eds), Tectonic Development of the Eastern Mediterranean Region. Geological Society, London, Special Publication 260, 557-590.

Westaway, R., 2009. Active crustal deformation beyond the SE margin of the Tibetan Plateau: constraints from the evolution of fluvial systems. Global and Planetary Change, 68, 395-417.

Westaway, R., Demir, T., Seyrek, A., 2008. Geometry of the Turkey-Arabia and Africa-Arabia plate boundaries in the latest Miocene to Mid-Pliocene: the role of the Malatya-Ovacık Fault Zone in eastern Turkey. eEarth 3, 27–35.

Westaway, R., Demir, T., Seyrek, A., Beck, A., 2006a. Kinematics of active left-lateral faulting in southeast Turkey from offset Pleistocene river gorges: improved constraint on the rate and history of relative motion between the Turkish and Arabian plates. Journal of the Geological Society, London 163, 149–164.

Westaway, R., Guillou, H., Yurtmen, S., Beck, A., Bridgland, D., Demir, T., Scaillet, S., Rowbotham, G., 2006b. Late Cenozoic uplift of western Turkey: Improved dating of the Kula Quaternary volcanic field and numerical modelling of the Gediz river terrace staircase. Global and Planetary Change 51, 131-171.

Wilkinson, T.J., 1997. The history of the Lake of Antioch: A preliminary note. In: Young, G.D., Chavalas, M.W., Averbeck, R.E. (eds), Crossing Boundaries and Linking Horizons: Studies in Honor of Michael C. Astour on his 80th Birthday. CDL Press, Bethesda, Maryland, pp. 557–576.

Wilkinson, T.J., Friedman, E., Alp, E., Stampfl, A., 2001. Geoarchaeology of a lake basin: spatial and chronological patterning of sedimentation in the Amuq Plain, Turkey. In: Fortin, M. (ed.), Recherches Archéométriques, Cahiers d'archéologie du CELAT. Laval University, Quebec, pp. 211–226.

Woodside, J.M., Mascle, J., Zitter, T.A.C., Limonov, A.F., Ergun, M., Volkonskaia, A., 2002. The Florence Rise, the western bend of the Cyprus Arc, Marine Geology, 185, 177–194.

Yener, K.A., 2005. The Amuq Valley regional projects. Volume 1, Surveys in the Plain of Antioch and Orontes delta, Turkey, 1995-2002. Publication no. 131, The Oriental Institute of the University of Chicago.

Yener, K.A., Edens, C., Harrison, T.P., Verstraete, J., Wilkinson, T.J., 2000. The Amuq Valley Regional Project, 1995-1998. American Journal of Archaeology, 104, 163-220.

Yener, K.A., Wilkinson, T.J., 1999. The Amuq Valley Projects: 1998-99 Annual Report. The Oriental Institute of the University of Chicago. http://oi.uchicago.edu/research/pubs/ar/98-99/amuq.html

Yıldırım, M.Z., 1999. Türkiye Prosobranchia (Gastropoda: Mollusca) türleri ve zoocoğrafik yayılışları. 1, Tatlı ve acı sular. Turkish Journal of Zoology 23, 877–900.

Yurtmen, S., Guillou, H., Westaway, R., Rowbotham, G., Tatar, O., 2002. Rate of strike slip motion on the Amanos Fault (Karasu Valley, southern Turkey) constrained by K–Ar dating and geochemical analysis of Quaternary basalts. Tectonophysics 344, 207–246.

Figure captions

Figure 1. Regional map, adapted from Fig. 2 of Westaway (2004), which lists original sources of information, and Fig. 1 of Seyrek et al. (2008), showing a schematic interpretation of faults forming the boundaries between the Turkish, African and Arabian plates in central-southern Turkey and NW Syria, in relation to selected GPS points from Reilinger et al. (2006) and Alchalbi et al. (2010). The Anatolian crustal province is unshaded where offshore; its southern limit, at the northern margin of the Arabian Platform, marks the suture of the former Southern Neotethys Ocean. The Jabal Nusayriyah or Syrian Coastal Range runs N-S to the west of the Ghab Basin and the Misyaf Fault. The Amanos Mountains run SSW-NNE to the west of the Karasu Valley between the coast west of Antakya and the northern margin of the Arabian Platform. Normal faults are indicated with hanging-wall ticks; left-lateral faults with lines with no ticks. However, many of the faults depicted are transtensional, the 'strike-slip fault' ornament being used for the major structures. Abbreviations denote particular faults or fault zones discussed in the text, thus: A.F., Amanos Fault; Ar.F., Armanaz Fault; A.S.F.Z., Antakya-Samandağ Fault Zone; A.T., Aakkar Thrust; D.O.F., Düziçi-Osmaniye Fault, with its suggested northward continuation dashed; E.H.F., East Hatay Fault; K.F., Karataş Fault; Ky.F., Kythrea Fault; L.T.F.Z., Latakia-Tripoli Fault Zone; M.F., Misyaf Fault; M.L.T., Mount Lebanon Thrust and associated reverse faults; N.F.Z., Narlı Fault Zone; N.K.F., Nahr el Kebir Fault Zone; O.F., Ovgros Fault Zone; Q.B.F., Qanaya-Babatorun Fault; R.F., Roum Fault; R.A.F., Rankine-Aabdeh Fault; R.R.F.Z, Ras al Basit – Ras Ibn Hani Fault Zone; S.F., Serghaya Fault; Ya.F., Yammouneh Fault; Y.F., Yumurtalık Fault. Mount Lebanon Thrust and associated reverse faults are simplified from Elias et al. (2007). Latakia Ridge, related structures, Cyprus subduction zone, Erastothenes Seamount and intersections with seismic lines are from Vidal et al. (2000a). Faulting onshore in Cyprus is simplified from Kinnaird and Robertson (2013).

Figure 2. Part of the up to 500 m high scarpment formed in Palaeocene limestone (overlain, in the top left of this view, by Lower Miocene conglomerate and Middle-Upper Miocene limestone) looking SSW from Universal Transverse Mercator (UTM) co-ordinates BA 46301 10804 at Saint Peter's Church (Sanpiyer Kilisesi) on the eastern edge of Antakya. A fault, part of the Antakya-Samandağ Fault Zone (Fig. 1), is evident within what appears to be cemented calcite fault gouge (cf. Verberne et al., 2013), striking SSW and dipping at ~80° to the WNW. Like Boulton and Robertson (2008) and Boulton and Whittaker (2009), who called this the 'Inner Boundary Fault' of the 'Hatay Graben', we

interpret this as an active fault with components of normal and left-lateral slip (cf. Karabacak et al., 2010; Karabacak and Altunel, 2013) and suggest the new name 'Antakya Fault' for this structure. Before this phase of slip began, the footwall escarpment may well have been overlain by Messinian evaporates and Early Pliocene marine sediments, with a probable thickness – estimated from the regional context (e.g., Boulton et al., 2006) – as >100 m; we infer that the ~600 m of normal slip thus estimated during the present phase of deformation indicates a time-averaged rate of ~0.17 mm a^{-1}, along with probably a much higher rate of left-lateral slip (the GPS data in Table 1 suggest that the rate of left-lateral slip across the ASFZ may be as as high as ~5 mm a^{-1}).

Figure 3. Field photograph looking ESE across the lower Orontes valley downstream of Antakya, providing another illustration of the escarpment of the Antakya-Samandağ Fault Zone. The photograph is taken from the surface of a low terrace of the Orontes at BA 41430 06993, where this fluvial terrace is transected by a cutting for the new ring road around the western outskirts of Antakya, at locality 3 in Fig. 12(a) of Bridgland et al. (2012), which provides a detailed topographic map of the area. The village in the centre of the view is Bostancık and that partway up the fault escarpment on the right is Harbiye. The escarpment of the 'Inner Boundary Fault' of Boulton and Robertson (2008) and Boulton and Whittaker (2009) (for which we suggest the new name 'Antakya Fault'; cf. Fig. 2) enters the view from the left at valley floor level, whereas their 'Outer Boundary Fault' (for which we suggest the new name 'Harbiye Fault'; cf. Fig. 4) forms the limestone escarpment in the distance, some 2 km farther SE. Stream gulleys entrenched into this escarpment are visible; these lead into stream 23 of Boulton and Whittaker (2009), whose long profile provides – in their view – evidence of a normal component of slip on these faults during the Quaternary. Both escarpments repeat the same succession of Palaeocene limestone overlain by Lower Miocene conglomerate and Middle-Upper Miocene limestone.

Figure 4. Map illustrating the linkage between offshore and onshore active (or post-Early Pliocene) faulting in and adjoining the easternmost Mediterranean Sea. Offshore faulting (SW of Ras al Basit) is from Bowman (2011) and is based on a dense grid of seismic lines illustrated in that reference. Hanging-wall ticks have been added on faults across which bedrock is downthrown. Onshore faulting in the Banyas / Jableh area of western Syria is from Ponikarov et al. (1963). Onshore faulting in the Amik Basin is from the present study, based on field evidence and reassessment of legacy seismic lines (see section 6). Onshore faulting in central-southern Turkey, SW of the Amik Basin, is from Boulton and Whittaker (2009); narrow ornament in this zone denotes very minor normal faults noted by these authors. SE-and SW-dipping offshore normal faults west of Samandağ (which we call the Samandağ and Kızıldağ faults) are from Hall et al. (2005). The disputed 'Nahr el Kebir Fault Zone' (extending onshore NNE of Latakia) and northward prolongation of the 'Banyas Fault' are discussed in the text (cf. Hardenberg and Robertson, 2013). Outcrop of Homs Basalt is simplified from Chorowicz et al. (2005). The 'misplaced seismic line' is seismic line 5 of Vidal et al. (2000a, 2000b) as plotted by Hardenberg and Robertson (2013; their Fig. 2). These authors have plotted this seismic line in the wrong place, locating its southern end (which is in reality ~9.5 km SSE of point 5C) ~30 km too far north and also orienting it parallel to ~N10ºW rather than the correct ~N17ºW (Fig. 1). In the northern part of the map area, abbreviations denote individual normal faults, thus: A.F., Akçaova Fault; An, Antakya Fault; B.F., Balıklıdere Fault; Ba.F., Banyas Fault; D.F., Denizgören Fault; H.F., Harbiye Fault; K.F., Karaköse Fault; Ka.F., Kasab Fault; Kı, Kızıldağ Fault; M.F., Meydan Fault; N.D.F., Nagar Dağı Fault; S.F., Sutaşı Fault; Sa.F., Samandağ Fault; Y.F., Yeşiltepe Fault; and Z.D.F., Ziyaret Dağı Fault. A complicating factor affecting this and other maps of the study region concerns the choice of co-ordinate system. The UTM system based on the WGS-84 reference frame will be used to define site co-ordinates throughout the present study. This divides the Earth's surface into UTM 'zones', each spanning 6º of longitude, which results in non-conformal joins between zones, one of which follows the 36ºE meridian through the present study region. Azimuths measured from UTM-oriented maps (such as the large-scale maps produced by the Harita Genel Komutanlığı and synthetic

maps generated using Shuttle Radar Topographic Mission imagery and rendered using UTM co-ordinates) therefore differ from those measured geographically. The difference is ~2°, or $\delta\phi$ x sin(θ) where $\delta\phi$ is the difference in longitude relative to the points where the co-ordinate systems are aligned, ~3°, and θ is the latitude, or ~36°. This difference causes UTM azimuths to exceed 'geographical' azimuths at sites east of the join; as a result, this and other maps are labelled using both geographical and UTM co-ordinates and north arrows are omitted.

Figure 5. Google Earth synthetic perspective view looking obliquely downwards towards S32^{o}E from a height of 11.2 km a.s.l. towards the coastal escarpment in the vicinity of Denizgören, near the Turkey-Syria border. This escarpment rises out of the sea to a height of ~700 m a.s.l., forming a large part of the WNW face of Keldağ, and has the characteristic facetted morphology of the footwall escarpment of a normal fault, which we call the Denizgören Fault (Fig. 4). On the right of the view, a smaller (≤200 m) escarpment that we interpret as the footwall of the Kasab Fault is also visible. The mid-point of the base of the view is above YE 62251 81900; the length of coastline depicted extends from YE 66773 86947 (left, near Karamağara, Turkey) to YE 60275 74632 (right, near Badrusiyeh, Syria), a distance of ~14 km. (a) un-annotated image. (b) image annotated with location information.

Figure 6. Map of the western foothills of the Amanos Mountains and the head of İskenderun Gulf, modified from Fig. 3 of Seyrek et al. (2008), based originally on part of Fig. 2 of Parlak et al. (1997), labelled like Fig. 4 with geographical and UTM co-ordinates. Numbers denote basalt outcrops within the Quaternary Ceyhan-Osmaniye volcanic field: 1, the Düziçi or Atalan basalt; 2, the Karagedik basalt; 3, the Karatepe basalt; 4, the Pınarözü / Aslantaş Dam basalt; 5, the Küçük Gertepe basalt; 6, the Büyük Gertepe basalt; 7, the Üçtepeler basalt; 8, the the Karataş Tepe basalt; 9, the Toprakkale basalt; 10, the Delihalil Tepe / Hama Tepe basalt; 11, the Botaş basalt. To avoid clutter, the River Ceyhan is only depicted upstream of the Aslantaş Reservoir; farther downstream, it flows SW from the Aslantaş Dam to Cevdetiye where it is joined by the Akarsu tributary. The SW end of the Savrun Fault is depicted after Duman and Emre (2013); farther SSW, where the Yakapınar-Göksun Fault Zone Zone passes beneath the Quaternary alluvium of the Cilician Plain, this fault zone is depicted schematically. Note that Parlak et al. (1997) depicted active left-lateral faulting along the Akarsu Valley consistent with the concept that the 'Karataş-Osmaniye Fault Zone' links in-line to the EAFZ at Türkoğlu, which Seyrek et al (2008) regarded as an incorrect structural concept. This faulting was reinterpreted as normal by Duman and Emre (2013) and regarded by them as part of their newly-designated Düziçi-Osmaniye Fault. See text for discussion.

Figure 7. Field photographs of the western escarpment of the spine of the Amanos Mountains in the Düziçi area (see Fig. 6 for locations). **(a)** View ENE from BB 65572 33490 adjoining distal limit of the Düziçi basalt near Abacılar (adjacent to the basalt sampling site in Fig. 6). In the foreground is the valley of the River Sabunsuyu, a left-bank tributary of the Ceyhan, and above it the ~185 m a.s.l. Ceyhan terrace, which we assign to MIS 8 (see text), as it is inset just below the distal limit of the ~280 ka basalt (Table 2) that is to the right of the view. In the distance in the centre of the view is the outlet where the Ceyhan exits Berke Gorge through the footwall escarpment of the Düziçi-Osmaniye normal fault, near Haruniye hot springs (BB 73466 38830). On the right of the view this escarpment rises from ~300 m a.s.l. to the mountain summit at ~2300 m a.s.l., Mesozoic limestone being upthrown relative to the younger rocks farther west the Düziçi-Osmaniye normal fault of Duman and Emre (2013). However, the in-line continuation of the mountain range front north of the river (to the left), likewise in the Mesozoic limestone, also shows the facetted morphology expected for the footwall escarpment of a major normal fault, suggesting the same normal fault zone (cf. Duman and Emre, 2013). **(b)** View looking northeastward, from BB 65052 35844 (~2 km north of the viewpoint in (a)), between the villages of Güzelyurt and Gümüş (~14 km NW of Düziçi; Fig. 6), towards the western escarpment of this mountain range from a different direction to the view in (a). The flat in the foreground, at ~300 m a.s.l., is formed of Early-Middle Miocene subduction-related sediments

(the Aslantaş Formation) that are locally overlain by ? Late Miocene - ? Early Pliocene gravels (the Kadirli Formation) and also partially covered by the ~280 ka Düziçi basalt. This flat is entrenched by the River Ceyhan, which flowed at a local level of ~100 m a.s.l. before the valley was flooded to a depth of >140 m a.s.l. behind the Aslantaş Dam. The outlet from Berke Gorge, also seen in (a) is visible on the right of the view. On the far side of the Ceyhan valley, to the left, is a higher flat at up to ~1000 m a.s.l., formed in Eocene-Oligocene subduction-related sediments (the Bulgurkaya Formation, also known as the 'Misis-Andırın mélange'). The distinctive mountain at the northern end of the range front is Dündül Dağı (circa BB 76500 51500), which rises to 1569 m a.s.l., adjoining the village of Boynuyoğunlu. This view is looking along the line of the 'Toprakkale Fault' of Duman and Emre (2013), which these authors have interpreted as a NE-striking left-lateral fault that terminates near Boynuyoğunlu at a rightward step onto an active west-dipping reverse fault on which the flat below the range front is being uplifted relative to the mountain range behind it on a reverse fault. The work by Seyrek et al. (2008) and our own follow-up investigations have revealed no evidence of such an active fault in this area, although an ancient reverse fault is locally present (Fig. 6). Stratıigraphic information used to illustrate these field photographs is from Tolun and Erentöz (1962), Parlak et al. (1997) and Robertson et al. (2004). See text for further discussion.

Figure 8. Synthetic topographic contour map, produced using Shuttle Radar Topographic Mission digital altitude data and rendered using UTM co-ordinates, of the Amanos Fault and newly identified Kızılyar Fault around Aktepe, showing localities discussed in the text. Dashed line oriented SSW from the Aktepe volcanic neck indicates the course of the Aktepe basalt flow, the distal part of which seems to be banked against the Kızılyar Fault. This basalt can be readily traced to circa P (BA 73807 60253) and is also visible circa Q (BA 73248 59346) and R (BA 72945 58282), before dying out circa BA 72329 56589, beyond the southern edge of this map. It appears distinct from the basalt farther west (e.g., at N, mentioned in the text), there being no continuity of outcrop in the field. This map is drawn with 20 m contours in black and intermediate 5 m contours in grey; the data processing used to render it is explained in previous publications (e.g., Demir et al., 2007, 2012; Seyrek et al., 2007, 2008; Westaway et al., 2009).

Figure 9. Google Earth image, used with permission, illustrating the left-lateral offset of the East Hatay Fault (the Yesemek Fault of Duman and Emre, 2013) near Karakaya (Fig. 1). This is a vertical view, centred over CA 03426 94824, looking downward from a point at 726 m a.s.l., ~200 m above the local land surface, with the top to the southeast. A small stream flowing southwestward is offset left-laterally between points CA 03441 94841 and CA 03413 94817, by ~37 m, having become entrenched into an older alluvial fan that has been shed from a bluff within the Hatay Ophiolite. Arrows at the sides of the view indicate the line of the East Hatay Fault through the site. See text for discussion.

Figure 10. Geological map of the Küreci basalt flow unit, adapted from part of Plate II of Atan (1969), with UTM co-ordinates added, showing his stratigraphic nomenclature and the location of the outcrop that we have named the Yünlü Tepe Basalt. Points denoted by letters are site locations discussed in the text, the upper case letters denoting the same points as in Fig. 8. Line segments linking c-g and east of J indicate positions of strands of the Amanos Fault deduced from fieldwork by Seyrek et al. (2007). Dashed line b-g illustrates Atan's (1969) tentative alternative interpretation. Point e is the location where basalt sample 99YW95, which yielded the ~253 ka K-Ar date, was collected, at BA 73857 65985. Point f is the viewpoint where the photographs in Fig 5b and 5c of Seyrek et al. (2007) were taken. Note that Atan's (1969) formation names are unofficial and other terminologies also exist; later studies (e.g., Schwan, 1971; Dean and Monod, 1985) discuss how these different nomenclatures correlate.

Figure 11. Montaged field photograph looking between westward and northward towards the Kızılyar Fault from BA 75054 67504: (a) original image; (b) annotated version. The ground in the foreground, east of this fault has been cleared (1), possibly for agriculture or in connection with chromite mining, but is bounded to the west by the fault-line bluff (2-3), in which a section through the Yünlü Tepe basalt is exposed (3-4), and is banked against ophiolite to the left of the view (4-5). Dating sample 06TR27 was collected ~30 m away at BA 75032 67528, at the foot of this bluff near the centre of the field of view, at G in Fig. 8 (6). Behind this bluff the land surface can be seen to rise higher, across a second bluff along the line of the Amanos Fault (7-8), to the summit area of Yünlü Tepe. On the right of the view is the distinctive flat-topped hill Keltepe (9), formed in basalt and bounded to the east by another basalt bluff that likewise marks the Amanos Fault and indeed adjoins the point (C in Fig. 8) where we envisage that the Kızılyar Fault Fault splays off. Yurtmen et al. (2002) and Seyrek et al. (2007) have published other field photographs illustrating this general area. Note the pervasive scrub vegetation, which obscures much of the potential exposure in this area.

Figure 12. Google Earth image, used with permission, illustrating a ~3 km length of the Amanos Fault (AF) and the adjacent Kızılyar Fault (KF) to the NW of Aktepe, between Yünlü Tepe on the right and the vicinity of Hacılar on the left. This rendering of satellite imagery has been processed to illustrate the view one would have looking downwards towards N80°E from a height of 2.87 km above sea-level, the field of view being centred at UTM co-ordinates BA 75351 68655. Field photographs presented by Yurtmen et al. (2002) and Seyrek et al. (2007) document several sites along this segment of fault at ground level in addition to that illustrated in Fig. 1. B, C, D, E, F and G denote the sites with the same labelling as on Fig. 8. Progressing from left to right, the Amanos Fault cuts across Yünlü Tepe separating Upper Cretaceous limestone (the Karadağ Limestone of Atan, 1969) to the WNW from the Hatay Ophiolite to the ESE. At F, basalt (the outcrop that we have named the Yünlü Tepe Basalt) first appears, banked against the northern edge of the ophiolite. A separate outcrop of basalt begins WNW of the Amanos Fault north of Yünlü Tepe, its southern edge (banked against the Cretaceous limestone) following the Aktepe-Eğribucak road. This basalt oucrop, which includes the distinctive hill Kısık Tepe (E), is bounded by an abrupt bluff with downthrow to the ESE along the Amanos Fault. Seyrek et al. (2007) discussed the possible location of the offset counterpart of this basalt on the ESE side of this fault, favouring a location consistent with a slip rate of ~3 mm a^{-1} that we now consider to be too conservative. B is the well-known ~450 m left-lateral offset of the Hacılar gorge through another basalt flow unit, dated by Seyrek et al. (2007) to 159±15 ka (±2σ), the use of which to constrain the left-lateral slip rate is discussed in the main text. The Kızılyar Fault entes this area from the right at the base of the bluff, forming the ESE face of Yünlü Tepe, in the Hatay Ophiolite, then passes the disused mine site (visible in this view as a scar on the landscape) and continues along the bluff at the truncated margin of the Yünlü Tepe Basalt at our sampling site (G; see also Fig. 11). D is the narrow outcrop of basalt that we regard as offset from the Yünlü Tepe Basalt at G as a result of ~1010 m of left-lateral slip on the Kızılyar Fault; C is our estimate of the point where the Kızılyar Fault terminates as a splay from the Amanos Fault; this adjoins another distinctive hill, formed in basalt, Keltepe, illustrated in Fig. 11.

Figure 13. Field photograph looking southward from BA 75054 67504, near G in Fig. 8, the same viewpoint as for Fig. 11. On the right is the ~220 m high escarpment in ophiolite, forming the ESE face of Yünlü Tepe, the southward continuation of the bluff illustrated in Fig. 11. We infer that the Kızılyar Fault continues along the foot of this escarpment, oriented circa N15°E-S15°W, as depicted in Fig. 8. In the left foreground (for example, circa BA 75118 67305, H in Fig. 8), east of the Kızılyar Fault, is outcrop of our 'highly weathered basalt'.

Figure 14. Map showing our interpretation of the most important active faults within the Amik Basin along with sources of information indicating when each has previously been documented, combining both field evidence and the seismic reflection evidence from Perinçek and Eren (1990) and Coşkun

(1994). For reasons stated in the caption to Fig. 6, this map has been provided with both geographical and UTM co-ordinates. The upper text beside each borehole is an identifying name or number; the lower number is the depth below sea-level of the base of the 'alluvium', which we take as marking the base of the post-Early Pliocene fluvio-lacustrine succession. The data for oil industry boreholes are as reported or deduced from Perinçek and Eren (1990). The other boreholes, from the DSİ (1975) dataset, have been re-plotted at their published UTM co-ordinates, which places many of them kilometres away from the positions where they were plotted by Karabacak et al. (2010): circular symbols indicate boreholes that bottomed in what Rojay et al. (2001) called 'pre-Pliocene basement' (i.e., rocks older than the fluvio-lacustrine succession), rectangular symbols indicate boreholes that did not. Unshaded symbols indicate boreholes that penetrated Plio-Pleistocene basalt. This map is modified from Fig. 7a of Karabacak et al. (2010) and can be compared with this original version and with the alternative scenario in Fig. 7d of Karabacak and Altunel (2013); in both these versions an in-line continuation of the Qanaya-Babatorun Fault is depicted as extending northward across the Amik Basin to roughly the location where we infer the southern end of the inferred Danaahmetli Fault, an idea that we regard as incorrect for reasons discussed in the main text. The Qanaya-Babatorun Fault has not been newly discovered in the past few years, as Karabacak et al. (2010) have claimed; it is depicted on old maps (e.g., Dubertret, 1962; Tolun and Erentöz, 1962; Ponikarov et al.., 1966) and has featured in discussion of the regional kinematics in many publications from Freund et al. (1970) onward. This fault was named by Westaway (2004) to facilitate discussion and shown by him to have accommodated significant left-lateral slip on the basis of existing geological mapping. The 'Antakya-Samandağ Fault Zone' depicted is a schematic representation of the set of en-echelon left-lateral transtensional faults mapped by Boulton and Robertson (2008) and others subparallel to the lower Orontes valley.

Figure 15. Two-way-time contour map for the Amik Basin, from Fig. 4 of Perinçek and Eren (1990). For reasons stated in the caption to Fig. 6, this map has been provided with both geographical and UTM co-ordinates. Contours in the eastern half of the map are for the top of the Eocene, those farther west are for the top of the Middle Miocene. Faults are ornamented to indicate our identifications of those that have experienced significant slip during the present phase of crustal deformation. A denotes Akçaova; Al, Alaattin Köyü, and H, Hasanlı.

Figure 16. Alternative map of the Amik Basin, modified from Fig. 2 of Coşkun (1994), showing the Amik-1 and Reyhanlı-1 boreholes and the seismic lines used by Coşkun (1994) to determine the depth to Mesozoic bedrock beneath the basin surface, which is expressed as the two-way time for seismic waves. This borehole reached 1629 m depth (Hemer et al., 1988), a few metres below the top of the Hatay Ophiolite, indicating a mean seismic velocity of ~1.7 km s^{-1} in the overlying Cenozoic sediments. Assuming the same seismic velocity, the maximum two-way time to the top of the ophiolite corresponds to a depth of ~2.3 km. However, Coşkun and Coşkun (2000) inferred that the 'lows' between the ophiolite 'highs' are largely filled with Cenozoic marine limestone, for which a higher seismic velocity and a correspondingly greater depth can be inferred, although they seem to have underestimated the thickness of Plio-Pleistocene sediment as discussed in the main text. The positions depicted for the Amanos Fault and Qanaya-Babatorun Fault mark where they cut the top of the Mesozoic bedrock; in the overlying Cenozoic sediments these faults have been interpreted as forming flower structures that can extend across distances of up to several kilometres perpendicular to each of the faults. The 'duplex zone' denotes the zone of overthrusting within the Hatay ophiolite; the cross-section is depicted in Fig. 8 of Coşkun (1994).